Instituto de Ciencias
Centro de Investigaciones en Dispositivos Semiconductores
Posgrado en Dispositivos Semiconductores

SOLUTION-PROCESSED ELECTRODES FOR PRINTED ELECTRONICS

Thesis submitted as a requirement to obtain the degree
PhD. Semiconductor devices

Presented by:

Sonia Patricia Cerón García # 220570140

Directed by:

Dr. Miguel Ángel Domínguez Jiménez
Director

Dr. David Barba
External Co-Director

CONACyT scholarship# 849805

Acknowledgements

The first person I would like to thank is Professor Miguel A. Domínguez, who has supported me with the freedom and confidence to carry out more than one research project that has been part of my professional growth. I appreciate the ease with which he has allowed me to propose and contribute solutions to the problems that have arisen during the development and completion of this doctoral thesis.

I would like to thank Dr. David Barba. I sincerely appreciate his continuous interest and feedback to my research work and the conclusion of this dissertation. His recommendations and observations were an important key for the continuous improvement of this research project and training for collaborative work and peer discussion.

I thank the Program in Semiconductor Devices, the professors and the colleagues who comprise it, for the help and learning provided during the conclusion of my Ph.D. I would like to thank all the jury members who took the time to review and evaluate my thesis.

I thank Conacyt for awarding me the scholarship #849805.

Thanks to my friends: Daniel, Aránzazu, Teresa, Pablo, and Gabriela, for their company and friendship in moments of joy and discomfort.

To Miguel G., for the calm, wellbeing, company, support and learning that you have given me.

Abstract

Printed electronics is a technology based on the deposition of films of conductive, dielectric, or semiconductor materials using printing mechanisms, called contact and non-contact, which are characterized by being fast, controllable and compatible with low-cost techniques, and with the use of flexible substrates made of natural and synthetic polymeric structures, attracting attention of the scientific community. In printed electronic technology, the use of functional and printable inks contributes to the quality of conductive contacts. The composition of the inks is mainly based on the presence of metallic nanoparticles dispersed in different organic solvents that provide stability and resistance to oxidation, resulting as a favorable electrical behavior for a printed circuit.

In this dissertation, the synthesis of a conductive ink based on silver nanoparticles (AgNPs), obtained by the chemical reduction method for the fabrication of conductive patterns deposited by direct deposition printing techniques, is demonstrated. The significant finding of this work lies in the optimization of the synthesis method and the eco-friendly reagents, where it was found that there is a preferential concentration for growth, size distribution, stability, and growth control through the addition of a limiting reagent. At the same time, the compatibility of the particles with flexible substrates such as bond paper, opaline, photographic paper, PET, and acetate is confirmed, along with the electrical performance of the particles dried at room temperature, with ohmic resistances ranging from 1.80 to 5.78 Ω. We would like to point out that the scope of the physical, chemical, optical, electrical properties, relies on the synthesis routes of metallic nanoparticles, as well as the influence of the reagents used during the processes. Ferreira-Oliveira *et al* [In Talanta open, **5**, 100085 (2022)] report a silver nanoparticle-based ink synthesized by the polyol method with a similar resistance (1.53 Ω). Although the reported result confirms the conductive nature of the ink, the polyol method involves suspending a metallic precursor in a glycol solvent and heating the solution by reflux, which implies higher energy cost and temperature control during synthesis to prevent oxidation of the polyols used [K. Eid *et al*, Supra-Materials Nanoarchitectonics, Elsevier inc., (2017) Amsterdam, 135-171].

Additionally, the synthesis of ink based on 20 wt.% AgNPs with hydrogen peroxide is presented, and the addition of any stabilizing or wetting compound was not necessary to maintain stability and allow ink flow. The synthesized ink maintains the properties of AgNPs and ensures the absence of contaminating elements. The electrical properties of the ink were assessed using photographic paper, demonstrating through bending and 1000 cycles of torsion the appropriate electrical behavior of the ink without reaching the pattern breakage.

Table of Contents

List of figures

List of tables

List of abbreviations

Abbreviation	Meaning
$AgNO_3$	Silver nitrate
AgNPs	Silve nanoparticles
Al	Aluminum
Au	Gold
$C_6H_5Na_3O_7$	Sodium citrate
CIJ	Continuous Ink Injection
CMOS	Complementary Metal-Oxide Semiconductor
Cu	Cooper
DEG	Diethylene gycol
DLS	Dynamic Light Scattering
DoD	Drop on Demand
EDS	Energy Dispersive X-ray Spectroscopy
EG	Ethylene gycol
EtOH	Ethanol
FET	Field-Effect Transistor
FR4	Flame Retardant 4
H_2O_2	Hydrogen peroxide
HFE	Hybrid Flexible Electronics
IC	Integrate Circuit
ITO	Indium Tin Oxide
I-V curve	Current-Voltage curve
LCP	Liquid Crystal Polymer
LED	Light-Emitting Diodes
MEA	Ethanolamine
MtOH	Methanol
N_2H_4	Hydrazine hydrate
$NaBH_4$	Sodium borohydride
NaOH	Sodium hydroxide
$NaNO_3$	Sodium nitrate
Ni	Nickel
OFET	Organic Field-Effect Transistor
PA	Polyamide
PAA	Poly (acrylic acid)
PC	Polycarbonate
PCB	Printed Circuit Board

PDI	Polydispersity index
PDF	Powder Diffraction Files
PE	Polyethylene
PEDOT:PSS	(poly(3,4-ethylenedioxythiophene)poly(styrenesulfonate)
PEN	Polyethylene naphthalate
PES	Polyether sulphone
PET	Polyethylene terephthalate
PI	Polyimide
PVC	Polyvinylchloride
PVP	Polyvinyl pyrrolidone
RA1, RA2	References sample 1 and 2
SEM	Scanning Electron Microscopy
SC1, SC2, SC3, SC4	Sodium citrate samples 1 to 4
SN1, SN2, SN3	Silver nitrate samples 1 to 3
TFT	Thin Film Transistor
TPUR	Thermoplastic polyurethane
XRD	X-Ray Diffraction

Results obtained

Publication

S. Ceron, D. Barba and Miguel A. Dominguez, “Solution-Processable and Eco-Friendly Functionalization of Conductive Silver Nanoparticles Inks for Printable Electronics”, Electronic Materials, 5, 45 (2024).

Contributions to national conferences

1. **S. Ceron**, D. Barba, M. A. Dominguez, “Synthesis of conductive silver nanoparticles for printing electronic applications.”. In Latin American Electron Devices Conference. July 4th-6th, 2022. Puebla, Mexico. [POSTER]
2. **S. P. Cerón García**, D. Barba, M. A. Domínguez Jiménez, “Synthesis of silver nanoparticles and its application as a conductive ink for flexible and printing electronics”. In XV International Conference on Surface, Materials and Vacuum, Sociedad Mexicana de Ciencia y Tecnología de Superficies y Materiales. September 26th–29th, 2022. Puerto Vallarta, Jalisco, Mexico. [POSTER]

Chapter 1
Introduction

Electronic waste or e-waste, according to Suja *et al* [1], is any electrical appliance or electronic component that has reached the end of its useful life cycle due to its operation, where eventually its use or consumption will be part of a set of waste. The e-waste is considered as a fastest-growing category because the consumption demand for electronic products continues growing every year, estimating a projection in consumption growth of 4.52% with monetary profits of $538 billion USD per year from the sale of electronic products [2, 3]. However, the high demand in consumption from various socioeconomic profiles increase the level of e-waste and limits the collection of waste, impacting and damaging environment and human health [4].
The continued use of devices, such as household appliances, televisions, smartphones, electronic hardware, and others that have generated and will continue to producing a significant new amount of e-waste in the near future [5, 6]. The main components of these devices are PCBs (printed circuits boards). These are constituted by a substrate know as Flame Retardant 4 (FR4), which is a composite material made of woven fiberglass cloth, epoxy resin binders, and toxic substances such as bromated flame retardants. Other components that are included in such PCBs are capacitors, batteries, plating for corrosion protection, and solder alloys that include toxic chemicals [7, 8].

Choosing ways to reduce polluting materials, can provide better alternatives that reduce environmental and health risks. Figure 1.1 shows a comparative perspective of the PCB e-waste problem and the possible eco-friendly solutions. However, now a days the waste and handling the materials that constitute PCBs requires a manufacturing processes were non-toxic materials are necessary. Also, not all the materials in PCBs have property to be recycle or being biodegradable to minimize adverse environmental and human health.

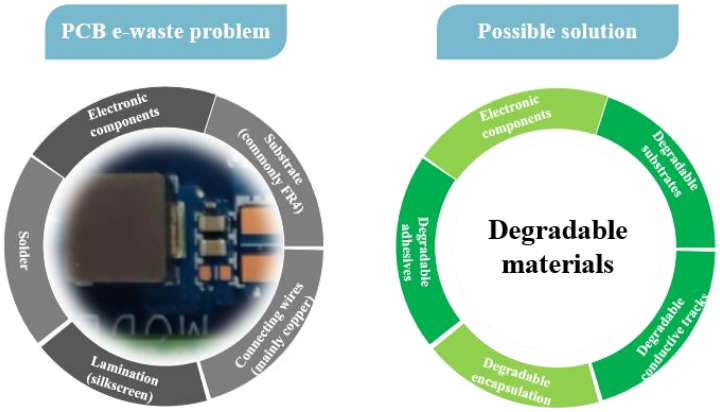

Figure 1.1. Desing guidelines of future degradable PCBs. Modified from reference [7].

For these reasons, new technologies are currently being developed to improve the maintenance of sustainable production routes in the industry, from the manufacturing stage up to disassembly [2, 8]. If electronic devices are manufactured with characteristics that contribute to their recycling, the reduction of risks in human manipulation of rare earth metals would be favored and the recovery of materials and metals would even be enhanced [7, 9].

The eco-design of electronics serves as an alternative solution to reduce waste by employing materials that can enhance recycling efficiencies (Figure 1.2). This involves constructing devices using materials such as polymers, adhesives, and active layers that can degrade naturally. Additionally, implementing materials with versatile production processes and easy-to-handle chemicals not only eliminates the environmental risks, but also facilitates disposal, while ensuring compatibility with environmental standards [9].

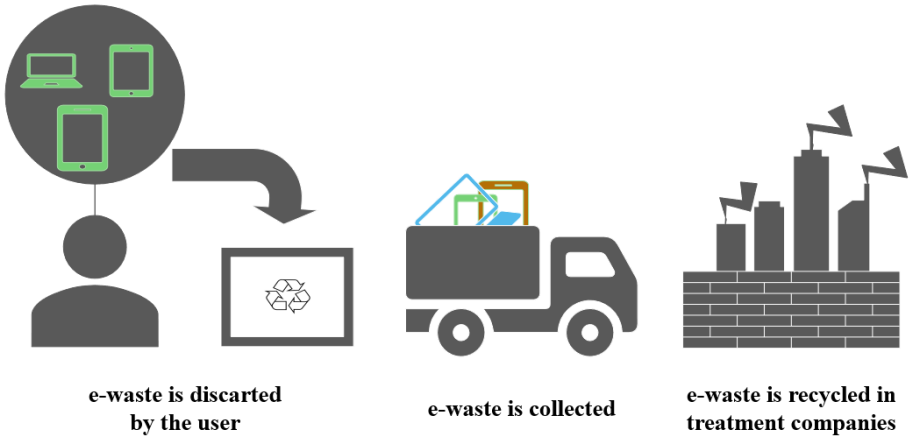

Figure 1.2. Possible routes to formal e-waste collection. Modified from reference [6].

Biodegradable materials, such as natural and synthetic polymer substrates (e.g., paper, polyvinylchloride or PVC, Polyethylene terephthalate or PET, among others), facilitate recycling, usage, and cost-effectiveness, making them attractive conventional materials for use in electronics. These materials form the basis of a field of application known as flexible electronics, offering the possibility of transferring the construction of PCB boards to a biodegradable electronics analogue, like Hybrid Flexible Electronics (HFE) that integrate printed electronics and conventional silicon ICs (integrate circuits) [10, 11].

The design and construction techniques of HFE involves that their active layers and conductive tracks do not produce toxicity, and the electronic components can be disassembled for reuse contributing to the e-waste recycling.

In addition to considering the technological development of printed electronics based on sustainable and eco-friendly development, it is also important to consider the electrical performance of different devices made with printed electronics comparing them with silicon based technology. In the following section, the historical development of devices based on

printed electronics will be briefly mentioned and, in general terms, its contrast with microelectronics is mentioned.

1.1 Background

In the late 1960s, the first tests of printed electronics were carried out. These tests involved the deposition of inorganic materials on Thin-Film Transistors (TFTs) placed on paper and other types of substrates using a vacuum chamber to construct flexible circuits. The aim was to integrate these circuits into credit cards, electrical sensors for medical and biological uses, teaching materials and toys [12, 13]. Later, devices printed on paper, such as a light-emitting diode (LED) with a capacitance response of 0.1 nF and field-effect transistor (FET) fabrications, were reported. The scale-up of these devices has been tested without altering the electrical properties [14, 15]. Currently, the development of printed circuits using inks containing metallic nanoparticles start to become a sustainable manufacturing process. These nanoparticles primarily act as electrodes, including materials such as Cu (copper), Ni (nickel), and Al (aluminum) [16]. Such breakthroughs made possible the implementation of Complementary Metal-Oxide Semiconductor (CMOS) technology at a low cost and with low environmental impact by avoiding the production of various toxic metals that affect the environment and health [17]. Multiple electronic devices as solar cells, LEDs, Organic Field-Effect Transistor (OFETs), capacitors, supercapacitors, batteries, antennas, PCBs, sensors, among others, can be fabricated on flexible substates [18-24]. The manufacturing of these devices has replaced high-cost and difficult-to-recover materials and elements such as platinum and Indium Tin Oxide (ITO). This has been achieved by using materials obtained in a more versatile way that exhibit competitive properties, including ternary and quaternary materials, metal oxides, carbon-based compounds such as graphene, or even nanomaterials.

Compared to traditional silicon electronics, printed materials are cheaper due to the design approach in creating devices that address a range of applications requiring disposability, reusability, better performance, and operational features, thus reducing production cost. Figure 1.3 outlines the key points in device manufacturing considering that printed electronics technology adopts flexible and large-area substrates with fast, simple and low-cost integration, as well as low switching operation times, compared to microelectronics that, despite providing extremely short switching times and high-density integration [see figure 1.3], however, sophisticated manufacturing in small areas implies high costs. The incorporation of HFE provides the qualities of both technologies from materials adaptation, manufacturing design, circuit design and incorporating integrated systems [11].

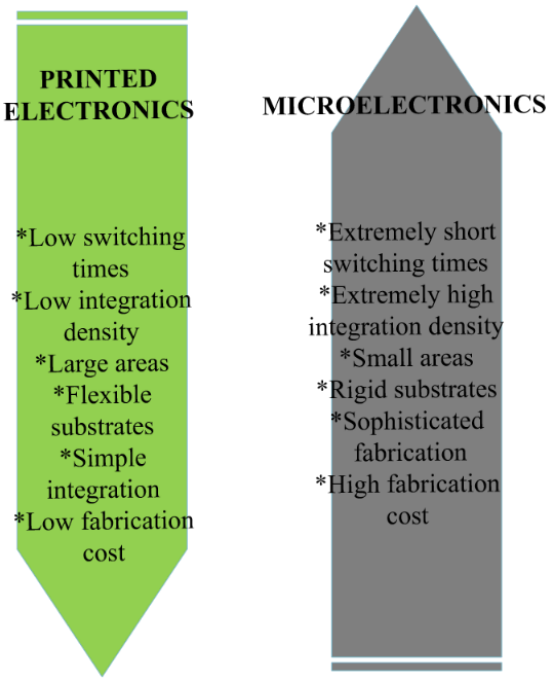

Figure 1.3. Comparison between printed electronics and microelectronics [25-28].

Individually, both techniques provide advantages, however, if there is an integration of both, then the substitution of mechanical properties that limit the scope of the application of the built systems is provided, for example, replacing an FR4 structure and etching on Cu plates by flexible substrates and conductive ink applied by a printing method. Teng *et al* [29] were the pioneers in achieving integration using microelectronics with the inkjet technique when manufacturing contacts for solar cells using a silver neodecanoate solution, from there, the development of solution-processed electronics has spurred the advancement of electronic device manufacturing processes, considering material performance from acquisition to implementation.

1.1.1 Functional printed electronics

Printed electronics involve layer-by-layer deposition to create continuous and uniform patterns. Ambient temperature drying is expected to be favorable; however, the use of temperature, with drying up to 500°C, may be required, first to evaporate the solvents that formulate the ink, and secondly, to enhance the electrical behavior of the printed materials [30-32].

Another important aspect of this technology is the flexible electronics and the requirements it entails for achieving the manufacturing of electronic devices. Flexible electronics presents limitations which, according to its development and applications, can be adaptable to the field applied. This implies considering aspects such as the flexibility of the materials used as

substrates compared to the rigid substrates that compose traditional microelectronics. This leads to the basic and simple realization of highly conductive, insulating, or semiconducting systems using flexible materials as substrates, although the performance is not yet comparable to silicon-based technology. However, the development and applications of flexible electronics are achievable in interdisciplinary fields such as medicine and health, energy, optoelectronics [33], and its manufacturing is based on material preparation, deposition, modeling, and encapsulation [34].

The manufacturing of inks for printing systems, like inkjet printing, is of interest due to their low fabrication costs, large areas, high efficiency, variability in low and high temperature, absence of mask usage, high resolutions, high compatibility with both natural and synthetic polymers, flexibility, low material consumption, etc. [34]. The formulation of inks, whose composition provides adequate flow, substrate compatibility, and controls the quality of printed films, is crucial. The choice of solvent is primarily focused on particle compatibility, as well as toxic and environmental implications. Hence, the use of organic solvents aims to avoid the generation of volatile compounds [35, 36].

The synthesis of water-based inks, besides not being based on a toxic solvent, implies no residue, and water is a much more economical and readily available solvent. However, the disadvantage of using this solvent is its limited compatibility with plastic polymeric substrates, which poses challenges for drying, adhesion, and uniformity of printed patterns due to surface tensions present, which are crucial in printed electronics technology [37].

Commercially, silver-based inks can be found in a range of prices due to their properties. For example, prices can vary from $300 USD for 10 g to $500 USD for 200 g [38-40]. The main characteristics of these inks depend on their deposition method and preparation, and compatibility with intended substrates is not guaranteed. Additionally, drying temperatures higher than 100°C are often recommended.

Inks primarily made of silver nanoparticle-based formulations have been reported and exhibit efficient conductivities [41-44] The difference among the reported inks lies in their formulation, synthesis routes, reagents used, adaptability of particles to specific solvents, variability in drying times and temperatures, and the routes for their applications in printed electronics, primarily through inkjet printing techniques. For example, Fernandes *et al* [41] report the mixtures of silver particles with ethylene glycol (EG), ethanol (EtOH), PEDOT:PSS [(poly(3,4-ethylenedioxythiophene)-poly(styrenesulfonate)], water, ethanolamine (MEA), and hyperdispersant (Solsperse 20000) in the same formulation, yielding resistivities of 5.4 $x10^{-6}$ Ω·cm. Additionally, Mo *et al* [42] reported resistivities ranging from 1.5 to 2.9 $x10^{-6}$ Ω·cm for silver nanoparticle inks with dodecylamine and dodecanothiol.

The manufacturing of electronic products through printed electronics still involves the search for accessible, economical, and reproducible processes. However, this is a field that is potentially envisioned in the industry's future. An ink that exhibits conductive characteristics and is low-cost, easy to prepare, store, and apply is indicative that manufacturing processes lead to high yields for various research and industrial applications, from their deposition to post-processing.

1.2 Main objective

Due to the scope, reproducibility, stability, and adaptability of using silver nanoparticle-based conductive inks, the main objective of this work is focused on a simple synthesis of these inks through the chemical reduction method. Simultaneously, on the selection of synthetic and natural polymeric materials, the goal is to evaluate the compatibility of nanoparticles and their application in printed electronics. Thus, more precisely, the main objective is described as follows:

Synthesize silver nanoparticles inks from chemical reduction method and functionalize them as electrodes by printing techniques for applications in flexible electronics.

The general idea is to use a precursor agent that generates silver ions ($AgNO_3$) reacting with a reducing agent ($NaBH_4$) in an aqueous medium, and through the use of sodium citrate ($C_6H_5Na_3O_7$) at different concentrations, evaluate the control of nanoparticle growth, their stability, morphological, compositional, optical, and structural properties. Subsequently, conductive nanoparticles will be identified, which will be measured through I-V characterization to confirm ohmic behavior. Similarly, one of the main challenges in particle suspension is to find a dispersing medium that allows creating a stable system without the need to implement wetting agents or organic stabilizers as conventionally found in the literature [45], as well as using low concentrations by weight ($\leq 20\%$) of nanoparticles in a larger volume aqueous medium ($\sim 80\%$) that allows good electrical properties [46-48].

As a detailed approach, individual objectives were established and pursued one by one as follows:

1. Synthesis of silver nanoparticle through the use of a reducing agent.
2. Determination of chemical and physical properties.
3. Determination of the electrical properties of conductive particles onto different flexible substrates.
4. Study and application of a conductive AgNPs-based ink.
5. Adaptation of the synthesized conductive ink in a conventional cartridge through handwriting technique.

1.3 Justification and structure of the thesis

Printed electronics refers to the application of printing techniques, both conventional and digital, to manufacture electronic structures, devices, and circuits, regardless of what functional materials (ink) and substrates are used, allowing it to be carried out economic [49].

The adaptability of conductive materials used as electrodes on flexible substrates increases the possibility that the electrodes printed on the substrate improve the compatibility on its surface and the improvement of the electrical characteristics in flexible electronics with a highly recyclable material. Using a conventional printer is expected conventional to favor the costs of the method, even from the choice of synthesis method to the costs of the reagents and materials implemented for the synthesis of inks with high conductive yields on large area surfaces. The aim is to ensure that deposition mechanisms could simulate both high-cost industrial methods and conventional, easily adaptable, and more economical methods. These methods fulfill the requirements of coating and direct deposition processes [50-52].

This dissertation is divided as follows: in Chapter 2, we discuss the general aspects of the state of the art involving printed electronics. We also describe the technology of printed electronics and deposition mechanisms for nanoparticle-based conductive inks. In Chapter 3, we describe the synthesis methods of silver nanoparticles using the chemical reduction method, evaluating the effect of adding two agents, one potentially reducing and the other with both reducing and protective characteristics. Conductive nanoparticles were obtained based on optical, compositional, morphological, size, and stability characterization, and their electrical behavior was measured on five flexible substrates. In Chapter 4, the synthesis of conductive ink from the reaction between nanoparticles and hydrogen peroxide (H_2O_2) is described. Characterization includes I-V measurements along with mechanical tests of bending and torsion cycles. Additionally, the construction of a simple PCB system using the direct deposition method of handwriting is presented. The dissertation concludes with Chapter 5, describing the conclusions and reviewing the main contributions and results of the thesis.

Chapter 2

General aspects of printed electronics

Printing electronics includes techniques that allow the replacement of conventional processes found in ICs. The main goal is to create an electronic system using printing electronics [53]. Figure 2.1 shows the comparison in the manufacturing of traditional integrated circuits, which involve different processes such as applying resin for lithography and etching of a circuit. On the other hand, printing involves fewer steps such as depositing conductive ink, primarily, and drying, making it a more controllable and sustainable process to obtain a circuit pattern on a functional substrate.

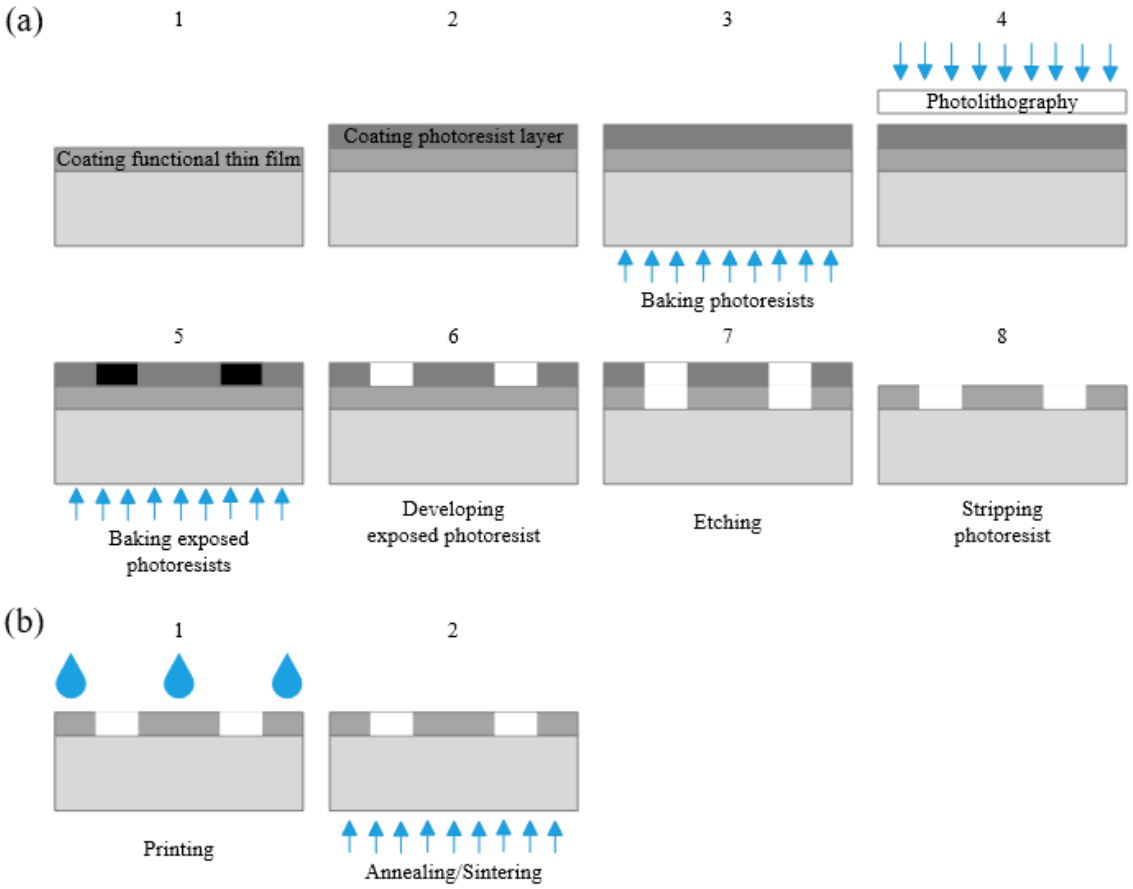

Figure 2.1. Comparison of manufacturing steps between (a) IC and (b) printing process [53].

Another objective of printing electronics is to reuse and achieve a circuit that is 100% closed-loop in terms of materials, with profitable heat and energy consumption, reliability, high

lifespan, yields, repairability, and maintenance, as offered by silicon-based technology [7, 54].

Printed electronics is still under development, but it provides solutions by adopting new methods for manufacturing thin, flexible, lightweight, and low-cost electronic devices from sustainable designs, thereby reducing the consumption of toxic and harmful materials. It also implements eco-friendly materials to provide a lasting solution [7; 49]. Today, hybrid flexible electronics combine silicon ICs with flexible and printed electronics, providing high-performance operation on large-area surfaces without expensive processes [10].

In addition to flexible, degradable, and recyclable substrates, using printing electronics also involves making inks from materials whose processes require low energy consumption. Moreover, the final properties and raw materials of these inks should not pose negative health or environmental risks during handling [49]. Another important aspect is that the inks are formulated based on solvents. In the literature, countless solvents are applied in different processes for the synthesis of these materials [30, 55].

In printing electronics, three groups of inks are classified based on the nature of the conductive material, where: (1) inks made from metallic particles, (2) inks based on carbon compounds, and (3) inks based on particle-free polymeric materials (for example, PEDOT:PSS ink) [46]. According to this classification, this section will describe the use of metallic nanoparticles as the reference for analysis.

In the following sections of this chapter, a brief review of the ink formulations from printed electronics will be addressed. Also, general aspects of the state of the art that connect flexible electronics and of impression will be described. The types of printing techniques are mentioned with the classifications and types of printing mechanisms. Finally, the general characteristics of inkjet printing technology and its use for the manufacture of conductive contacts on flexible substrates will be mentioned.

2.1 Nanoparticles ink technology

Inks based on nanotechnology focus on the functionality of the inks based on their chemical composition, particle size and shape, ink viscosity, and surface tension [47]. Different authors have mentioned a variety of synthesis methods for preparing nanoparticles such as chemical vapor deposition [56], photochemical reduction [57], ion sputtering [58], laser ablation [59], chemical reduction [60], among others. The chemical reduction method is one of the most commonly used to synthesize metallic nanoparticles because one of its main characteristics is the controlling of the temperature and reaction time, where the size and shape of the nanoparticles can be controlled as well [61].

Referring to metallic nanoparticles, the most common are made of silver (Ag) AgNPs and gold (Au), as they provide high conductivity and other qualities such as resistance to oxidation. When they are integrated into an ink, these aspects do not substantially affect the ink's conductivity over time. Gold nanoparticles show greater resistance to oxidation over time, and their conductivity is higher. However, gold is an inert metal, making the formulation of an ink based on these nanoparticles complicated. Additionally, the cost is considerably higher, and synthesis processes, even by using methods such as chemical reduction (which is one of the simplest methods), involve the use of higher temperatures and longer synthesis periods [62]. On the other hand, metals like copper (Cu), aluminum (Al), or nickel (Ni) are cheaper but oxidize, forming insulating layers that in turn alter the conductivity of the inks. Therefore, the use of vacuum may be necessary to delay oxidation [30, 35, 62]. Considering these characteristics and comparing them with particles of Au, Cu, Al, and Ni, silver nanoparticles (AgNPs) are the conductor material par excellence for use in the synthesis of conductive inks [63].

Recent studies report the synthesis of AgNPs using the chemical reduction method, taking into account various aspects such as the reagents used and reaction conditions. Gangwar *et al* [64] have reported the synthesis, using silver nitrate ($AgNO_3$), with tannic acid as the reducing agent and sodium hydroxide (NaOH) at 30°C for 30 minutes. The reported particle size is 5-40 nm, and they exhibit a spherical shape. The authors describe the effect on particle growth with changes in the concentrations of the reducing agent and precursor. Additionally, they report the effect of the reducing agent concerning time.

Ma *et al* [65] demonstrate that under the reaction of $AgNO_3$, hydrazine hydrate (N_2H_4), and polyvinyl pyrrolidone (PVP) at 60°C for 30 minutes, spherical particles of 81 nm are obtained. On this study, they compare the variation in the concentration of $AgNO_3$ to evaluate the electrical behavior in relation to the effects of agglomeration.

On the other hand, besides using $AgNO_3$, N_2H_4, and PVP to obtain spherical particles. Some other authors also use ethyl cellulose, acetone, and terpentine alcohol to synthesize conductive ink [66]. Zhuo *et al* also mention printing patterns on polyimide (PI) with drying temperatures ranging from 140°C to 250°C since the organic compounds formed are removed at these temperatures.

Using sodium borohydride ($NaBH_4$) with PVP and $AgNO_3$ to obtain spherical particles by the chemical reduction method has also been reported. However, Kant *el al* [67] do not provide information about the reaction conditions even though, they obtain an ink based on their synthesized AgNPs with particles ranging from 10-50 nm in size dispersed with EtOH, methanol (MtOH), propanol, diethylene glycol (DEG), toluene, and water. The authors conducted tests on photographic paper with drying at 100°C. The authors conducted tests on PET and photographic paper with drying temperatures ranging from 50 to 300°C for 30 minutes.

By the same synthesis method, the processes of obtaining nanoparticles can be accelerated depending on the properties of the reducing agent. For example, benzene-1,3,5-triol reacting with $AgNO_3$ at 25°C for 5 minutes results in particles of 12 nm [68]. Finally, Shen *et al* [44] report spherical AgNPs particles ranging from 20-230 nm in size using $AgNO_3$, MEA, poly (acrylic acid) [PAA], and water at 65°C for 1 hour. The ink that mention is based on EG and water, tested on photographic paper with drying temperatures ranging from 50 to 180 °C over 15 minutes.

2.2 Conductive inks design

Ideally, the design of an ink formulation assumes that its composition addresses different issues that may arise during the printing process. For example, nanoparticles tend to aggregate or sediment over time, which adversely affects the ink's stability. Additionally, during printing, bulging lines and cracks may form during pattern drying [69]. Therefore, it is common to find in the literature inks where dispersing agents are added mixed with binders and other additives [30, 55].

Although multiple synthesis routes and ink formulations are mentioned in the literature, there is no precise way to determine which one is the most favorable. Therefore, it is important to create a design that takes into account solutions to the problems that arise during and after printing using a printed electronics technique. This will favor processes and yields from ink synthesis to its use and promote proper functioning and application in the printing system.

Tam *et al* [45] propose three steps for designing an ink. The first step involves identifying the specifications of the desired product, which means achieving the transition from a solution with nanoparticles to a solid track after drying. Another aspect to consider is the surface properties of the substrate and the printing mechanism or technique intended to be adopted. Additionally, formulating an ink based on metallic nanoparticles implies that the nanoparticle size influences stability, as sedimentation can be accelerated by increased density resulting from larger particle size. Regarding the electrical characteristics of the particles, it is preferable to minimize porosity and cracks when the printed pattern is already solidified. The second suggested step is the ink formulation. As mentioned, an ink may consist of a conductive material, a dispersing agent, a dispersing medium, a cosolvent, or a binder, and the choice and incorporation of these components are based on the properties that are need for improvement. For example, in Figure 2.2, the key aspects that can be improved are shown. According to the figure, these properties are associated with stability and printability, which depend on the suspension of the conductive material or the conductivity that relies on the printed pattern. Additionally, if conductivity improvement is expected by making the conductive pattern with fewer pores and cracks, then a binder can be added, using curing conditions, modifying viscosity, and changing the thickness of the printed pattern. On

the other hand, if ink stability improvement is desired, then the amount of conductive material should be varied. The variation in the compounds related to the ink composition (see "related ingredients" in Figure 2.2) will change the properties of the ink or the printed pattern.

			Product use conditions					Product specifications						
								Suspension			Printed track			
		Product attributes	Substrate	Droplet diameter and nozzle diameter	Droplet velocity	Transverse printing speed and droplet spacing	Curing conditions, e.g. drying or sintering	Shelf life	Ink viscosity	Ink specific surface energy	Track width	Track thickness	Track volume resistivity	Related ingredients
Suspension	Stability	Stable against sedimentation						x						Conductive material
		Stable against aggregation		x	x			x						Dispersant
	Printability	Stable droplet formation	x						x	x				Dispersing medium
		Good wettability on substrate				x				x				Dispersing medium
		Droplets coalescence to form uniform lines							x	x	x			Dispersing medium
Printed track	Conductivity	Free of coffee ring stains								x				Cosolvent
		Fully sintering with minimum pores and cracks					x		x			x	x	Binder

Figure 2.2. Matrix for conductive ink-based metal nanoparticles formulation. Modified from [45].

The third step is the verification and modifications to the formulation. After synthesizing the ink, the test to validate its performance is printing, bringing the material to be adapted to the printing system. Subsequently, it needs a validation and verification if any additional processes are required to form a solid pattern, allowing the determination of pattern measurements and electrical characterization appropriately and functionally. If there are no favorable effects after deposition, alternatives are sought to improve the compatibility of the ink with the substrate and the printing system, which implies a new challenge to solve the new problems that have been observed.

The design proposed previously is suitable to provide a general perspective on the key points that may arise during the development of a functional ink. However, the chemical, physical, and electrical properties of the conductive material can lead to variability in adopting this scheme.

Therefore, as mentioned in section 2.1, finding the best properties of the conductive material may lead to the search for new synthesis routes.

2.3 Silver nanoparticles for printing electronics

In section 2.2, it was mentioned that it is crucial that the particle size needs to be reduced, as it facilitates the suspension of the particles in the medium and also contributes to uniformity of the printed pattern. In a printing system, such as inkjet printing, the particles should not

obstruct the nozzle, which typically has a droplet expulsion size of 30 μm in diameter [70]. Various studies report inks containing particles with sizes up to 200 nm [71-73]. Furthermore, to adapt an ink to a commercial printer, it is also considered that the particle size should be less than 200 nm [74]. Another aspect to consider in order to avoid a nozzle obstruction and achieve a uniform pattern, is that the inks, for example, based on AgNPs, are generally composed with 20% of the total content [46, 75].

2.4 Spherical nanoparticles and size control

In section 2.3, it was mentioned that particles with sizes less than 200 nm are required to avoid obstruction of printing systems and minimize defects in printing. Regarding shape, Winter *et al* [76] have mentioned that spherical particles are preferred because they provide fluidity during ink injection or application, and with this geometry, they can acquire electrically conductive charges [77, 78]. Spherical nanoparticles can be obtained via the chemical reduction method. Also, from this chemical reduction method, metallic nanoparticles of gold, silver, and copper can be rapidly formed with controllable sizes and stable characteristics [79, 80]. Conventionally, the synthesis process simplifies temperature and reaction time control for shaping, sizing, and other material properties during synthesis. Obtaining silver nanoparticles involves dissolving a precursor metal salt, a reducing agent, and sometimes the use of a stabilizer. In section 2.1, cases reported in the literature using this method were mentioned. Under all aspects mentioned in this chapter, it is considered feasible to produce a conductive ink based on AgNPs using a simple, adaptable, rapid synthesis process with controllable conditions to promote nanoparticle growth and the presence of conductivity. Additionally, the design contemplates formulating a water-based ink without the need for stabilizers or dispersants.

2.5 Printable and flexible electronics technology

Printing electronics enable the implementation of organic, inorganic and hybrid materials, through low-temperature, low-cost processes, and the use of easily accessible materials such as synthetic (see figure 2.3) or natural (see figure 2.4) polymer substrates. These materials can be used as large-surface substrates for the manufacturing of devices in biodegradable electronics [10, 81-83], aerospace [84-87], automotive [88-90], packaging [91, 92], and medicine [93-96]. For printing electronic products, the term “print quality” refers to the surface roughness and thickness of the printed ink or paste, as well as to the electrical properties of the achieved components and devices.

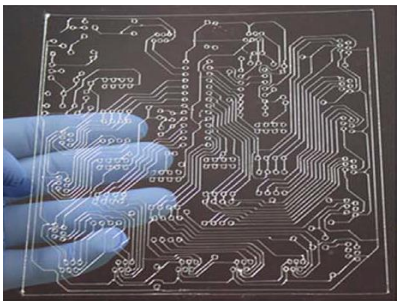

Figure 2.3. Printed circuit on PVC substrate [97].

Figure 2.4. Three-dimensional structure of conductive material printed on paper [98].

In direct printing electronics applications, conductive materials are the most commonly used. These materials offer a more affordable approach and are suitable for the large-scale production circuits [97, 99].

2.5.1 Printing processes technology

In the development of printed electronics, the technology is categorized into two types of processes, contact and non-contact printing, which are distinguished by the process of depositing a material. In contact printing, the plating plate or base of the mechanism maintains direct fixation with the surface of the substrate, while in non-contact printing, only the material of interest has direct contact with the substrate surface. Various deposition mechanisms are employed to achieve material fixation using either of these two techniques [26, 100], as illustrated in figure 2.5. For example, contact printing methods, [see gray zone of figure 2.5], imply greater disregard for material and present limitations in terms of the resolution of printed materials, for example, screen printing consists of a flat system constructed of a "woven mesh" that requires direct contact with the substrate in order to deposit the material. However, the printing mechanism requires deep cleaning to avoid contamination between different deposits and the width of the lines cannot be less than 30 µm [26]. In this method there may be waste of material, since the control in the deposit depends on the viscosity of the material and there is no control in the fall of the drop, potentially altering the outline of the printed pattern [101]. On the contrary, non-contact printing techniques [see green area in figure 2.5], since there is only contact between the deposited material and the substrate, there is the advantage of presenting less contamination or even eliminating waste, reducing the risk of damaging the substrate and alignment of printed patterns are more precise and uniform, allowing for the deposition of multiple layers [26, 102]. For example, the mechanism of an inkjet printing system contains a head that allows the drop to be ejected continuously, however, there is the disadvantage that the deposited material clogs the head due to its chemical and physical properties [71]. In the following section, some characteristics that favor this deposit method will be described.

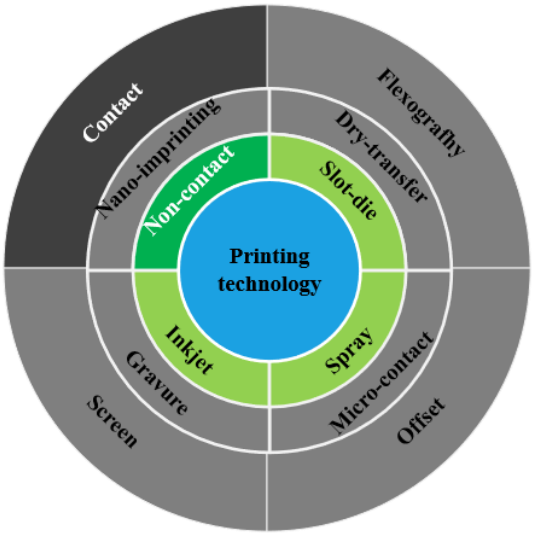

Figure 2.5. Classification of printed techniques by the contact methods (gray zone) and non-contact methods (green zone) [99, 103].

Printing technology offers several advantages, for example, in the printing mechanisms of printing technology, the applicable printable materials can present advantages in their use by requiring low drying temperatures, good electrical properties which can show high resolution in the pattern printed. In addition, printing systems offer the possibility of carrying out rapid printing processes, using masks or not, and using large surface substrates [103, 104].

2.6 Characteristics of inkjet printing technology.

Among all the aforementioned techniques, inkjet printing is one of the simplest methods for achieving material functionalization on flexible substrates. One of the main advantages of this technique is its ability to produce uniform structures or films with thicknesses and dimensions lower than 100 nm. Also, as a non-contact techniques, it minimizes the contamination by impurities and facilitates the fabrication of stacked structures [18].

This process enables to wide-scale deployment print of any shape or pattern, whose composition can be changed by simply modifying the drawing in the printing system software. This technique is well-suited for a wide range of production scales, including prototyping and large-scale industrial production [105]. It is also a relatively eco-friendly processing tool that causes few materials wastes since it can be easily implemented for the quick deposition of inks (in picoliters) without requiring the use of great quantity of corrosive chemicals [106].

Conventionally, sophisticated inkjet printing equipment has other qualities such as controllable drop, also called drop on demand (DoD) or continuous ink injection (CIJ). Microdroplet formation occurs either through piezoelectric systems that creates mechanical compression through a nozzle, or by heating the ink to increase its volume and pressure [99]. In the first mode, DoD, the printers are characterized by high precision in the placement of ink drops, efficient control, and no waste of ink due to temperature control during operation [107]. In the DoD printer, an electrical current is passed through a small heater that heats the liquid above its boiling point. The rapid expansion and collapse of the droplets generates a pressure pulse. In the second mode, CIJ, as its name indicates, the flow is continuous due to the vibration of a piezoelectric actuator, which makes the deposition less controllable and gives rise to a waste of the materials [55].

The DoD and CIJ modes are more conventional and have more accessible equipment such as commercial printers for daily use. However, the material deposited cannot be controlled, but the printed patterns could be obtained with a notable reduction of production costs.

Figure 2.6 depicts the inkjet printing process. To implement this technology, an inkjet printer is required, which can be a common office printer. The ink can be integrated into printer cartridges, and a polymer or paper can be the substrates.

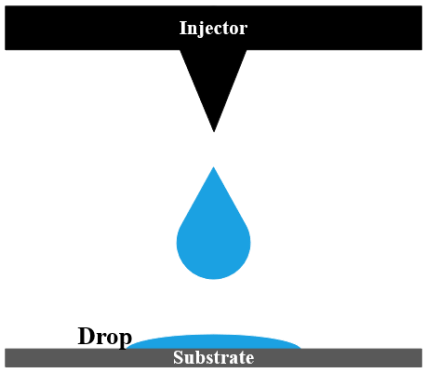

Figure 2.6. Representation of the inkjet printing process. Modified from reference [108].

Although commercial printers facilitate fast and low-cost production, there are limitations such as making the nozzles capable of expelling ink with volumes of several picoliters, as would occur in material printers or that do not include a mechanism to precisely control the position of the nozzles [101]. These limitations can be addressed by improving the physical and chemical properties of inks through their preparation, which provides moisture to allow flow during printing [103]. An approach of this type aims is to optimize printing patterns and at the same time improve rheological conditions depending on the viscosity and surface tension of the ink [109].

Chapter 3
Synthesis methods of metal nanoparticles

The technology of nanoparticle synthesis includes two general approaches that describe the obtaining of nanoparticles, known as constructive or destructive methods, which involves various biological, physical, and chemical processes. The construction method, also called bottom-up, involves building a material from atoms to form clusters [110-112]. The bottom-up method is more versatile because nanoparticles are formed from more common substances that are easier to find or manipulate. The bottom-up method requires a suitable soluble source of metals, typically metal cations in the form of soluble salts, to which a reducing agent is added [113]. On the other hand, the destructive or top-down method involves the reduction or decomposition of bulk material into molecules, and subsequently into particles on a nanometric scale [110-112]. This method involves the mechanical grinding, cutting, and milling of bulk metals and requires a significant energy consumption to maintain high-pressure and high-temperature conditions during these synthesis processes [114, 115].
Different types of nanoparticles of can be synthesized from inorganic, organic, carbon based, or biological sources using a top-down or bottom-up approach. Biosynthesis involves the use of microorganisms such as bacteria, fungi, viruses, yeasts, and plant extracts [114-116]. Physical methods, generally used in the top-down approach, include mechanical pressure, thermal energy, electrical energy, or high-energy radiation to cause abrasion, melting, evaporation or condensation of the material in order to obtain nanoparticles [114, 116]. Chemical methods include chemical reduction processes using organic and inorganic reagents in a soluble system [116]. Within these methods, various synthesis routes are employed to obtain particles with specific properties, such as different forms of nanoparticles (nanocage, nanocrystals, nanobelt, nanofiber, nanoparticle, nanotube, nanorod, quantum dot, nanocomposites), classified according to their dimensions (0D, 1D, 2D and 3D), as well as characteristics such as size, morphology, and stabilization. Furthermore, Ealias *et al* [110] lists properties such as surface area, volume ratio, pore size, surface charge, surface charge density, crystalline and amorphous structures, reactivity, and sensitivity to environmental factors. These parameters influence the application of the nanoparticles. Figure 3.1 shows the synthesis methods and their corresponding properties.

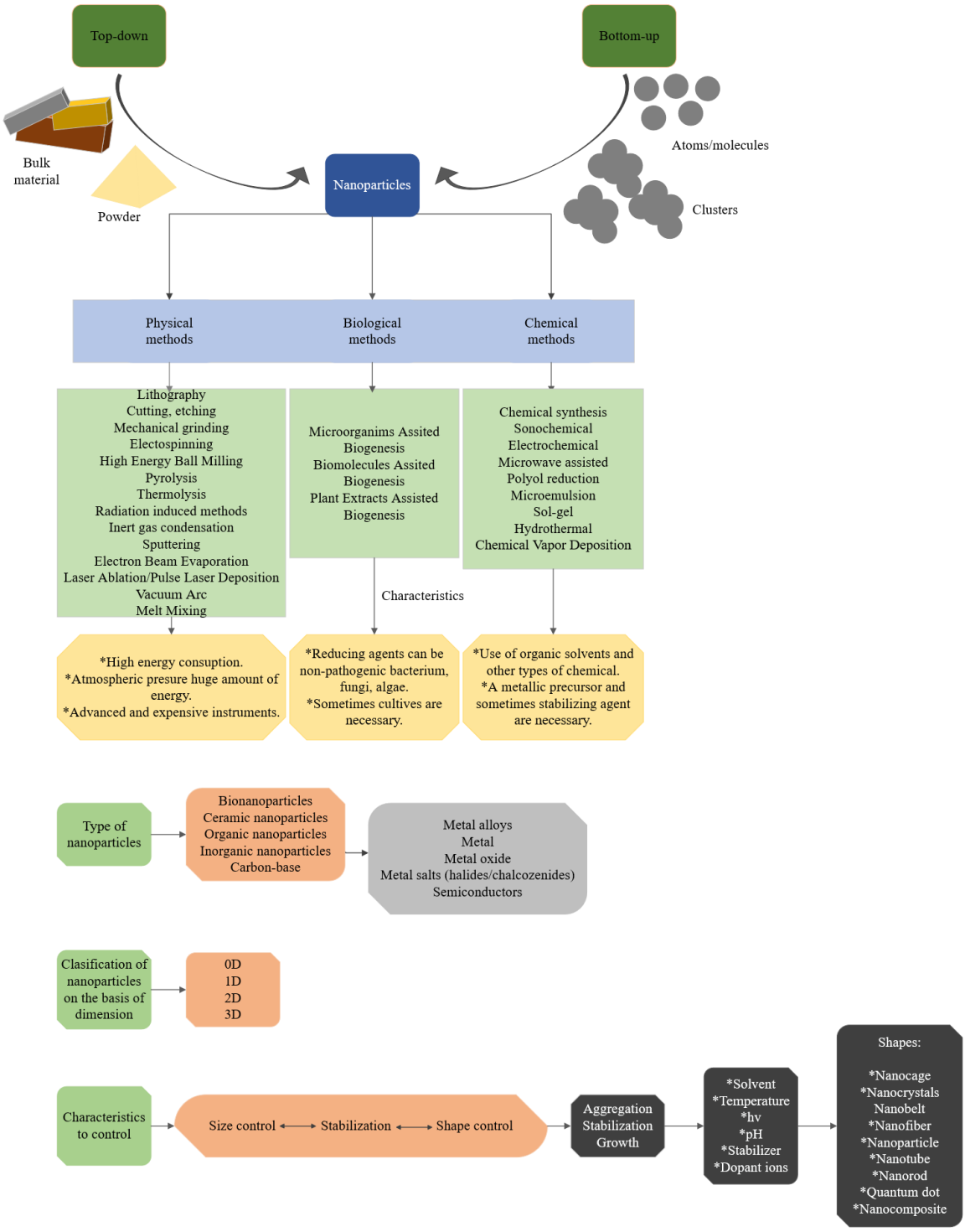

Figure 3.1. Nanoparticle synthesis approaches and their characteristics. Figure based from [61, 110, 111, 115, 116-120].

3.1 Synthesis of metallic nanoparticles

Metallic nanoparticles typically have diameters ranging from 1 to 100 nm. They offer the advantages of easy reproducibility, readily available chemicals, high efficiency, and economy. During their production process, they require a minimum number of reagents, and it is possible to control the shape and size of the particle, and prevent agglomeration through factors such as temperature, concentration of the reagents, and the selected synthesis method. However, it is possible that the particles may exhibit instability and impurities. Optimal conditions can minimize residues and improve stability [121, 122].

The chemical reduction method is the easiest, most affordable, and fastest route to obtain nanoparticles. In general, there are two stages involved: nucleation and growth, which occur during the phases of metal (M°) incorporation and aggregation [118, 123, 124]. The LaMer mechanism proposes an 'instantaneous nucleation' and simultaneous growth of colloidal particles and nanoparticles simultaneously [125]. During the kinetics, there is a competition between nucleation, growth, and aggregation [126]. The LaMer mechanism consists of three stages [124, 125, 127]:

Stage I: Formation of soluble monomer and accumulation in solution.

Stage II: Nucleation begins in the solution when the concentration of the soluble monomer reaches a higher level (saturation concentration). Each nuclei (seeds) formed then undergoes a burst nucleation, partially relieving the supersaturation or monomers formed.

Stage III: Growth by diffusion begins when the supersaturation concentration is decreased to a lower level (minimum supersaturation).

The formation of nuclei depends on the medium's temperature, the reducing capability of the reagent and the metal's affinity to be reduced. High temperatures can lead to undesired products, while even low temperatures can result in the formation of non-spherical nanoparticles, affecting the control of the size [61].

The synthesis of metal nanoparticles in solution is carried out using a metal precursor, reducing agent, and stabilizing agent. The reaction time, temperature, reducing agent, protective agent, and precursor agent determine size control, which is crucial as it influences the physicochemical properties of the particles, such as optical, electronic, chemical, and magnetic properties [118, 128, 129].

A more comprehensive synthesis process is shown in figure 3.2. In this process, a chemical reduction effect occurs due to charge transfer, where the precursor metal is in ionic form (M^+) and interacts with an electron donor, reducing the metal, reaching a zero-oxidation state (M^0), initiating the nucleation and subsequently growth. Once growth is completed, the particles can be suspended in a liquid medium to prevent oxidation and organic additives (stabilizing

agents) can be added to avoid agglomerations. The following section describes the general aspects of the chemical reduction process.

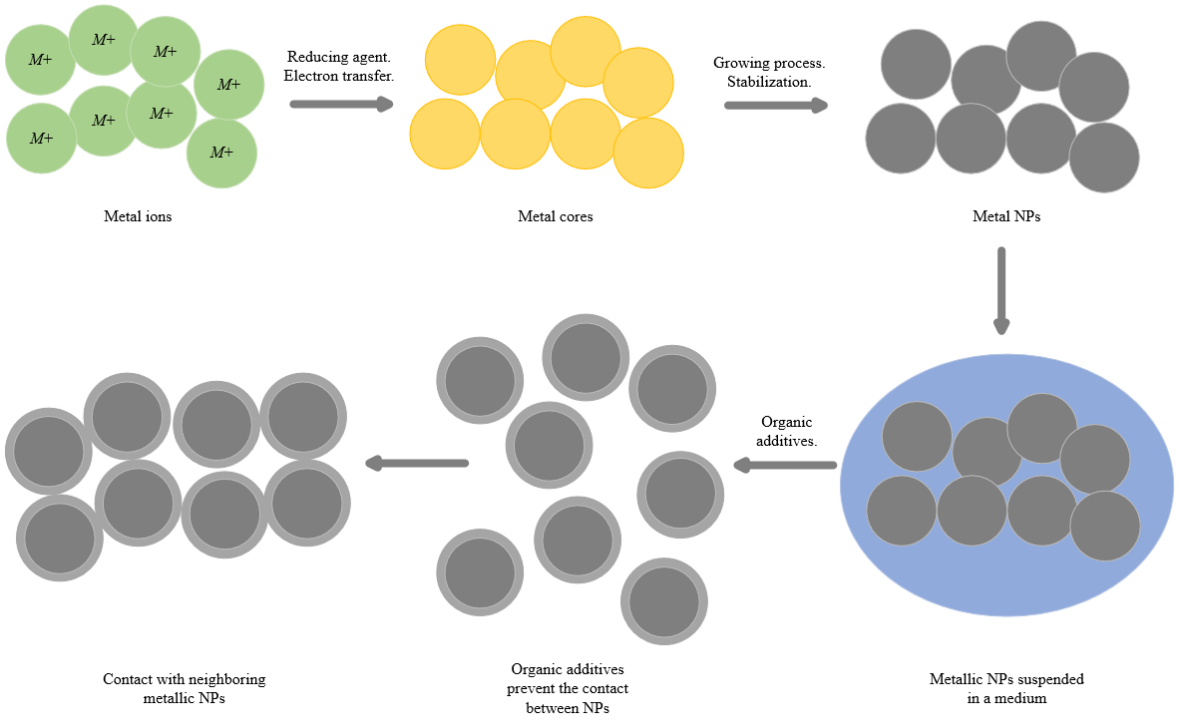

Figure 3.2. General steps for the formation of metal nanoparticles.

3.2 Synthesis of silver nanoparticles by the chemical reduction method

The chemical reduction method involves the reduction of a noble metal ion (M^+) to elemental metal nanoparticles through electron transfer. A metal precursor can be dissolved in either aqueous or organic solvents. If the metal precursor is particularly sensitive to oxidation, such as Cu and Al dispersing it in an organic solvent is preferred [114, 130]. The use of a metal precursor such as metal oxides, chlorides or nitrates provides a better stability. The use of $AgNO_3$ is advantageous because silver resists oxidation, and the precursor can be dissolved in water, making it cheaper compared to gold precursors.

During the formation of silver nanoparticles using the chemical reduction method, parameters such as particle size and aggregation state are influenced by initial $AgNO_3$ concentration, reducing agent, and stabilizer concentrations [131]. The one-pot method reduction of AgNPs using different reducing agents such as $C_6H_5Na_3O_7$ and $NaBH_4$ is applied for the reduction of silver ions (Ag^+) in both aqueous and non-aqueous solutions (see Fig. 3) [114].

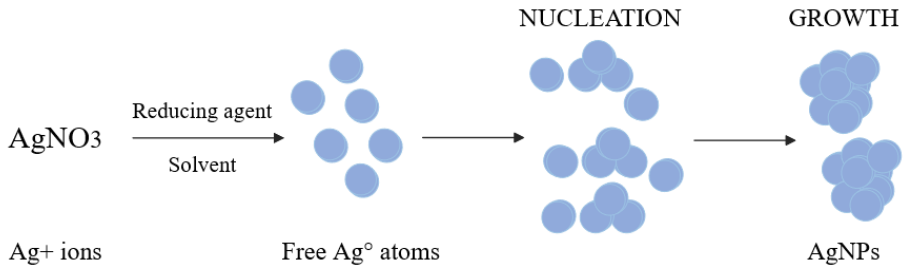

Figure 3.3. Mechanism formation of AgNPs from the reduction of Ag^+ [131].

With the use of $C_6H_5Na_3O_7$ and $NaBH_4$ the Turkevich or Lee-Meisel method and Creighton method, respectively, are commonly reported [118, 123, 132]. The reduction of $C_6H_5Na_3O_7$ is reported as the Turkevich method for the synthesis of gold nanoparticles. By the same route, to obtain AgNPs, the method is renamed as the Lee-Meisel method and is carried out under reflux involving the $AgNO_3$ solution as the precursor agent, with citrate implemented simultaneously acting as the reducing and protective agent. A boiling method is required with the temperature at 100 °C. Then, aliquots of samples are extracted and immediately cooled down to room temperature [133-136]. The diameter of synthesized aggregates of different shapes varied in the range of 60-200 nm with high polydispersity [137]. An optimal citrate concentration controls the size and shape of AgNPs using a [citrate]/[Ag^+] relationship [122]. However, the choice of concentration can influence the rate of nucleation, reduction and growth, as citrate may act more favorably as a stabilizing agent rather than as a reducing agent. To control this, it may be necessary to create unfavorable conditions, such as reducing the temperature (to room temperature or below), to achieve reduction of silver ions (Ag^+) [137]. Moreover, the Creighton method consists of the reduction of $AgNO_3$ with a cold solution of $NaBH_4$, ideally at 0 °C to stop the spontaneous reactivity produced by $NaBH_4$ when it interacts with Ag^+ [138]. Both techniques are cost-effective and do not require complicated equipment or manipulation.

The $NaBH_4$ has a higher reducing capacity than citrate, and under ideal reaction conditions, controlling the size, shape, and homogeneity of the particles can be controlled most precisely. Different authors report the silver nanoparticles with an average size of 10-80 nm [139, 140]. However, obtaining 60 nm silver particle size is better achieved with citrate as the reducing agent [140]. In [141], the authors report a gradual reduction process, accelerating the reduction of Ag^+ with the addition of $NaBH_4$ forming particles of 4 nm in size, then with citrate the growth of the particles and the reduction of Ag^+ is concluded. They also mention that heating the solution after the addition of citrate allows the growth of the particles to occur, obtaining particles of 100 nm in size. They mention that the precursor material ($AgNO_3$) is consumed in a period of 20 h. Therefore, with the use of two reducing agents, an external source is conventionally required as a sonochemical method to accelerate the reaction completion of all products [123]. The addition of different reducing reagents in the same reaction is known as the "seed-mediated growth" process [142, 143], which consists of the growth of seeds of a reduced size, for example 4 nm, grown through an initial reduction

and which continues and concludes with the addition of another reducing reagent. Figure 3.4 shows the order of addition for the growth of these seeds.

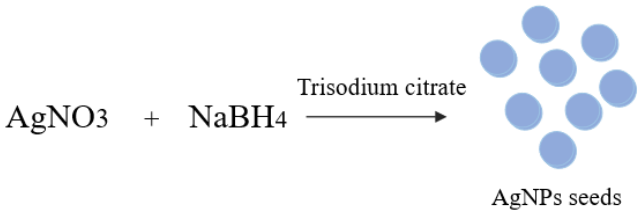

Figure 3.4. Formation of AgNPs seed from the addition of $NaBH_4$ and $C_6H_5Na_3O_7$.

3.3 Reagents properties and environmental impact

Silver nitrate is an inorganic silver salt with high solubility in water and stability at room temperature. Its structure corresponds to a triangular planar arrangement. It is commonly used as an astringent for antimicrobial and antibacterial purposes. Additionally, it has been used for a long time in the fabrication of photographic films and as a reagent for the visualizing of proteins in gels [144-146].

Sodium borohydride is a white solid known as a reducing agent commonly used in organic chemistry and pharmaceuticals synthesis. $NaBH_4$ converts aldehydes and ketones into alcohols. It is also used as a precursor material to produce other borohydrides and implemented as a hydrogen fuel cell generator in hydrogen storage applications. During its decomposition (hydrolysis) when reacting with water, sodium metaborate ($NaBO_2$) is generated, which is nonpolluting and nontoxic, and can be recycled to produce $NaBH_4$ again [147-150].

Trisodium citrate is a salt of citric acid. It is a white crystalline powder, soluble in water and insoluble in alcohol. It is stable at room temperature and its decomposition will occur at its the melting point. Because trisodium citrate has three carboxyl groups, these can be protonated/deprotonated, leading to an acid-base buffer. It exists as a metabolite in many plants and animals. Its extraction involves the microbial fermentation process. Citric acid and its salts, such as trisodium citrate, are recognized as safe for use in foods. It is commonly used as a flavoring or preservative in the food industry, in the manufacture of detergents products, or as an anticoagulant due to its alkalinizing capacity in the field of medicine [151, 152].

3.4 Methodology

3.4.1 Chemical reduction of silver nitrate

In section 3.2, the reaction conditions for obtaining AgNPs with sizes less than 100 nm were mentioned. However, it is mentioned that, mainly, the particle size can vary according to the concentration of the reagents added and the completion of the reactions, it can vary according to the reaction time. Next, in order to find the optimization of the growth of AgNPs, three experimental stages are described. The first consists of the use of $NaBH_4$ and $C_6H_5Na_3O_7$ (both reducing agents) when they react separately with $AgNO_3$ (precursor reagent) to evaluate their reducing capacity under the established experimental conditions mentioned below. In the second experimental stage of this thesis, $NaBH_4$ and $C_6H_5Na_3O_7$ are used from the "seed-mediated growth" process. Finally, the third experimental stage consists of varying the concentration of $AgNO_3$, keeping the concentrations of $NaBH_4$ and $C_6H_5Na_3O_7$ fixed under the same "seed-mediated growth" process.

3.4.1.1 First experimental stage

To carry out the first reaction:

A solution of 0.05 M $C_6H_5Na_3O_7$ (99.0% Sigma-Aldrich) dissolved in tridistilled water is prepared. In an ice bath, place a flask with 25 mL of tridistilled water, add a 0.05 M $C_6H_5Na_3O_7$ solution and then add the $AgNO_3$ solution drop by drop. Then it is left to react for 30 minutes. Figure 3.5 schematizes the order in the addition of the reagents. To identify this sample in the discussion of the results, the sample obtained has been named RA1.

Reaction 1: Mix of $AgNO_3$ and $C_6H_5Na_3O_7$.

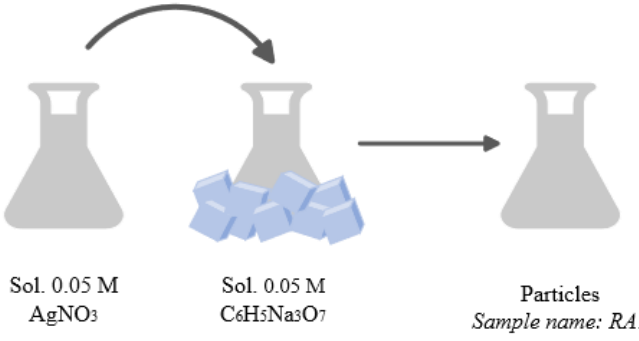

Figure 3.5. Reaction and order of addition of reagents to obtain the first reference sample.

The reaction proposed in this method is described in eq. 3.1:

$12AgNO_3 + 4C_6H_5Na_3O_7 + 6H_2O \rightarrow 12Ag° + 12NaNO_3 + 4C_6H_8O_7 + 3O_2$ (Eq. 3.1)

To carry out the second reaction:

A solution of 0.05 M $NaBH_4$ (99.0% Sigma-Aldrich) dissolved in tridistilled water is prepared. In an ice bath, place a flask with 25 mL of tridistilled water, add a 0.05 M $AgNO_3$ solution (99.0% Sigma-Aldrich) and then add a $NaBH_4$ solution drop by drop. After the addition of the reagents, a reaction time of 30 minutes is established. Figure 3.6 schematizes the order in the addition of the reagents. To identify this sample, it has been named RA2.

Reaction 2: Mix of $AgNO_3$ and $NaBH_4$.

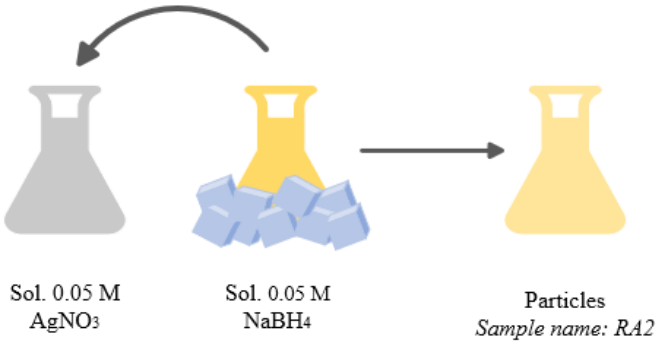

Figure 3.6. Reaction and order of addition of reagents to obtain the second reference sample.

The reaction proposed in this method is described in eq. 3.2:

$AgNO_3 + NaBH_4 \rightarrow Ag° + NaNO_3 + ½ B_2H_6 + ½ H_2$ (Eq. 3.2)

3.4.1.2 Second experimental stage

The second experimental stage consisted in the variation of the $C_6H_5Na_3O_7$ concentrations to find the particles with better stability, size, and other properties such as structural, morphological and optical absorbance characteristics. During this step, a mixture of reagents is used as a matrix, this mixture is composed of 0.05 M $AgNO_3$ and 0.05 M $NaBH_4$. To carry out the reactions, $C_6H_5Na_3O_7$ is first added different concentrations (from 0.01 M to 0.04 M with a variation 0.01M). A flask containing 25 mL of tridistilled water is placed in an ice bath, then a solution of $C_6H_5Na_3O_7$ is added. Subsequently, the $AgNO_3$ solution is added drop by drop, followed by the $NaBH_4$ solution, also added drop by drop. A total of four reactions are carried out. Each one is left to react for 30 minutes. It should be noted that the concentrations of $AgNO_3$ and $NaBH_4$ do not vary in any of the reactions. Figure 3.7 shows

the order of addition of each reagent and the names of the samples with which it will later be identified.

Reaction 1 to 4: Mix of the matrix reagents $AgNO_3$ and $NaBH_4$ with $C_6H_5Na_3O_7$ at four different concentrations.

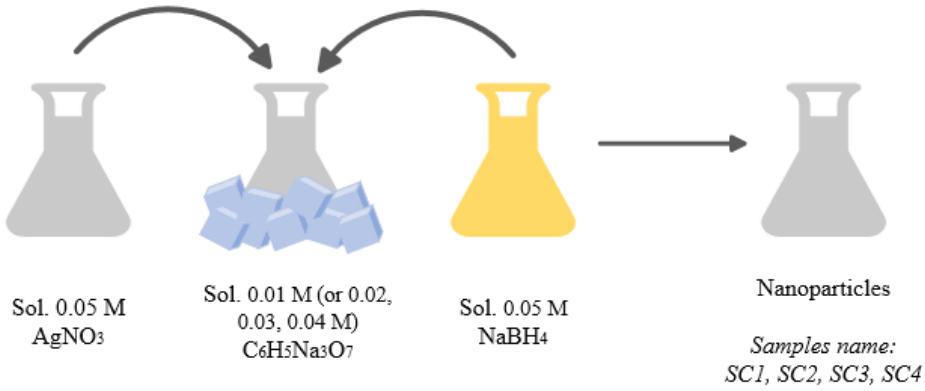

Figure 3.7. Reactions and order of addition of reagents to obtain the four samples with sodium citrate at different concentrations.

3.4.1.3 Third experimental stage

The third experimental stage consists in varying the concentrations of $AgNO_3$, which are 0.05, 0.10 and 0.15 M, in order to find the particles that could exhibit conductive properties. A total of three reactions were carried out, where in each of them the concentrations of 0.03 M $C_6H_5Na_3O_7$ and 0.05 M $NaBH_4$ were kept fixed. The reactions were out under the conditions described in the second experimental stage. To identify each of the samples obtained in each reaction with respect to the variation in the concentration of $AgNO_3$, they were named as SN1 (for 0.05 M), SN2 (for 0.10 M) and SN3 (for 0.15 M). Figure 3.8 shows the order of addition of each reagent. In this step, the formation of a sediment is observed, which, for each sample, was obtained through a centrifugation process at 1000 rpm for 30 min to measure the electrical properties of the synthesized particles.

Reaction 1 to 3: Mix of the matrix reagents $C_6H_5Na_3O_7$ and $NaBH_4$ with $AgNO_3$ at three different concentrations.

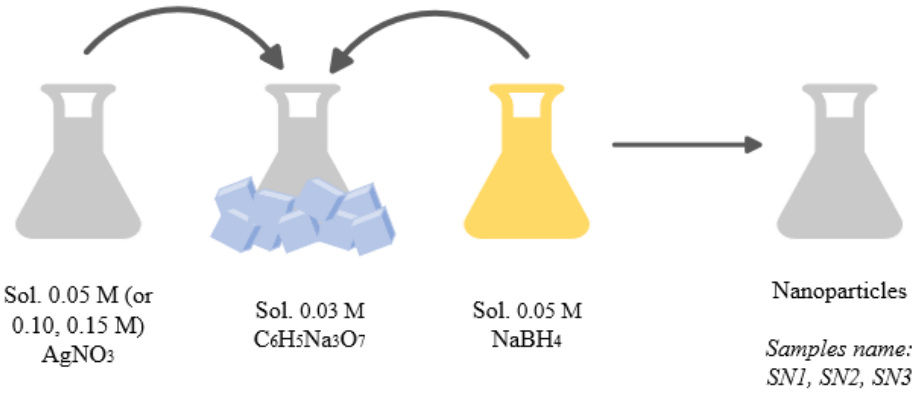

Figure 3.8. Reactions and order of addition of reagents to obtain the three samples with silver nitrate at different concentrations.

In table 3.1 are listed the concentrations of the reagents used in each sample obtained.

Table 3.1. Sample preparation at different concentrations.

Experiments	**Sample**	**[$AgNO_3$] M**	**[$C_6H_5Na_3O_7$] M**	**[$NaBH_4$] M**
First stage	RA1	0.05	0.05	---
	RA2	0.05	---	0.05
Second stage	SC1	0.05	0.01	0.05
	SC2	0.05	0.02	0.05
	SC3	0.05	0.03	0.05
	SC4	0.05	0.04	0.05
Third stage	SN1	0.05	0.03	0.05
	SN2	0.10	0.03	0.05
	SN3	0.15	0.03	0.05

3.4.2 Characterizations

For XRD, SEM and EDS characterization, the different obtained samples are deposited on a silicon wafer (100) and dried at 60 °C for 30 minutes. To carry out the characterizations using DLS techniques and UV-Vis spectroscopy, the AgNPs samples are diluted in water in at ratio of 10:1 (water:AgNPs). The crystalline structures of the nanoparticles were determined using a Discover 4 hours of sweep; with a Tescan Vega3 LMH (SEM) with SE detector, images of the morphologies of the samples were obtained. Diameter sizes, polydispersity indices (PDI) and zeta potentials were measured using a Zetasizer Nano-ZS90 equipment. Finally, electrical characterization was performed using a Keithley-4200 Semiconductor Characterization System at room temperature.

3.5 Results and discussion

In this section the results obtained in the three experimental stages described in sections 3.4.1.1 to 3.4.1.3 will be presented. In the first, two reference samples were obtained by taking the reaction between $AgNO_3$+$C_6H_5Na_3O_7$ and $AgNO_3$+$NaBH_4$ to evaluate the reductive potential of each of the reducing agents ($C_6H_5Na_3O_7$ and $NaBH_4$). In the second experimental stage, four reactions were obtained from $AgNO_3$ and $NaBH_4$ with fixed contractions and $C_6H_5Na_3O_7$ was added at four different concentrations. In the third experimental stage, three samples were obtained where $C_6H_5Na_3O_7$ and $NaBH_4$ were added at fixed concentrations and three different concentrations of $AgNO_3$ were added. This section will show the results obtained through Dynamic Light Scterring (DLS) techniques, Scanning Electron Microscopy (SEM), UV-Vis spectroscopy, X-Ray Diffraction (XRD), and Energy Dispersive X-ray Spectroscopy (EDS). In addition, the electrical behavior of the samples are shown through I-V measurements.

3.5.1 Dynamic Light Scattering (DLS) and Zeta Potential Analysis

Using the DLS technique, the size of the nanoparticles can be determined; the stability of the colloidal system can also be determined by determining the polydispersity index (PDI) and the zeta potential. The PDI is a parameter that describes the heterogeneity of a sample, which can be determined from the square of the standard deviation divided by the square of the average size, as is show in eq. 3 [153]:

$$PDI = \left(\frac{St.deviation}{Average\ size}\right)^2 \quad \text{(Eq. 3)}$$

The dispersity index is classified as low, moderate, or high. The PDI values less than 0.05 indicate monodisperse systems, while values greater than 0.70 indicate highly polydisperse system, in accordance with ISO standard 13321:1996 E and ISO 22412:2008 [154].

On the other hand, stability of the particles can be known through the zeta potential. This represents a balance between attractive van der Waals forces and electrical repulsion resulting from the net surface charge [155]. Nanoparticles system with zeta potentials greater than +30 mV or less than -30 mV are considered as stable colloidal suspension systems [155, 156].

The nanoparticles obtained in the first experimental stage, whose samples were named as RA1 and RA2 (see table 3.X) sowed average sizes of 312.0 and 304.0 nm, respectively. The sample named RA1 exhibits a PDI of 0.378, indicating moderate polydispersity. In contrast, sample named RA2 has a PDI of 1.000, indicating high polydispersity. The higher PDI in sample RA2 compared to sample RA1 suggests that under the same reaction conditions, $C_6H_5Na_3O_7$ can also exhibits a reductive effect, leading to a better control of particle size due

to its lower reductive capacity [157]. Zeta potentials found describe negative values of -24.5 and -24.3 mV, respectively. These values are consistent with those reported in literature [158, 159]. Another action that borohydride and citrate have in the reduction reaction is that when they are in ionic form, the nanoparticles already formed can absorb these ions, forming a monolayer that provides them stability. Because the ionic character of these compounds is negative [158, 160], the zeta potential found in the measurement is also negative. Furthermore, it is observed that the particles do not exhibit favorable stability, as their zeta potential is equal to or less than -30 mV, which is the established parameter.

For the samples obtained in the second experimental stage (SC1, SC2, SC3 and SC4 samples), it was found that the particle sizes decrease in the following order SC2>SC1>SC4>SC3. Additionally, the PDI value indicates that sample SC1 exhibits greater polydispersity compared to the other samples. For sample SC2, less polydispersity and, consequently, better uniformity in size distribution could be expected. However, in terms of zeta potential, sample SC3 demonstrate better stability. Also, a sample with lower particle size is preferred for the expected application (see sections 1.3 and 1.4). Table 3.2 lists the properties found under this technique for each of the samples already mentioned. Compared with the samples obtained in the first experimental stage, the addition of the three reagents ($AgNO_3$, $C_6H_5Na_3O_7$ and $NaBH_4$) provides better stability in the system and, as a consequence, in the growth control of the nanoparticles. This process called "seed-mediated growth" and is described in section 3.2.

Finally, for the samples obtained in the third experimental stage (SN1, SN2 and SN3 samples), it is observed that sample SN1 has a lower particle size and PDI compared to the other samples (see table 3.2). The three samples fall within the moderate range in terms of polydispersity description [161], however, sample SN3 shows higher stability according to the zeta potential. For this experimental stage, this analysis does not provide a trend towards the improvement of the properties of the colloidal solutions with increasing concentration.

Table 3.2. Particle size, polydispersity index, and zeta potential values of samples obtained in the three different experimental stages.

Experiments	**Sample**	**Particle size (nm)**	**Polydispersity index (PDI)**	**Polydispersity range**	**Zeta potential (mV)**
First stage	RA1	312	0.378	Moderate	-24.5
	RA2	304	1.000	High	-24.3
Second stage	SC1	85	0.627	Moderate	-30.9
	SC2	106	0.437	Moderate	-30.9
	SC3	52	0.528	Moderate	-31.7
	SC4	70	0.580	Moderate	-31.1
Third stage	SN1	51.9	0.528	Moderate	-31.7
	SN2	70.8	0.690	Moderate	-31.2
	SN3	64.0	0.571	Moderate	-32.2

3.5.2 Scanning Electron Microscopy (SEM)

To analyze the surface of the samples, a Scanning Electron Microscopy (SEM) was used to obtain images at a scale of 1 µm. For all the samples the formation of spherical nanoparticles was confirmed (figure 3.8) [162, 163]. In each image, approximately one hundred particles were measured using ImageJ software to know the average diameter size and their distribution was calculated using the standard log-normal distribution [164-166]. The average diameter size calculated for all samples are listed in table 3.3.

According to the first proposed experimental stage, the reaction of citrate with $AgNO_3$ is slow with the established reaction conditions. The formation of the particles will then be limited by the effect of the reducing material during the reaction. In the images of sample RA1, the low population of particles is observed. From the histogram, an average size of 335 nm was found for this sample. In the image of sample RA2 the growth of particles of different sizes is observed due to the spontaneous reaction that occurred in the sample [167]. An average size of 285 nm was calculated from the histogram. The calculation of the standard deviation reveals that a lower value indicates that the data are closer to the mean, implying greater homogeneity in particles growth, while at a higher deviation would show that the particles are dispersed with wider ranges of different sizes [168-170]. The standard deviations are large for both samples, indicating heterogeneity in the growth of the particles, as observed in the images of both samples RA1 and RA2. The PDI corroborate the disproportionate growth.

For the samples obtained in the second experimental stage, visible changes in the increase of the nanoparticle population are observed in the SEM images. Similar effects due to the variability of $C_6H_5Na_3O_7$ concentration as a reducing agent have been reported [171, 172]. On the other hand, populations of agglomerated particles with a size of 61 to 98 nm are observed in the histograms. The order of particle growth is the same as that one observed through DLS: SC2>SC1>SC4>SC3 (see section 3.5.1), where sample SC3 has the smallest particle size. The particle sizes of the samples are determined by the initial stoichiometry of the reaction with respect to the citrate concentration, where at low concentrations the particle size increases [163]. Additionally, it was observed that with an increase in citrate concentration, the PDI calculated using the standard deviation shifted from large to moderate polydispersity ranges (see table 3.2).

The SEM images of the samples obtained in the third experimental stage show the increase in the particle population with the increase of $AgNO_3$ concentration. From the histograms, particle sizes ranging from 58 to 77 nm were found. Sample SN3 is the one with the smallest average size, Zhang *et al* [173] indicate that the initial concentration of the precursor ($AgNO_3$) gives balanced concentrations of Ag^+. With the added concentrations of 0.03 M $C_6H_5Na_3O_7$ and 0.05 M $NaBH_4$, the reaction medium showed better stoichiometry, which suggests that the reaction maintains a thermodynamic and kinetic balance, allowing in turn the control of particle growth. On the other hand, as described in the DLS data (see section

3.1), sample SN2 exhibits the largest particle size (70.8 nm from DLS data). However, regarding the polydispersity index, all three samples fall within the moderate range.

Table 3.3. Average diameter size, standard error, and polydispersity index obtained from histograms of samples obtained in the three experimental stages.

Experiments	Sample	Average diameter size	PDI	Polydispersity range
First	RA1	335 ± 140	0.420	Moderate
stage	RA2	285 ± 80	0.280	Moderate
	SC1	85 ± 11	0.129	Moderate
Second	SC2	98 ± 19	0.200	Moderate
stage	SC3	61 ± 9	0.149	Moderate
	SC4	66 ± 12.199	0.185	Moderate
Third	SN1	61 ± 9.135	0.144	Moderate
stage	SN2	77 ± 12.461	0.162	Moderate
	SN3	58 ± 9.871	0.170	Moderate

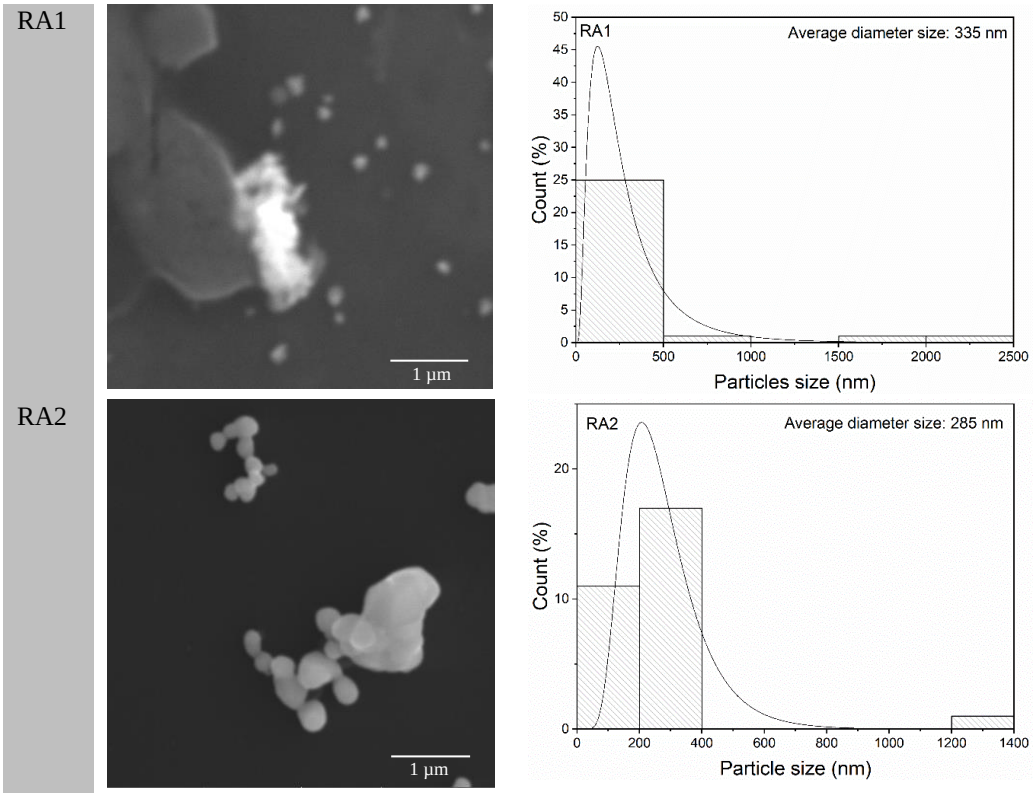

SC1

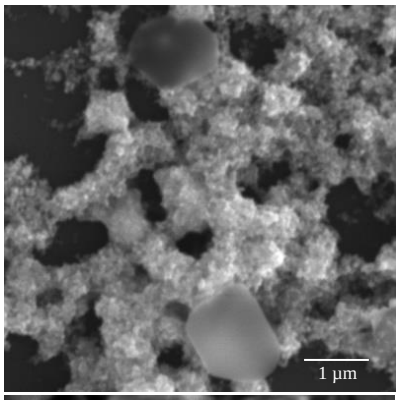

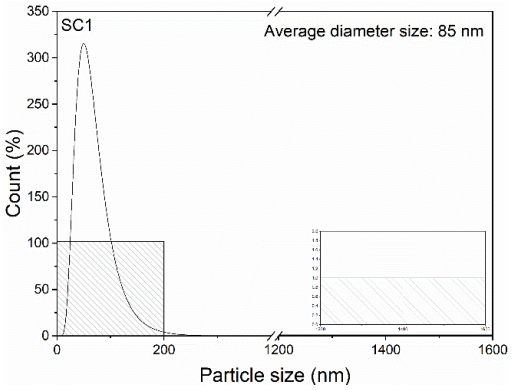

SC2

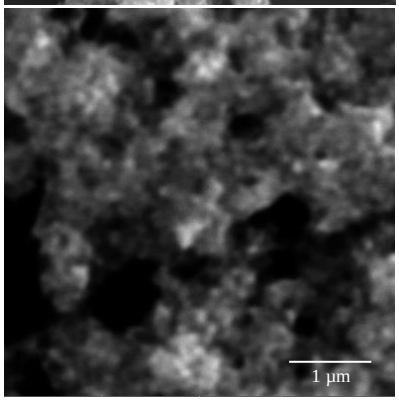

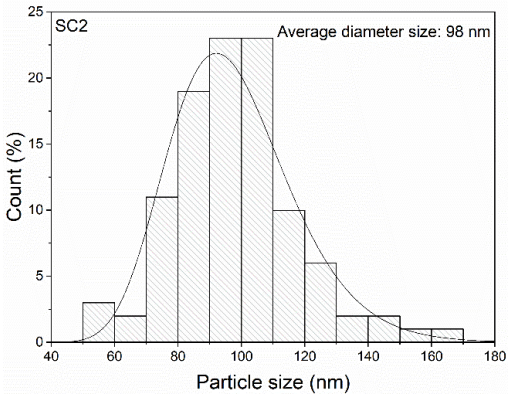

SC3

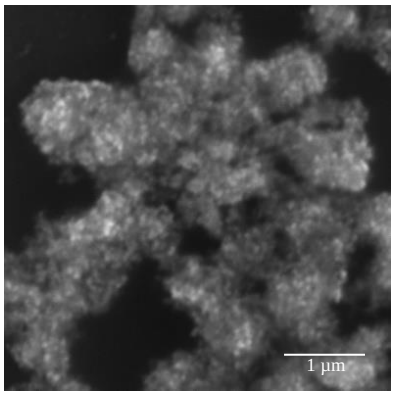

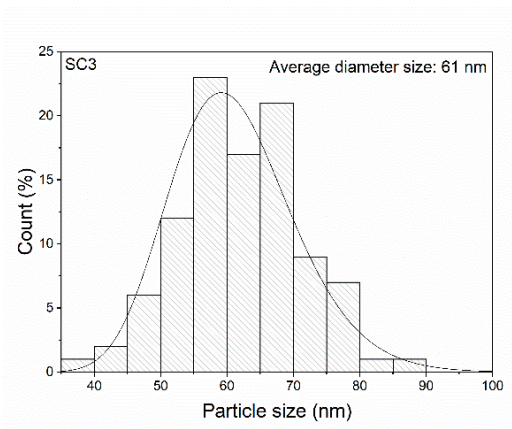

SC4

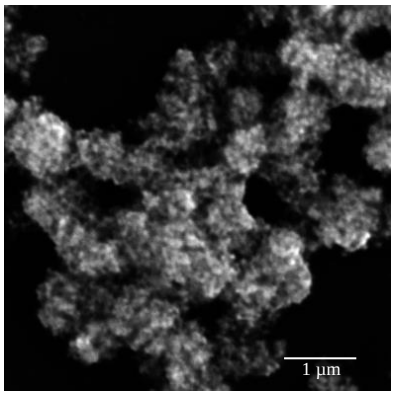

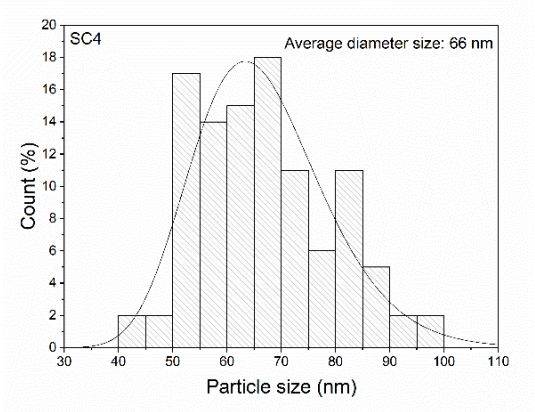

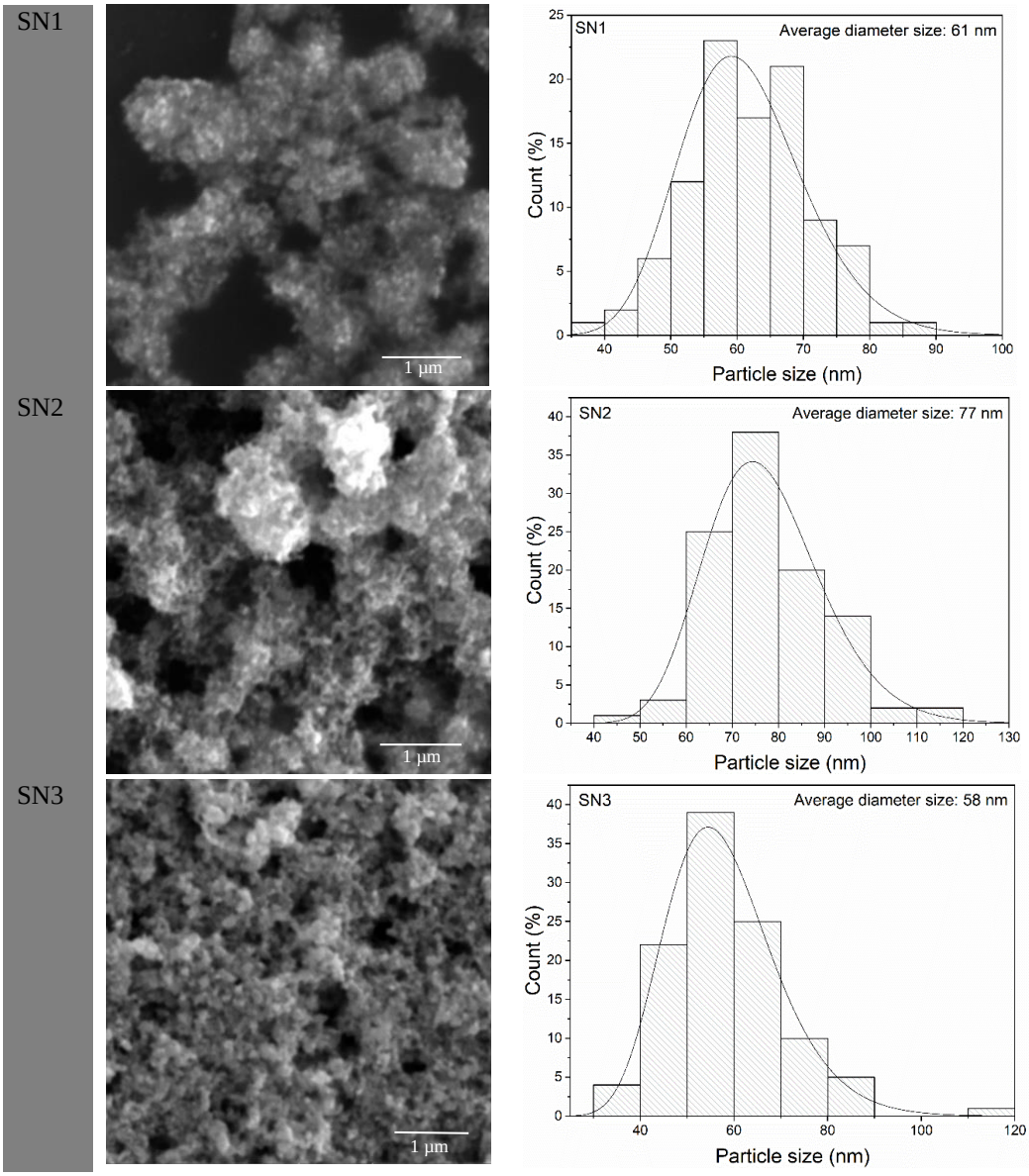

Figure 3.9. SEM images of AgNPs obtained from the three experimental stages.

3.5.3 UV-Vis spectroscopy

The optical absorbance of the samples was measured by UV-Vis spectroscopy. In the absorbance curves of the samples obtained (RA1 and RA2) in the first experimental stage, a low absorption is observed and the elevation of the baseline proportional to the maximum absorbance is presented in the samples [see figure 3.10(a)]. According to the analyzes observed in sections 3.5.2, a reduced particle population was observed for both samples, however, sample RA1 showed a limited particle population. On the other hand, for sample RA2 a disproportionate growth occurs due to the spontaneous reaction that occurred in the

sample [167]. A low intensity curve indicates the decrease in nucleation [163], this demonstrates that the concentrations of the initial reactions (RA1: 0.05 M $AgNO_3$ and 0.05 M $C_6H_5Na_3O_7$; RA2: 0.05 M $AgNO_3$ and 0.05 M $NaBH_4$) are supersaturated and nucleation is not possible in a controlled manner. Furthermore, an increase in the baseline is observed in both measurements with the increase in wavelength range, caused by the agglomerated states of the particles [174, 175].

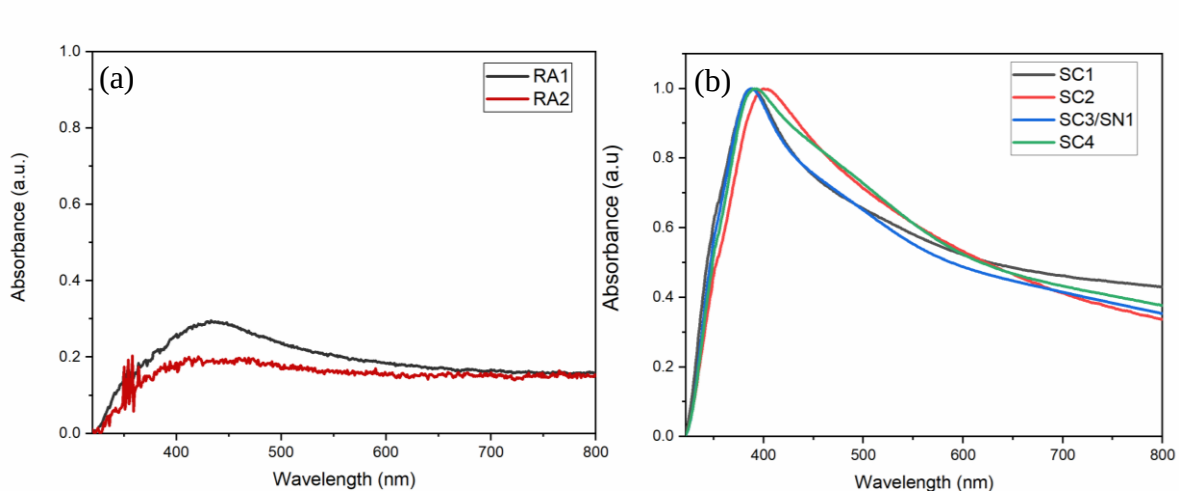

Figure 3.10. UV-Vis measurement of samples obtained in (a) first and (b) second experimental stages.

Conventionally, the particle size can be determined from the maximum absorbance found at a certain wavelength. Since the samples synthesized in this dissertation present agglomerations and polydispersity, (see sections 3.5.1 and 3.5.2), the samples do not have uniformity in the size distribution [176]. However, from the shift to a higher or lower wavelength, the increase or decrease in particle size can be observed by comparing the samples with each other. Regarding to the wavelengths where maximum absorbance is found, samples SC3 and SC4 are found at a similar wavelength close to blue indicating that these samples have lower particle sizes compared to samples SC1 and SC2 [see figure 3.10(b)]. According to McClary *et al* [163], the particle sizes are initially large at the lowest stoichiometries, these characteristic decreases as it reaches a concentration in kinetic and thermodynamic equilibrium. This is the case for samples SC3 and SC4, however, even though the maximum absorbance for these samples is very close to each other, the broadening of the absorption curve increases for sample SC4. This indicates a change in stability, being prone to forming greater coalescence effects between particles [163]. According to these analysis, sample SC3 has a smaller size and fewer agglomerated states. On the other hand, the absorbances show a greater elevation of the baseline at the longest wavelength with a red shift (in the range of 600 to 800 nm), indicating the presence of agglomeration in each sample. This confirms that this sample has a smaller particle size and fewer agglomeration,

suggesting that this synthesized sample has the greatest stability, as was observed in DLS (section 3.5.1) and SEM (section 3.5.2) analyses.

For the samples obtained in the third experimental phase [see figure 3.11], the maximums of the absorbance curves are found at wavelengths very close to each other, indicating that the samples have similar sizes or with non-significant variations. Also, it is observed that sample SN2 exhibits greater aggregation due of the baseline in the range of 600-800 nm. Regarding sample SN3, a lower baseline elevation is observed compared to samples SN1 and SN2, as well as a narrower bandwidth. Based on these characteristics, it is estimated that the sample synthesized with 0.15 M $AgNO_3$, 0.03 M $C_6H_5Na_3O_7$, and 0.05 M $NaBH_4$ would exhibit greater stability.

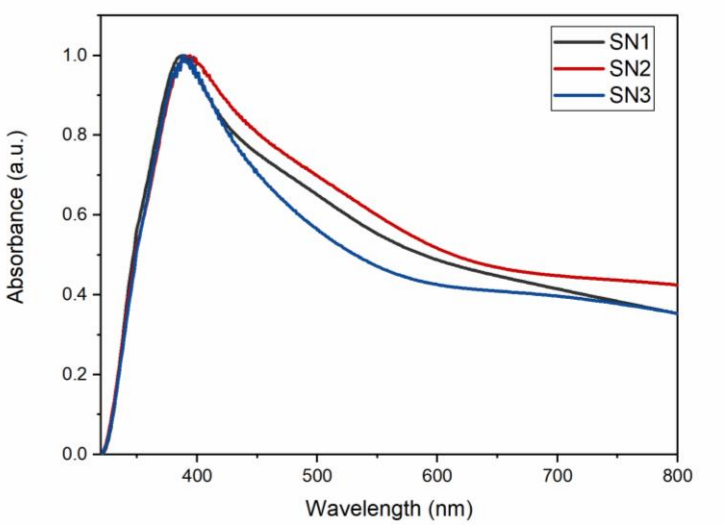

Figure 3.11. UV-Vis measurement of samples obtained in the third experimental stages.

3.5.4 Energy Dispersive X-ray Spectroscopy (EDS) measurements

The chemical composition of the synthetized samples was determined using Energy Dispersive X-ray Spectroscopy (EDS). To perform quantification, the surface of the samples was mapped in an area of 1 µm. The weight % (wt. %) and atomic % (at. %) of the elements found in each sample are listed in table 3.4, and the obtained spectra are show in figure 3.12

Table 3.4. Elemental quantification (wt. % and at. %).

Experiment	**RA1**				**RA2**			
First stage	*Element/ spectral line*	*wt. %*	*at. %*	*Abs. error %*	*Element/ spectral line*	*wt. %*	*at. %*	*Abs. error %*
	Ag	6.19	0.95	0.89	Ag	98.99	94.26	3.34
	N	6.92	8.14	3.43	N	---	---	---
	C	22.46	30.83	4.62	C	---	---	---
	O	44.22	45.58	6.81	O	0.63	4.06	0.79
	Na	20.22	14.50	1.00	Na	0.38	1.69	0.19
	SC1				**SC2**			
Second stage	*Element/ spectral line*	*wt. %*	*at. %*	*Abs. error %*	*Element/ spectral line*	*wt. %*	*at. %*	*Abs. error %*
	Ag	80.16	37.70	3.98	Ag	88.96	55.44	2.80
	N	1.18	4.26	2.24	N	---	---	---
	C	1.87	7.89	1.72	C	1.40	7.84	0.66
	O	13.57	43.04	6.04	O	6.70	28.14	2.07
	Na	3.22	7.12	0.69	Na	2.94	8.59	0.30
	SC3				**SC4**			
	Element/ spectral line	*wt. %*	*at. %*	*Abs. error %*	*Element/ spectral line*	*wt. %*	*at. %*	*Abs. error %*
	Ag	81.58	41.09	2.09	Ag	78.77	37.16	3.44
	N	0.16	0.63	0.34	N	---	---	---
	C	2.48	11.22	0.57	C	1.40	5.92	1.44
	O	9.46	32.14	1.68	O	13.45	42.77	5.15
	Na	6.32	14.93	0.36	Na	6.39	14.15	0.73
	SN1				**SN2**			
Third stage	*Element/spectral line*	*wt. %*	*at. %*	*Abs. error %*	*Element/spectral line*	*wt. %*	*at. %*	*Abs. error %*
	Ag	81.58	41.09	2.09	Ag	88.84	55.15	2.82
	N	0.16	0.63	0.34	N	0.35	1.68	0.38
	C	2.48	11.22	0.57	C	1.95	10.87	0.53
	O	9.46	32.14	1.68	O	5.10	21.37	1.27
	Na	6.32	14.93	0.36	Na	3.76	10.94	0.29
	SN3							
	Element/spectral line	*wt. %*	*at. %*	*Abs. error %*				
	Ag	88.81	55.49	3.24				
	N	1.05	5.05	0.76				
	C	1.31	7.36	0.60				
	O	4.85	20.42	1.71				
	Na	3.98	11.68	0.38				

On the other hand, figure 3.12 shows the spectra generated in the measurements of the samples. In the spectra, the peak at K_{α}=1.739 keV corresponds to the silicon substrate. The peak at $L_{\alpha 1}$=2.984 keV is corresponds to Ag, and for $L_{\beta 1}$=3.149 keV, the same element is found. The other satellite peaks (Lβ1) arise from the electron repulsion [177, 178].

RA1

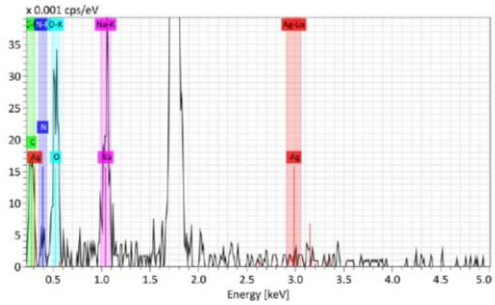

RA2

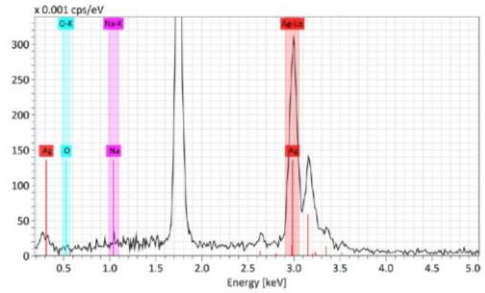

SC1

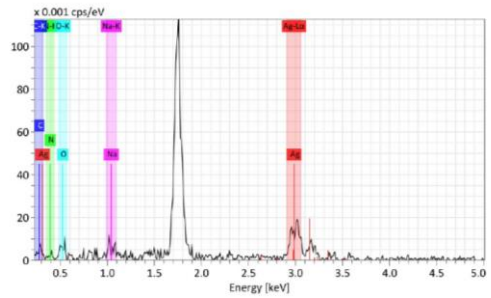

SC2

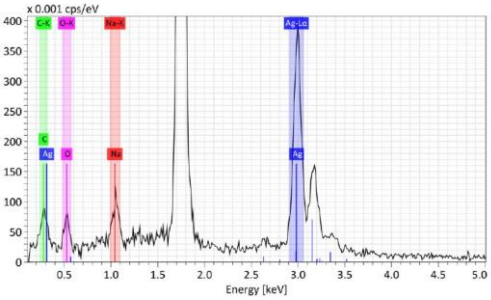

SC3

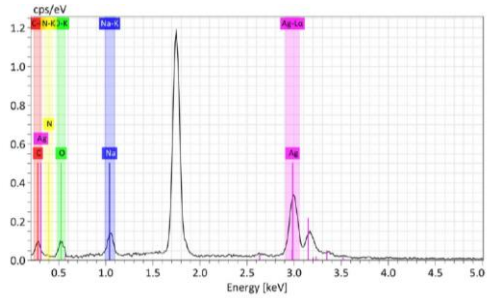

SC4

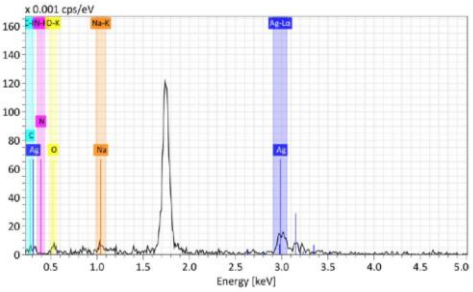

SN1

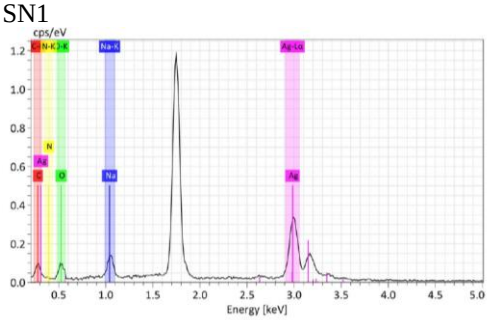

SN2

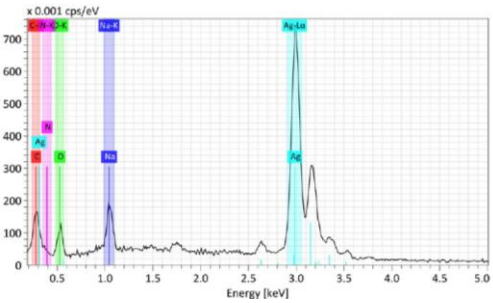

SN3

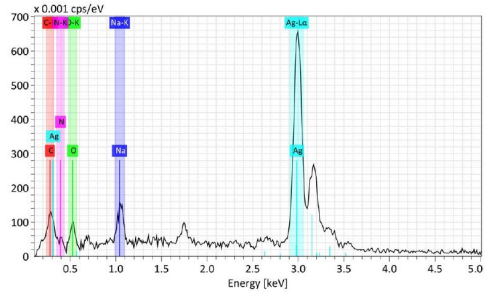

Figure 3.12. EDS spectra.

According to these results, for the samples obtained in the first experimental stage, the element silver was found for samples RA1 and RA2, however, the disproportion in the at. % for both samples is significantly different. In sample RA1, the low Ag content would indicate that the reaction cannot occur spontaneously. The reductive capacity of citrate would indicate that a medium of energy is needed to achieve the complete reaction between citrate and Ag with the integrated concentrations. As commonly mentioned in the literature, the reaction kinetics is accelerated when temperature (100 °C) is applied) to achieve the reduction of Ag^{+} ions [133-136]. On the other hand, for sample RA2, the quantification of Ag (94 at. %), Na and O are observed, and whose quantification is minimal and can be considered as elements of a residual compound present in the sample. The reduction in the high concentration of Ag indicates the high reductive potential of the sample; however, as observed in the SEM analysis (see section 3.5.2), the particles grew disproportionately, exceeding 100 nm in size. At the end of this section, the color maps corresponding to each elements found in each sample are shown (figure 3.13). For samples RA1 and RA2, the disproportion is observed in terms of the quantification of Ag and the presence of C, N, O and Na with higher concentration, which indicates that the citrate did not react.

Since, in this dissertation, the synthesis parameters were focused on ice baths (constant 0 °C for 30 minutes), as observed in section 3.4.1.2, the increase in the population of AgNPs when adding the two reagents $NaBH_4$ and $C_6H_5Na_3O_7$, allowed the reduction under cold bath conditions. In table 3.4, the presence of Ag greater than 37 at.% is observed for samples SC1, SC2, SC3 and SC4. This suggests that one of the reagents initiates the nucleation stage and the other controls the addition of particle growth [124]. In the elemental maps of figure 3.13, the presence of silver is observed with a greater population of AgNPs in samples SC2 and SC3. The high concentration of O (greater than 28 at.%) in all samples may be indicative of the presence of higher molecular weight compounds. Sample SC4 contains a higher concentration of this element (O 42.77 at.%), which indicates a greater amount of residual species. A solution of $C_6H_5Na_3O_7$ can form different citrate salts (H_3Cit, H_2Cit^{-}, $HCit^{2-}$, Cit^{3}, where Cit= $C_6H_5Na_3O_7$) [179], so it is possible that some ionic species of citrate are found in the systems.

For the samples of the third experimental stage, it was found that the quantifications of the element Ag in the samples (SN1, SN2 and SN3) compared to the samples of the second experimental stage do not increase with the increase in the concentration of $AgNO_3$. It is also observed that the quantification of O is reduced going below 20 at. %, being the SN3 sample with the highest content. However, the C and O content is lower for this sample (7 and 5 at.%, respectively), indicating that the presence of citrate ions and other compounds decreases for this sample. The stoichiometry in the reaction for this sample could provide more kinetic and thermodynamic stability so that the reaction can reach completion with the established experimental conditions [173]. Furthermore, the higher silver concentration suggests the increase in growth control, as shown in the DLS and SEM results.

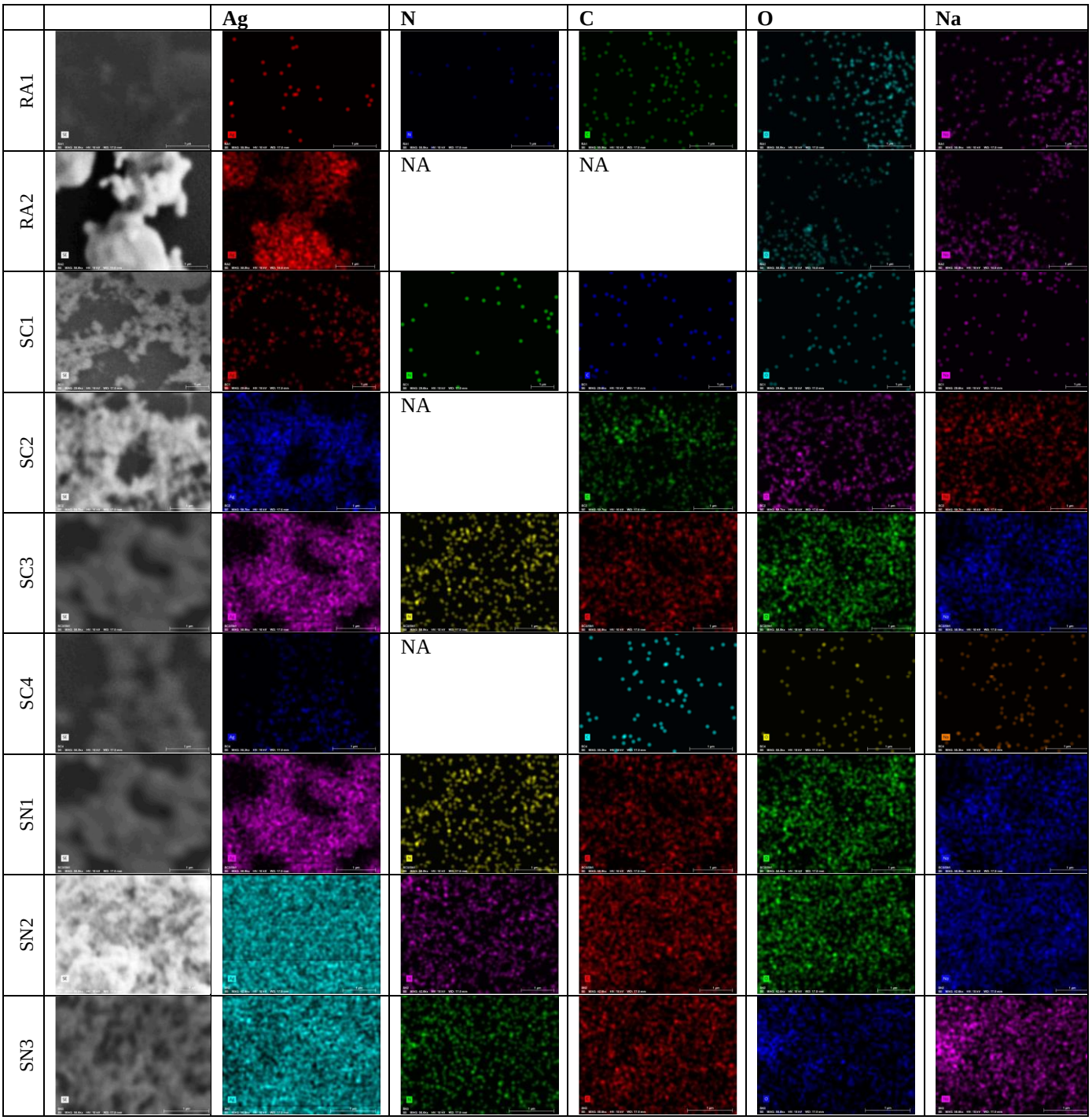

Figure 3.13. Elemental mapping of samples obtained in the three experimental stages.

3.5.5 X-Ray Diffraction (XRD) measurements

During the XRD measurement, experimental data was collected over the range from 10 to 50°, with a step size of 0.04 and corriment time of 14 s. The phase idenfication of the samples was determined by using the Powder Diffraction Files PDF from the PDF4 database format.

In the different samples, the phases were identified with the next PDF cards:

1. Ag: 00-004-0783
2. $C_6H_5Na_3O_7$: 01-088-6876
3. $NaNO_3$: 00-036-1474

In the analysis, no significant changes that modify the structure were observed, suggesting that the phases found correspond to the patterns obtained experimentally. Also, in figure 3.14, the patterns of the reagents used in the nanoparticle synthesis process are shown, which were also used as reference sources for phase identification.

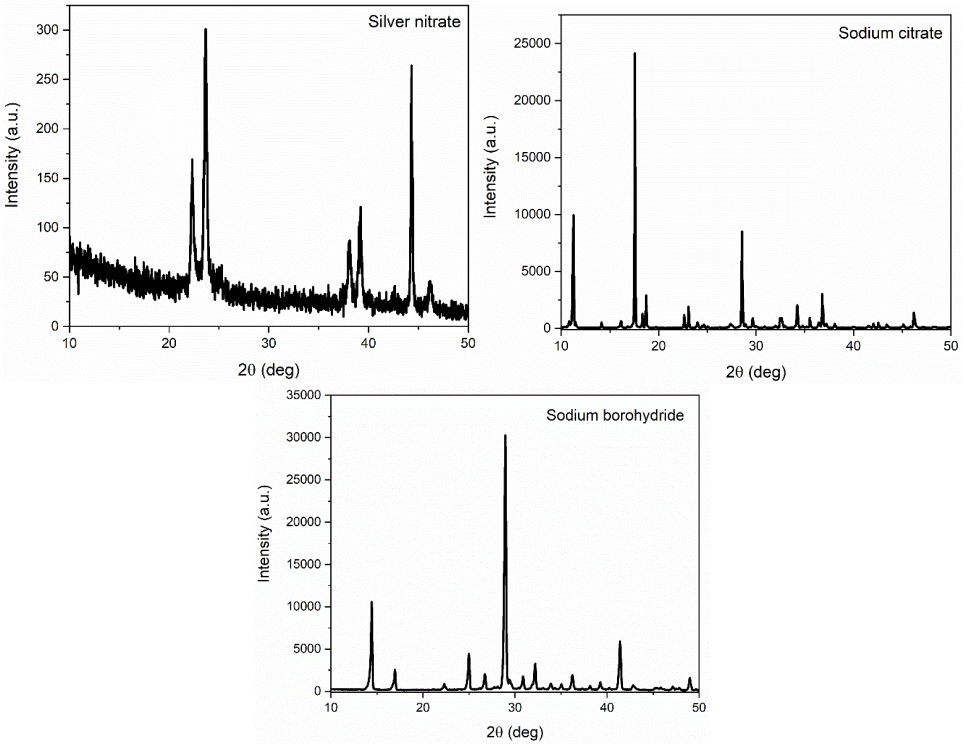

Figure 3.14. XRD patterns of reagents used during the different synthesis.

For the samples of the first experimental stage, in the measurement of sample RA1, Ag and $NaNO_3$ phases were identified (figure 3.15), however, the low concentration of silver show in the EDS spectra (see section 3.5.4) confirms that the sodium citrate is a weak reducing agent that limits the generation of seed nuclei [180, 181]. Also, the low number of counts for the silver phase indicates disorder in the crystalline arrangement. Additionally, the phase identification of the file $C_6H_5Na_3O_7$-01-088-6876 is observed in the pattern, along with a peak with high intensity at 10.46° (*), which is similarly identified in the reference pattern

of sodium citrate (figure 3.14). Also, according to the reaction of equation 3.1 (see section 3.1) it is expected to find the $NaNO_3$ phase. For sample RA2, all the peaks were identified with the Ag and $NaNO_3$ phases as described in the reaction of equation 3.2 (see section 3.1). In the figure 3.X, the particles show two peaks at 38° and 44 ° that correspond to the (111) and (200) face-centered cubic (fcc) crystalline planes [182]. A high intensity of the plane (111) suggests preferential growth of particles [183]. In both samples it is verified that the reduction reaction of the nanoparticles is determined by the reductive potential of the agents used.

For the samples of the second experimental stage, in the samples SC1, SC2, SC3 and SC4, the three phases were identified with the same PDF files for the four samples, suggesting that competition between reducing agents ($NaBH_4$ and $C_6H_5Na_3O_7$) does not cause structural changes during the reduction of Ag ions (figure 3.15). Likewise, as observed in the EDS analysis, the controlled growth of the particles is verified with the addition of the two reagents ($NaBH_4$ and $C_6H_5Na_3O_7$), showing that the intensity of the peak positions is significantly reduced in the number of counts for each sample compared to sample RA2. For all samples, a peak at 28.48° (*) was found, which was also observed in the pattern of sample RA1 (figure 3.15), suggesting the presence of another species originated from the dissolution between citrate and water (see section 3.5.4). These salts can form M-citrate complexes (where M is a metal) which in turn could dissociate, releasing M^+ ions, and these are rapidly reduced to the metallic state M^0 [184]. The reduction of silver ions is corroborated in both the diffraction patterns and the EDS spectra (see section 3.5.4).

For sample SC3, a greater intensity is observed for the $C_6H_5Na_3O_7$ phase planes compared to the other samples. This is an indication that the agents are reacting preferentially with respect to the stoichiometry for the added concentrations. Likewise, it is possible that in the reaction to obtain this sample involves the complexation of Ag^+ with citrate ions [163, 185]. Chadha *et al* [185] mention that the chemical balance of citrate ion concentrations and the influence of different citrate species in the reaction solution can decrease the rate of Ag^+ reduction. To determine the existence of other citrate species in the samples obtained, it is necessary to carry out different characterizations that provide compositional information. For this dissertation, this is proposed as future work.

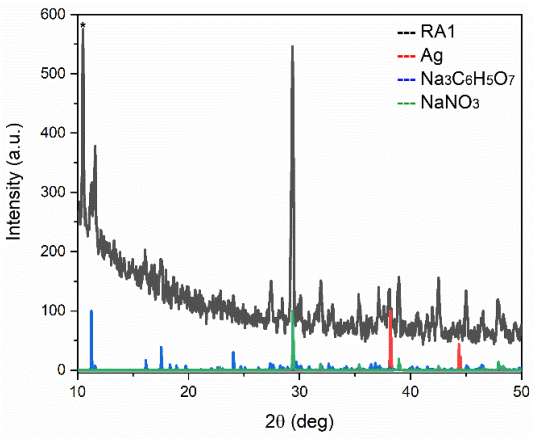
--- RA1
--- Ag
--- Na3C6H5O7
--- NaNO3
Intensity (a.u.)
2θ (deg)

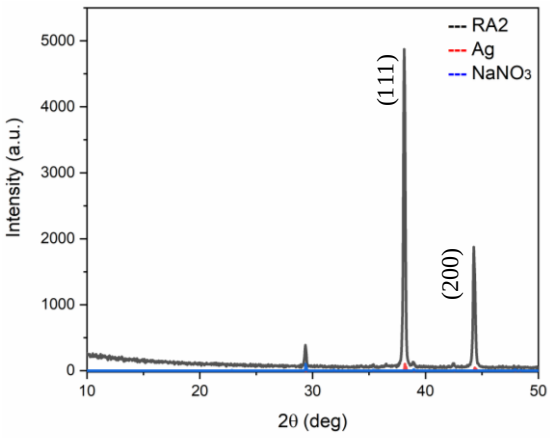
--- RA2
--- Ag
--- NaNO3
(111)
(200)
Intensity (a.u.)
2θ (deg)

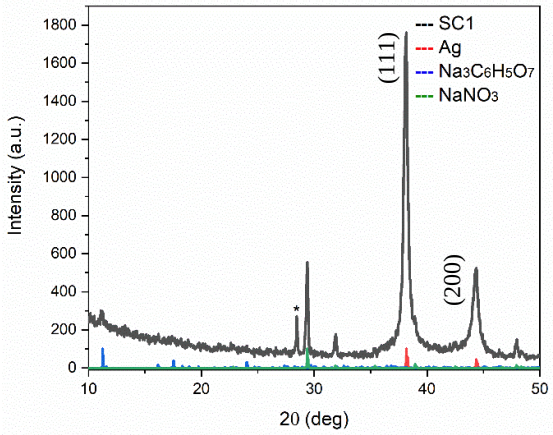
--- SC1
--- Ag
--- Na3C6H5O7
--- NaNO3
(111)
(200)
Intensity (a.u.)
2θ (deg)

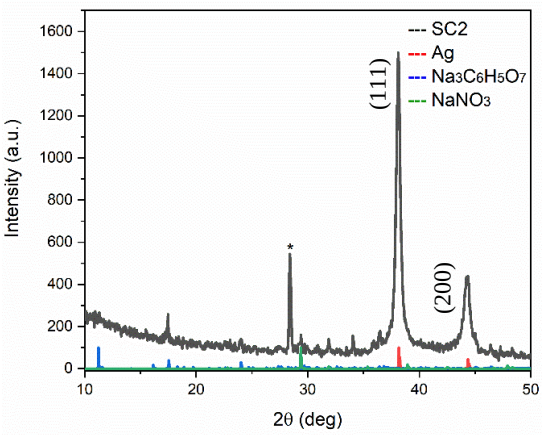
--- SC2
--- Ag
--- Na3C6H5O7
--- NaNO3
(111)
(200)
Intensity (a.u.)
2θ (deg)

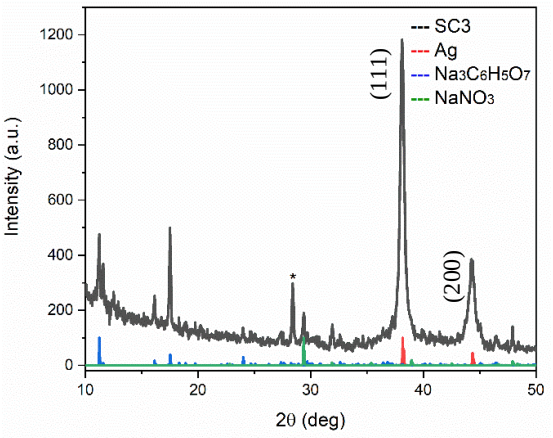
--- SC3
--- Ag
--- Na3C6H5O7
--- NaNO3
(111)
(200)
Intensity (a.u.)
2θ (deg)

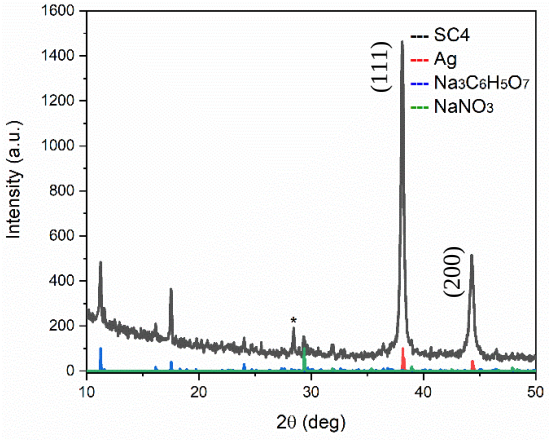
--- SC4
--- Ag
--- Na3C6H5O7
--- NaNO3
(111)
(200)
Intensity (a.u.)
2θ (deg)

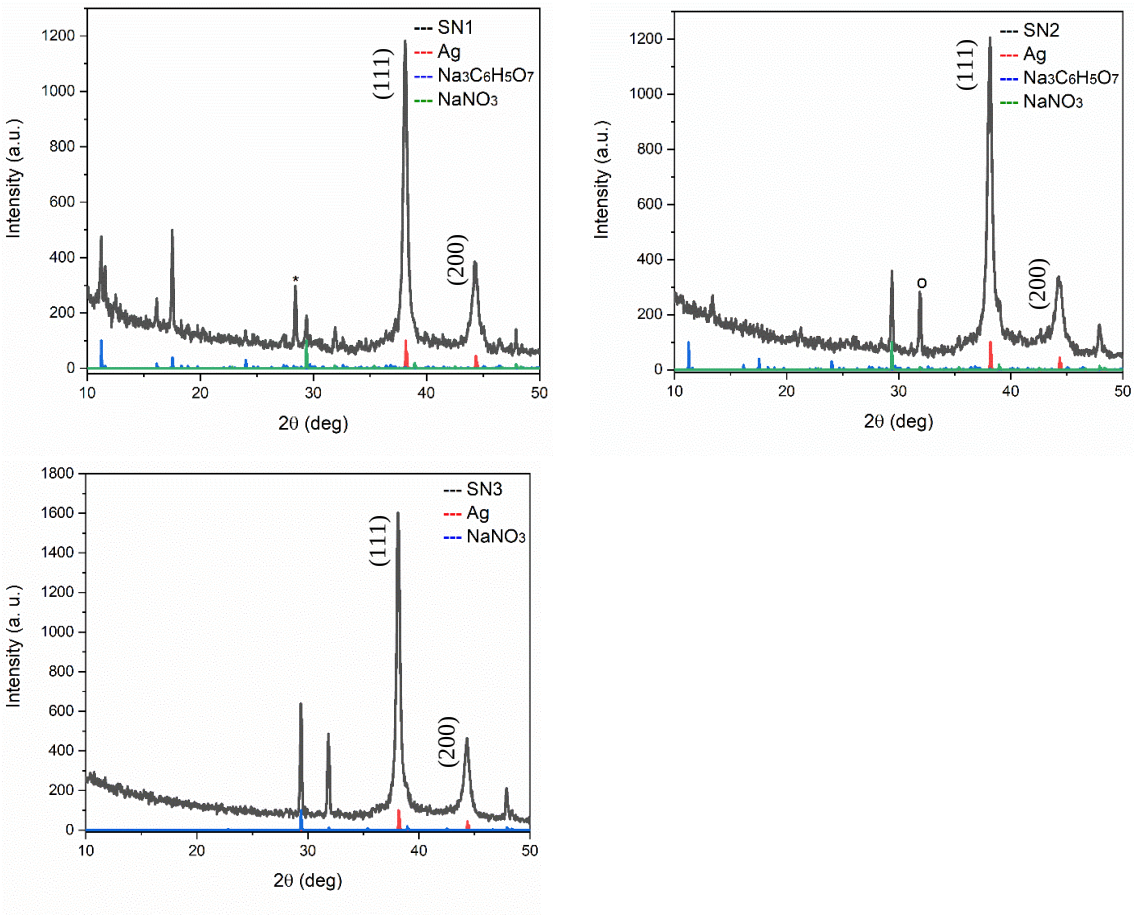

Figure 3.15. XRD patterns of samples obtained in the three experimental stages.

Figure 3.15 also shows the diffraction patterns of the samples obtained in the third experimental stage. According to the elemental quantification shown in section 3.5.4, the Ag concentration is proportional in the three samples (SN1, SN2 and SN3). However, the XRD analysis confirms that sample SN2 exhibits phases of $NaNO_3$ and $C_6H_5Na_3O_7$, indicating the continued favorable quantification of the elements C, O, and Na as also shown in sample SN1. In addition to this, in the pattern of sample SN2, a peak is identified at 29.40°, which is also identified in the reference pattern of sodium borohydride (see figure 3.14). This indicates that BH_4^- ions play a minor role in the reduction reaction under these experimental conditions. In sample SN3, $C_6H_5Na_3O_7$ was no longer found as the elemental quantification, as was shown for this sample, the balanced concentrations of Ag^+ depend on the initial concentration of the precursor material ($AgNO_3$) [173]. Moreover, in the SN3 sample, the system showed better stoichiometry which suggests that the reaction maintains a thermodynamic and kinetic equilibrium leading to the conclusion of the reaction.

3.5.6 Electrical characterization

Based on the DLS and SEM parameters found (see sections 3.5.1 and 3.5.2), it is estimated that concentrations of 0.05 M $AgNO_3$, 0.05 M $NaBH_4$, and 0.03 M $C_6H_5Na_3O_7$ offer better stability and balanced kinetics during particle nucleation and growth. Compared with all the samples, a minor increase in absorbance in the range of (600-800 nm) was noticed for sample SC3, indicating lower agglomeration of nanoparticles (see section 3.5.3). For this sample, under the reaction conditions and the molar ratio between $C_6H_5Na_3O_7$:$AgNO_3$ with the presence of $NaBH_4$, the Ag^+ can be rapidly reduced. To determine the resistance, an I-V measurement was realized to evaluate the electrical behavior of the sample. Figure 3.16 shows the experimental process for sample preparation and measurement. In the figure 3.16(a) shows the deposition of silver contacts (SPI-PAINT) with the help of a mask (see appendix A) on Corning glass used as a substrate, followed by the deposition of sample SC3. Figure 3.16(b) shows the drying of the sample at 60°C for 30 minutes. Finally, figure 3.16(c), the I-V measurement is schematized using two tips to determine the resistance of the samples.

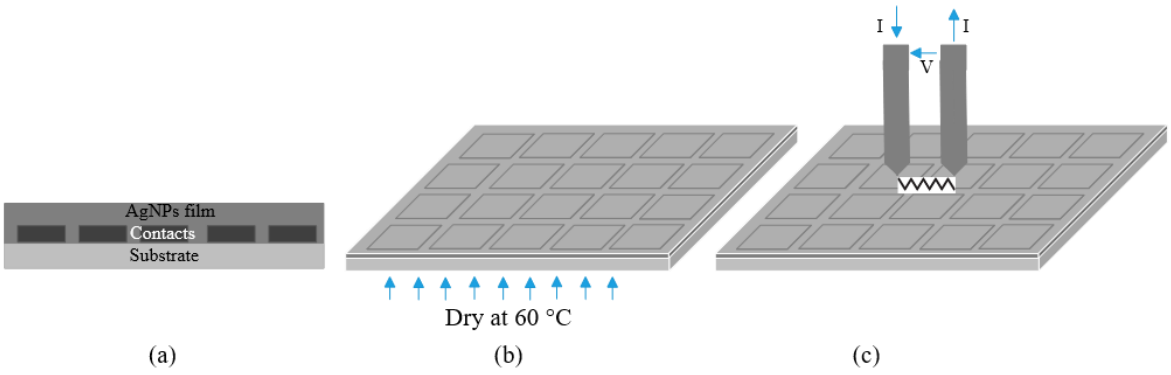

Figure 3.16. Schematic diagram of sample preparation for I-V characterization.

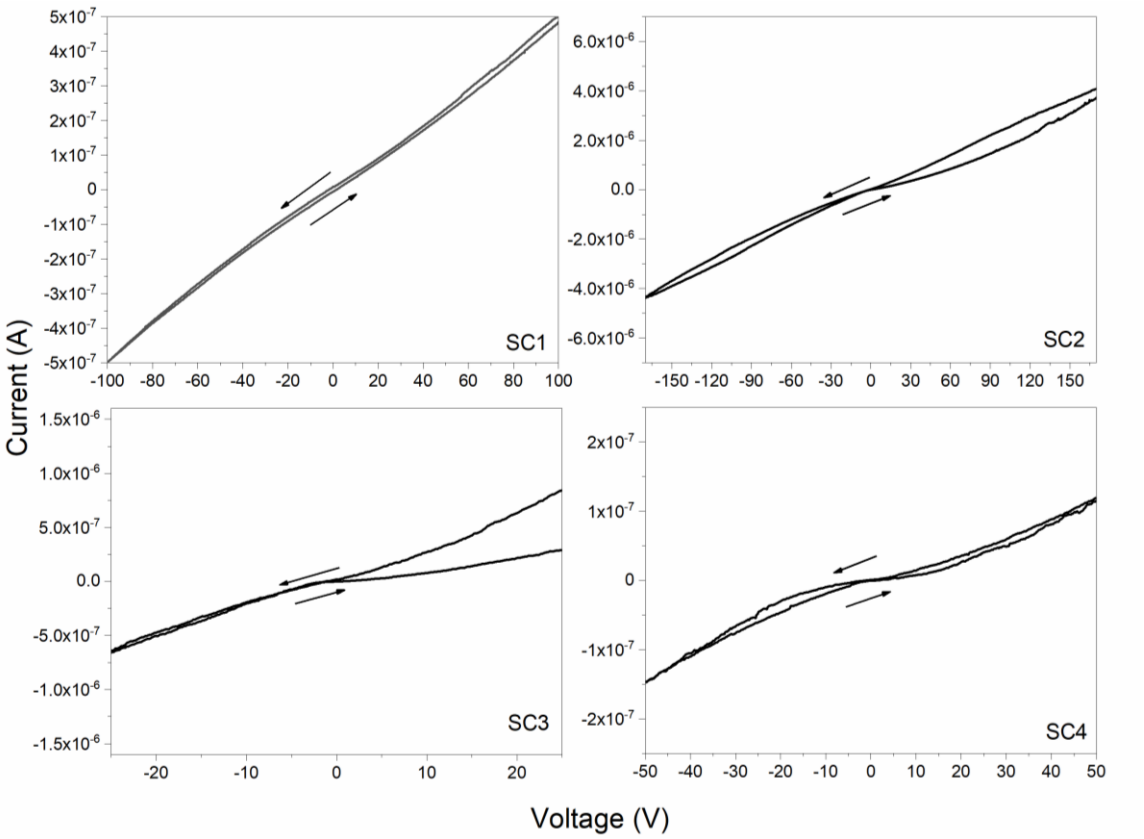

Figure 3.17. I-V curves of the samples obtained in second experimental stage deposited on corning glass.

Figure 3.17 shows the I-V curve measured for samples SC1, SC2, SC3 and SC4. The resistances calculated by Ohm's law are $2x10^8$ Ω, $4.2x10^7$ Ω, $2.9x10^7$ Ω and $2.2x10^8$ Ω, respectively. All the samples present high resistance, however, according to the experimental design for obtaining nanoparticles, the sample SC3 shows better properties and even lower resistance although it is not conductive. For this reason, it was chosen to increase the concentration of $AgNO_3$ and continue with the reaction conditions, as described in section 3.4.1.3, using 0.03 M $C_6H_5Na_3O_7$ and 0.05 M $NaBH_4$ as matrix, while varying $AgNO_3$ concentration to 0.05 M (sample SN1, previously SC3), 0.10 M (sample SN2), and 0.15 M (sample SN3).

Figure 3.18 shows the I-V forward and reverse sweeps performance of the three samples. It is observed that for sample SN1 and SN2, the I-V curves do not exhibit linearity, indicating that the samples do not have an ohmic behavior. Additionally, irregular, and unstable hysteresis is observed. In contrast, for sample SN3, the I-V curve exhibits linearity which demonstrated an ohmic behavior. The absence of hysteresis indicates electrical stability. This behavior is consistent with other reference [186]. Sample SN3 shows higher quality and a linear tendency while increasing the current with low applied voltage. Moreover, better symmetry of the curve is observed compared to the other samples. The resistance calculated

by Omh's law were 2.9x10^7 Ω, 7.71 x10^6 Ω and 5.78 Ω for samples SN1, SN2 and SN3, respectively.

Different studies report resistance values in the range of ~400 to 2000 Ω for AgNPs obtained by different synthesis methods using the same $AgNO_3$ concentration used to obtain our sample SN3 [186-189]. These results indicate that the SN3 sample is a good candidate for use as a conductive material to synthetize a conductive ink. As observed in the SEM images and as the DLS and UV-Vis results suggest the formation of the particles that could tend towards a connection between them in an orderly manner, which favors the electrical characteristics calculated for the SN3 sample.

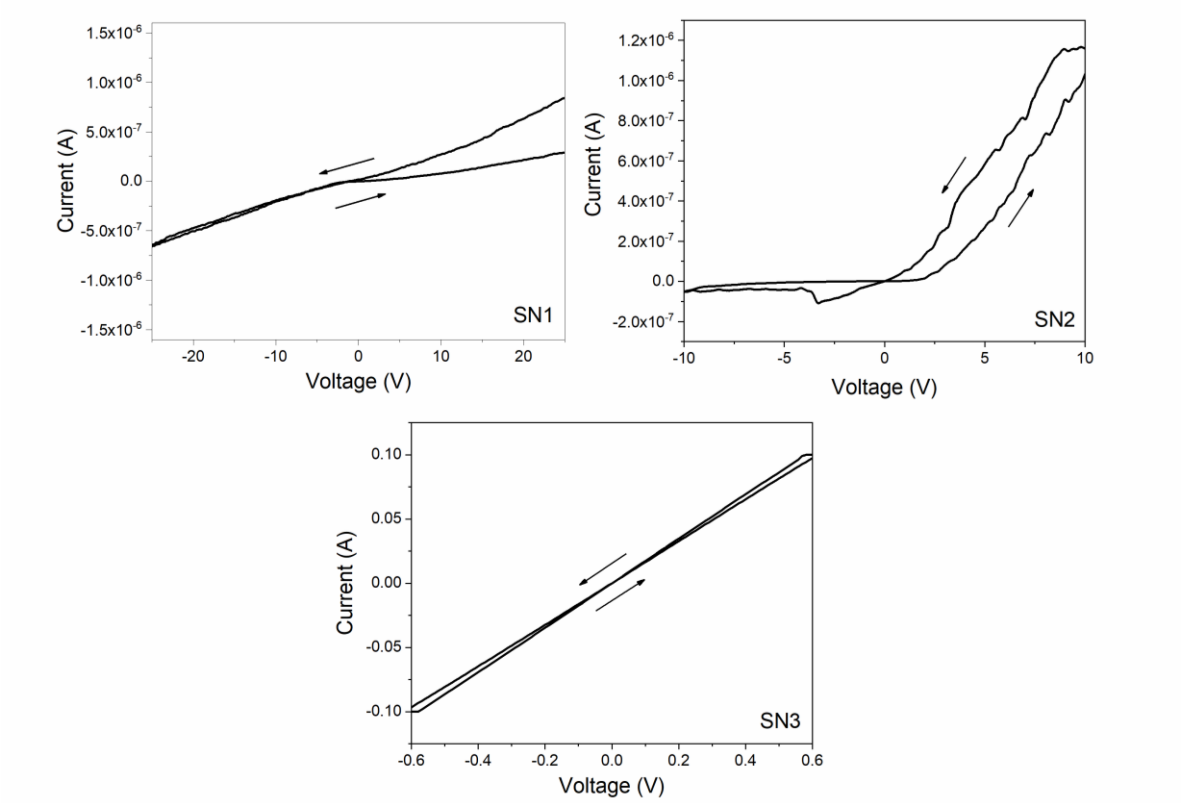

Figure 3.18. I-V curves of the samples SN1, SN2 and SN3 deposited on corning glass.

In other hand, to observe the behavior of the particles in the SN3 sample, they were deposited on acetate, bond paper, photographic paper, opaline paper, and PET substrates and dried at room temperature and 60 °C.

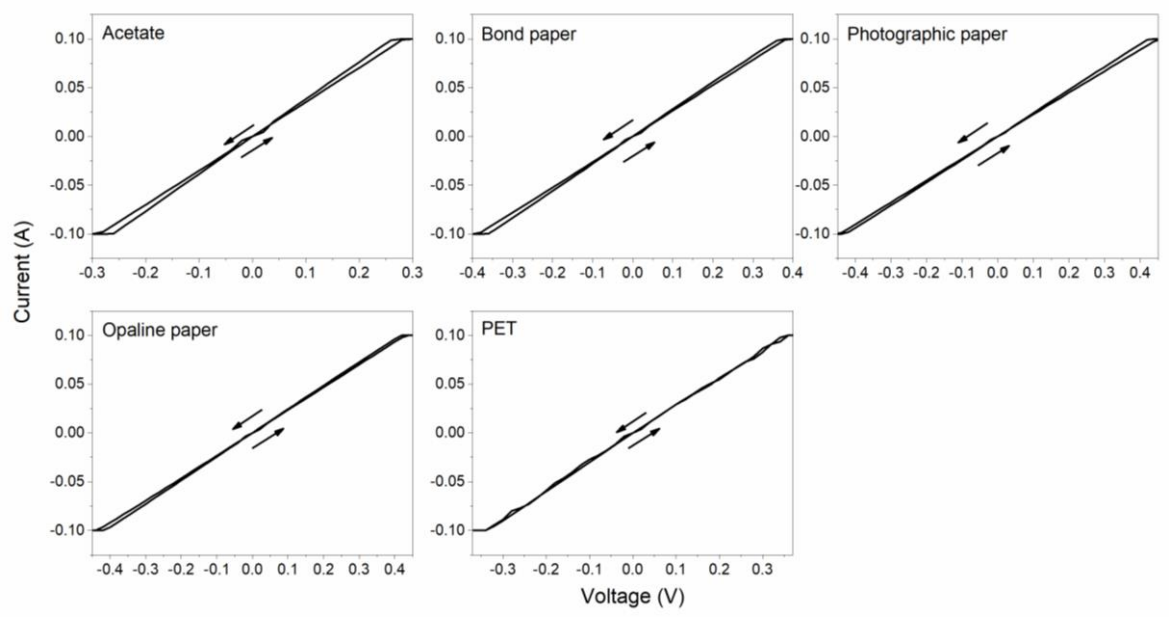

Figure 3.19. I-V curve of conductive AgNPs (sample SN3) deposited on different substrates dried at room temperature.

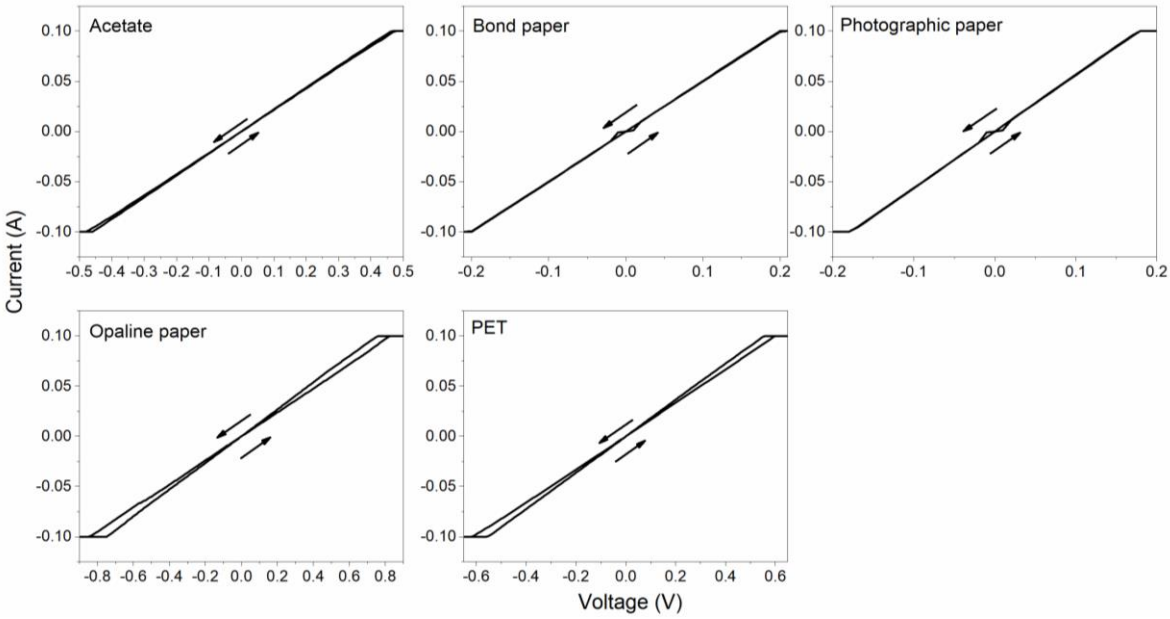

Figure 3.20. I-V curve of conductive AgNPs (sample SN3) on different substrates dried at 60 °C.

Figure 3.19 shows the I-V curves for the samples dried at room temperature, where it is observed that the applied voltages are low and remain similar among all the characterized substrates. Additionally, minimal hysteresis and low resistances are observed in all the samples. This indicates that despite the variability in the rheological properties of the implemented substrates, the nanoparticles of the SN3 sample demonstrate stability and

compatibility with both natural and synthetic polymeric substrates with minimal variability in the calculated resistances.

Table 3.5. Resistance of sample SN3 coated on different flexible substrates.

	Room temperature		**60 °C**	
Substrate	**Drying time of deposited nanoparticles**	**Resistance (Ω)**	**Drying time of deposited nanoparticles**	**Resistance (Ω)**
Acetate	2 hrs 30 min	2.86	5 min	4.74
Bond paper	20 min	3.80	5 min	2
Photographic paper	15 min	4.35	5 min	1.80
Opaline	25 min	4.00	5 min	4.74
PET	2 hrs	3.60	5 min	5.57

The table 3.5 lists the drying times and the resistances found for each sample. For the samples dried at room temperature, the drying time was variable. This variability can be attributed to differences in surface properties, which may arise from variation in cellulose content among different types of papers. Additionally, these samples may contain various types of load retention additives aimed at reducing surface roughness. The additives fill gaps between the paper fibers, facilitating homogeneous drying and preventing swelling or shrinkage of fibers, which could otherwise deform the paper structure and delay drying [51, 190]. Regarding the PET and acetate substrates (synthetic polymeric materials), they have low-energy surfaces, which hinder rapid adhesion and wetting due to their hydrophobic nature [191].

Regarding the samples dried at 60 °C a drying time of 5 min was applied (I-V curves of figure 3.20). It was observed that the use of temperature facilitates drying for PET and acetate substrates and does not significantly alter the resistance of the nanoparticles in all the substrates (see table 3.5). Ferreira-Oliveira *et al* [51] report a lower resistance value (1.53 Ω) for AgNPs on paper compared to this work. However, it is important to note that the reagents and synthesis method reported in the reference involves the use of a temperature higher than 100 °C, a longer reaction time, and the use of different solvents with the particles. Due to the favorable response observed in the I-V characterization of the SN3 sample on various flexible substrates, the functionality of the particles was measured on filter paper. The I-V curve shown in figure 3.21, exhibits irregular behavior, and a significant increase in hysteresis is also observed. The presence of the hysteresis could be attributed to the roughness of the paper, high pore size, and separation of fibers inside the filter paper, which disrupt the connection between the particles [192-194]. The filter paper can retain nanoparticles of 5 nm and larger; however, the lateral compaction of the paper would limit the lateral diffusion of

the particles, thus preventing the connection between them [195, 196]. On the other hand, at high Ag concentrations, many particles are widely distributed on the filter paper [197]. The calculated resistance is 10.18 Ω, so it is showing that there is no impediment to the functionality of the particles as a conductive material on the filter paper.

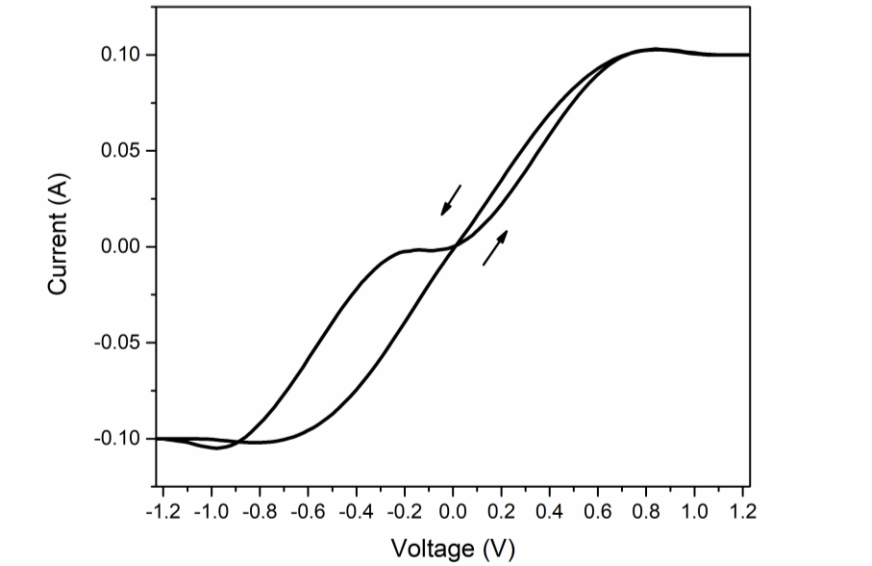

Figure 3.21. I-V curve of conductive AgNPs deposited on filter paper.

As the particles continued to exhibit adequate conductivity, a circuit was constructed by drawing two tracks on a filter paper. Figure 3.22(a) shows the deposition of the nanoparticles using the handwriting technique as a direct deposition method. The traced pattern was dried at room temperature. The length of the marked pattern was 5 cm, and then they were connected to an LED [see figure 3.22(b)]. As shown in figure 3.22(b), turning it on by connecting the tracks with a power source tested the functionality of the obtained nanoparticles for use as a conductive ink on different flexible substrates.

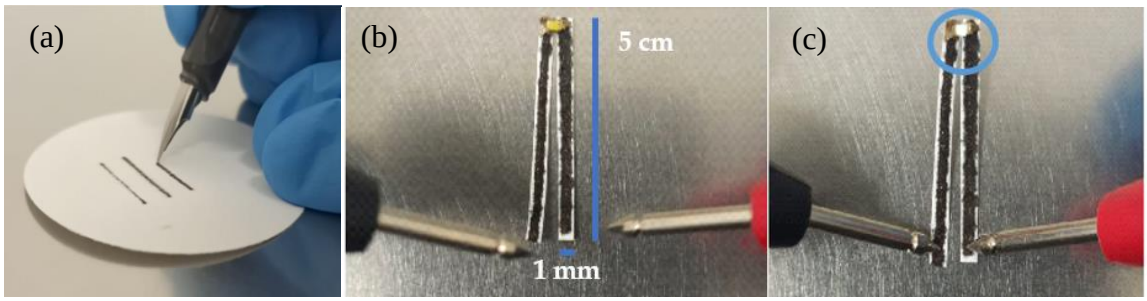

Figure 3.22. (a) AgNPs-SN3 placed on filter paper by handwriting as direct deposition and dry at room temperature. (b) Prototype of a conductive pattern and (c) its functionality on filter paper with an LED off and on.

Chapter 4

Functionalization of conductive inks using silver nanoparticles

Metallic nanoparticles inks are characterized by their chemical stability and high electrical conductivity. Here, the ink that is used for the suspension or solution of metallic nanoparticles in an aqueous solution of water-based or an organic solvent. Generally, the use of water as a dispersant requires the addition of an ionic surfactant to disperse the conductive materials, which typically require heat treatment for drying or activating the deposited material [198]. However, the use of water provides an eco-friendly and safe alternative solution compared to organic solvents, which can be corrosive or flammable. To functionalize the ink, thermal or chemical drying processes involving heat or room temperature are required to evaporate, dissolve, or dry any agent involved, thereby preventing material agglomeration [199]. Conventionally, dispersing agents ensure the adhesion of the printed ink to the substrate or any additive that can modify the properties of the ink [35]. In general, the inkjet deposition process with nanoparticles, depicted in figure 4.1, involves: (1) cleaning the substrate, (2) depositing the synthesized nanoparticles onto the printing system, and (3) thermally or room temperature drying and functionalizing the printed material on a substrate.

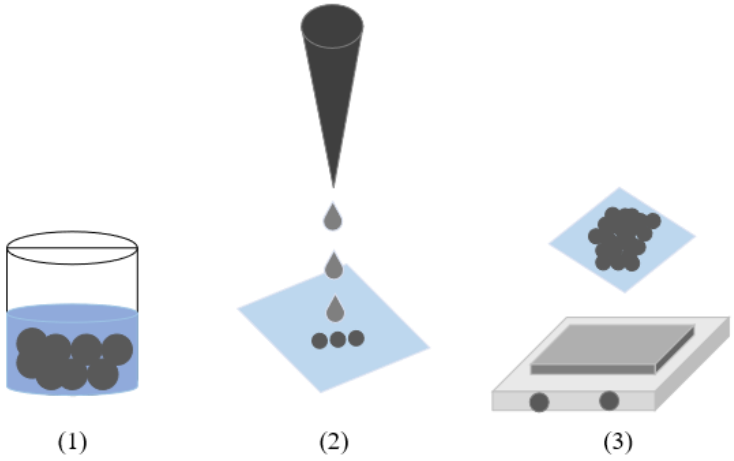

Figure. 4.1. Phases of the inkjet deposition process with nanoparticles. Modified from [200].

In the following sections of this chapter, for simplicity, we briefly describe the office inkjet printer and handwriting electronics that has been developed in last years, the functional patterns and types of materials as substrates, where several polymers and types of paper has been used, and a discussion of the parameters that are taken into account for measuring the conductivity of the ink. Meanwhile, in section 4.2 we describe the methodology of the AgNPs

ink synthesis and finally we show the characterizations, results, and discussion of the material.

4.1 Inkjet printing technique modifications: office inkjet printer and handwriting electronics

Conventionally, metal nanoparticles can be adapted to a commercial manufacturing machine known as a ‘research-use material printer’, which houses a single-use print head with multiple nozzles [201]. This equipment facilitates the manipulation of various parameters, including temperature control to regulate ink viscosity and drying, as well as the droplet fall control to enhance compatibility between the ink and the surface as well as substrate roughness. Additionally, it enables the incorporation of materials with different properties to produce large-area printed prototypes. This is achieved through substrate rotation and aligning, feature and location measurement, inspection and image capture of the printed pattern or drops, cartridges alignment, precise drop placement to match the patterned substrate [202]. Despite the convenience this equipment offers for printing tests, it comes with a price tag of 24,500.00 USD [203].

Similarly, the printing mechanism of an office inkjet printer involves the ejection of ink through a print head. However, this mechanism lacks controllable parameters, making it challenging to ensure proper functioning, especially concerning droplet expulsion [see top diagram 1 of figure 4.2]. Therefore, the implementation of externally controllable parameters is essential for effectively applying ink onto a substrate. This includes selecting the base solvent for ink formulation and conducting drying processes or printing layers to achieve optimal material performance [204-206].

On the other hand, pens, pencils, fountain pens, and brushes are currently used as ‘handwriting electronics’ tools for direct deposition. Through free design, ink functionalization can be carried out "in situ" for on-demand production of printed patterns via line drawing on substrates such as paper, plastic, and even textiles [51, 207-209]. Due to their versatility, commercial pencils with removable and refillable cartridges can be purchased for such applications [see bottom diagram 2 of figure 4.2].

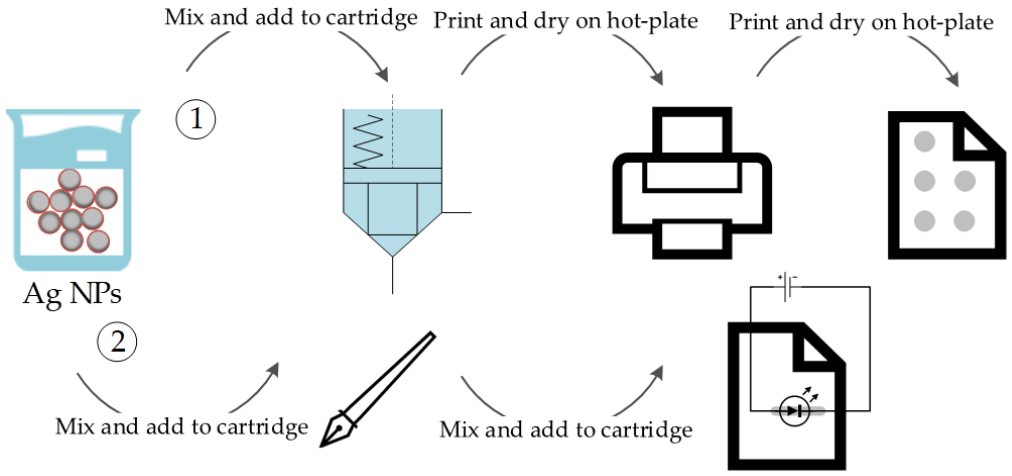

Figure. 4.2. Modifications to direct deposit routes by (1) office inkjet printer and (2) handwriting electronics.

4.2 Functional patterns and types of materials as substrates

Inkjet printing is compatible type of printing with many flexible substrates at a low cost, where various types of polymers can be used, such as polyethylene (PE), polyimide (PI), polycarbonate (PC), polyacrylate types, polyamide (PA), polyether sulphone (PES), polyethylene naphthalate (PEN), liquid crystal polymer (LCP), thermoplastic polyurethane (TPUR), and polyethylene terephthalate (PET) [35, 109, 210], for allowing the utilization and adaptation of a conventional office printers.

On the other hand, paper has also been an attractive option for inkjet-printed electronics due to its flexibility, affordability, environmental friendliness, and recyclability [109]. By implementing paper as substrate, the flow of the deposited liquid in the substrate's porous and rough surface is driven by its capillarity and adsorption capacity [211].

The choice of substrate type may be influenced by the quality of the ink. Factors such as printing speed, resolution, ink thickness, viscosity and surface tension are taken into consideration during printing [212]. The electrical conductivity of printed patterns on paper substrates can be enhanced by the composition of the paper due to the surface coating [12, 213], ensuring that the choice of paper type does not alter the electrical properties of the deposited ink.

In contrast, polymeric materials like PET have a longer absorption time as they lack of capillary effects like paper. The differences between using plastic and paper substrates are attributed to the humidity, absorption, and drying of the deposited drop [12]. Print resolution of the ink on paper substrates has been reported to be better compared to PES and PEN [214]. Even, photographic paper, with its matte or glossy surface, allows for better printing resolution [190, 215].

4.3 Conductivity measurement

A simple way to describe the functionality of a conductive pattern is by measuring its electrical behavior, specifically its resistance to the electricity flow. Resistance is independent of the shape or size of the sample; however, for conductors, resistance measurements will vary based on the length, width, and thickness of the sample [102]. This measurement is not only dependent on the geometry of the printed pattern; resistance values can also vary if the material undergoes sintering at different temperatures [216].

4.4 Methodology

4.4.1 Synthesis of ink based on silver nanoparticles

Conductive silver nanoparticles (see section 3.4.1.1) are washed with ethanol (EtOH) and centrifugated at 1000 rpm by 30 min. In 5 mL of a hydrogen peroxide solution at 3% the AgNPs (20 wt. %) are disolved, then the mix is sonicated for 3 hrs. Figure 4.3 show the steps of the synthesis process. A color change of colloidal solution from gray to black is observed. To corroborate the conductivity, the ink is placed on photographic paper as substrate (for sample preparation for electrical characterization, see section 3.5.6).

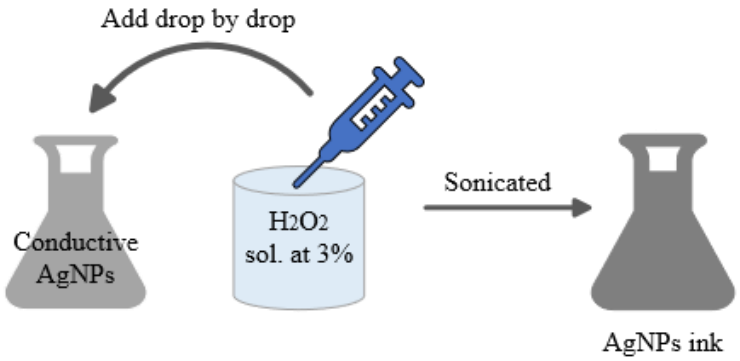

Figure. 4.3 Schematic process of adding hydrogen peroxide for AgNPs ink synthesis.

4.4.2 Characterizations

To carry out the characterizations using DLS techniques and UV-Vis spectroscopy, the AgNPs samples are diluted in water in at ratio of 10:1 (water:AgNPs). Crystalline structures of nanoparticles were determined through a Discover X-ray diffractometer (Bruker D8 Advance), operated at 40 kV and 25 mA with Cu-kα radiation source in a dispersion range of 20 to 90° (2θ); with a Tescan Vega3 LMH (SEM) with SE detector the morphologies of the samples were mapped. The diameter sizes, polydispersity indices (PDI), and zeta potentials were measured with a Zetasizer Nano-ZS90 equipment. Finally, the electrical characterization was performed using a Keithley-4200 Semiconductor Characterization System at room temperature.

4.5 Results and discussion

4.5.1 X-Ray Diffraction (XRD) measurements

To identify the crystalline structure of the particles, the PDF4 database format was used [217]. Figure 4.4 shows the diffraction pattern of the AgNPs (sample AgNPs-SN3, synthesized in the previous chapter) where a phase of $NaNO_3$ has also identified in the crystalline pattern as a secondary product. For the sample AgNPs dissolved in a 3% H_2O_2 solution (sample named AgNPs ink), only the silver phase has been identified from JCPDS file 00-004-0783, as shown in Figure 4.5. The different positions of intense peaks were identified at 38°, 44°, 64°, 77° and 81°, related to the x-ray diffraction pattern onto the crystalline planes of (111), (200), (220), (311) and (222) orientations, respectively. Although chemical reduction processes are simple to prepare and cost-effective [218], the secondary product was not identified, and no additional purification processes were required. According to Zhang et al. [219], Na^+ can act as a stabilizer in the solution, which reduces the spontaneous decomposition of H_2O_2. The effect of H_2O_2 on $NaNO_3$ may result in a remaining $NaNO_3$ precipitate, but also could lead to the formation of Na_2O through its decomposition at room temperature. However, the mixture of AgNPs with the addition of H_2O_2 as a redox reaction starts to occur since the H_2O_2 acts as a metal recovery process [220, 221]. A possible reaction mechanism is described in references [222-224], where there it is noted that the dissociation of H_2O_2 promotes the adhesion of OH^- ions onto the outer surface of AgNPs, generating Ag^+, then hydroxyl radical and superoxide anion, according to reactions (1) and (2)

$$AgNP + H_2O_2 \rightarrow Ag^+ + HO^{\cdot} + OH^- \quad (1)$$

$$HO^{\cdot} + OH^- + H_2O_2 \rightarrow O_2^- + 2H_2O \quad (2)$$

The superoxide anion transfers electrons to the AgNPs surface, resulting in the formation of highly reactive charged nanoparticles (Ag^{*-}) and induce the regeneration of AgNPs, according to reactions (3) and (4) [223, 224].

$$Ag^+ + O_2^- \rightarrow AgNP^{*-} + O_2 \quad (3)$$

$$Ag^+ + AgNP^{*-} \rightarrow AgNP + AgNP \quad (4)$$

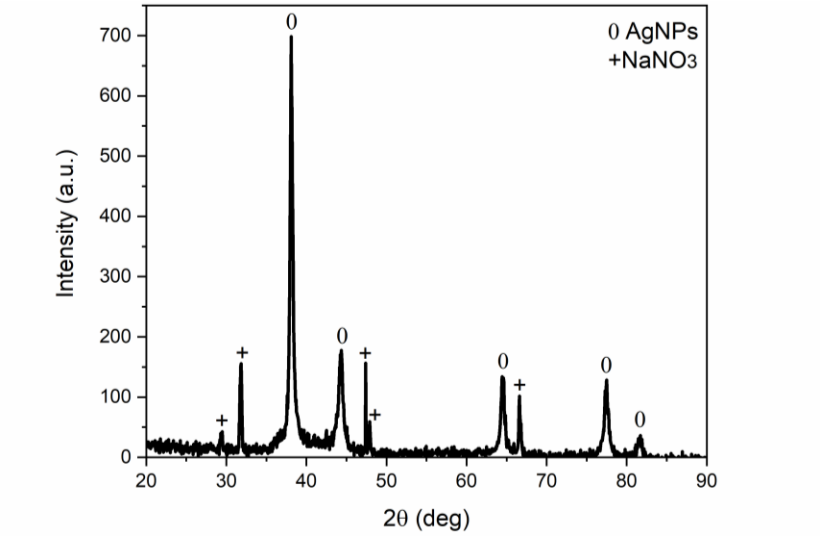

Figure 4.4. XRD pattern of AgNPs obtained in the SN3 synthesized sample.

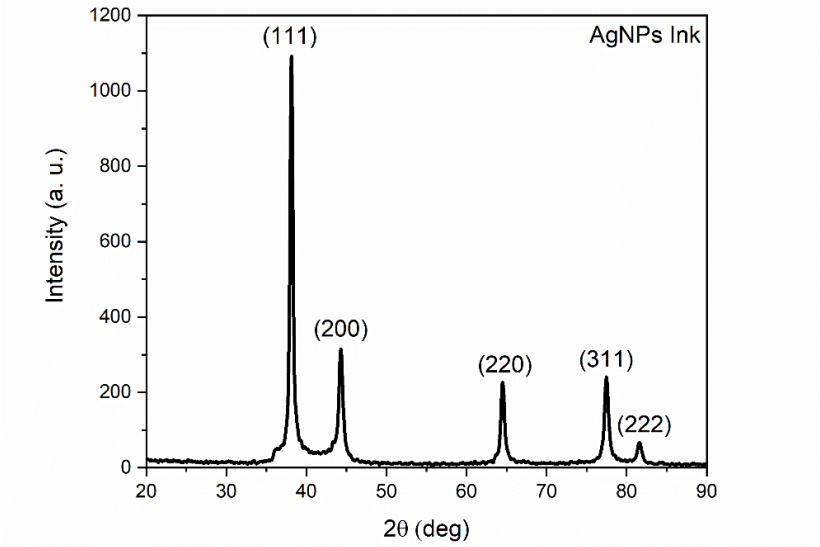

Figure 4.5. XRD pattern of conductive AgNPs ink after mixture in peroxide.

4.5.2 SEM/EDS analysis

To analyze the surface of a trace of AgNPs ink, a sample was deposited on a photographic paper as a substrate and dried at room temperature for 15 minutes. Subsequently, a scanning electron microscopy (SEM) was used to examine the surface. Figure 4.6 shows the SEM image of photographic paper surface at a scale of 20 µm, without particle coating. In Appendix B is show the SEM images of several substrates with and without ink coating.

To show a comparative analysis of the arrangement of AgNPs with and without H_2O_2 mix, a mapping (image at a scale of 1 µm) of the SN3 sample (as previously presented in section 3.5.2) has been taken [see figure 4.7(a)]. The film consists of particle agglomerations with

an average diameter of nanoparticles of ~58 ± 10 nm and have spherical shape, as calculated by the standard log normal function [164-166]. The diameter size was determined to be count around 100 particles using the ImageJ software. The histogram obtained is shown in figure 4.7(b).

On the other hand, for the sample prepared with AgNPs-based ink, shown in Fig. 8a, the diameter of nanoparticles is ~48 ± 12 nm [see figure. 4.8(b)] The observed decrease in average diameter is attributed to the effects of sonication [225, 226]. The formation of agglomerations facilitates the conductivity of the particles due to their union. The heating of the particles is not necessary as the samples already connected, and it is estimated that they have an affinity for the smooth surface of the paper [227].

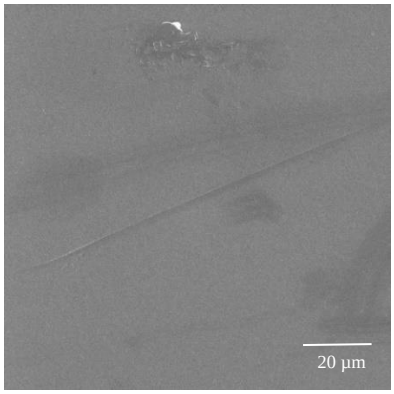

Figure 4.6. SEM image of the surface morphology of the clean photographic paper.

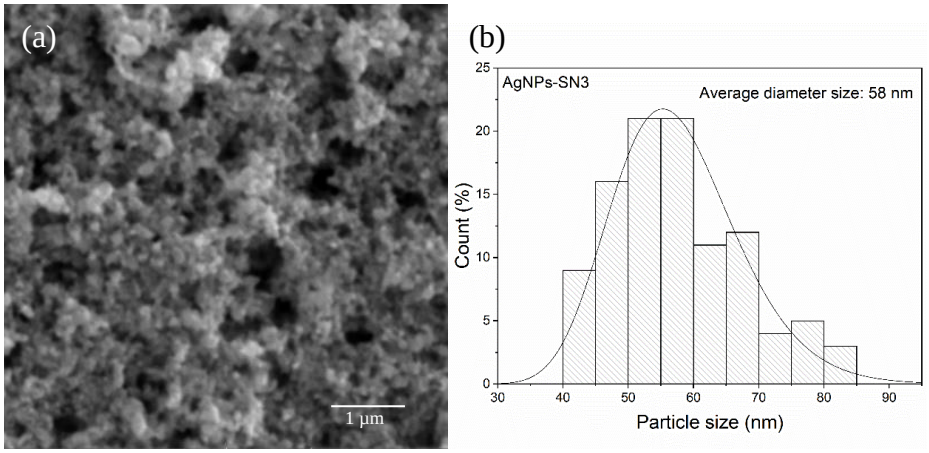

Figure 4.7. SEM images of (a) the surface morphology of the photographic paper after its coating by the sample AgNPs-SN3. (b) Size-distribution of sample AgNPs-SN3 determined from the SEM analysis.

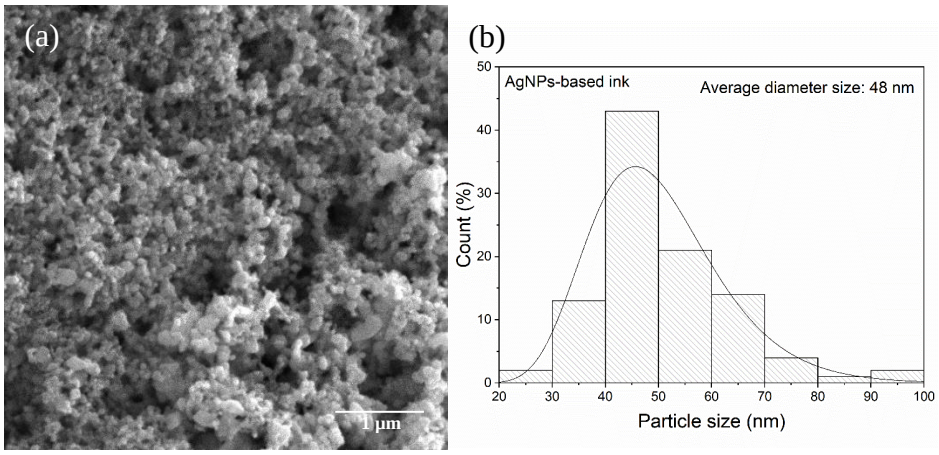

Figure 4.8. SEM images of (a) the surface morphology of the photographic paper after its coating by the AgNPs-based ink. (b) Size-distribution of AgNPs-based ink determined from the SEM analysis.

An elemental analysis was conducted using energy dispersive X-ray spectroscopy (EDS) to determine the chemical composition. EDS spectra (figure 4.9) from sample SN3 and the identified elemental lines are listed in Table 4.1. Figure 4.9 shows the EDS analysis of the sample with nanoparticles without H_2O_2, the detection of the elements N, O and Na were found. The relative quantity of each element is minimal compared to the one of silver. This suggest that the fraction corresponding to Na species should be also weal in the sample with H_2O_2, and its concentration could be possibly lower than the detection limit if the EDS apparatus.

Comparatively, figure 4.10 illustrates that the spectra of sample prepared with AgNPs-based ink exhibit a strong silver signal, indicating the presence solely of AgNPs. The silver percentage is high, and no other element from the reagents used during the synthesis were detected (Table 4.2).

The reagents used modify the cover surface composition of the particles, and consequently, their elemental composition determines the electrical resistance of the printed pattern [228]. In the case of our ink prepared with AgNPs in H_2O_2, the absence of other contaminants means that sample heating for solvent evaporation is not required, nor is it necessary for ink drying, which occurs at room temperature.

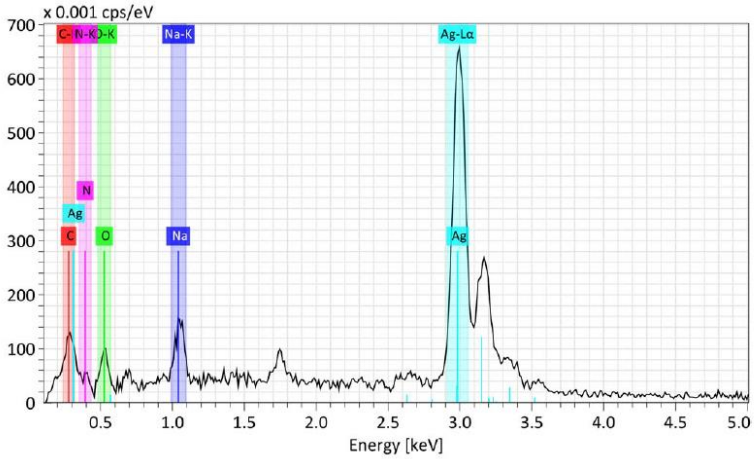

Figure 4.9. EDS analysis of conductive AgNPs (SN3 sample) photographic paper.

Table 4.1. Elemental quantification obtained from sample SN3 spectra.

Element/spectral line	wt. %	at. %	Abs. error %
Ag	88.81	55.49	3.24
N	1.05	5.05	0.76
C	1.31	7.36	0.60
O	4.85	20.42	1.71
Na	3.98	11.68	0.38

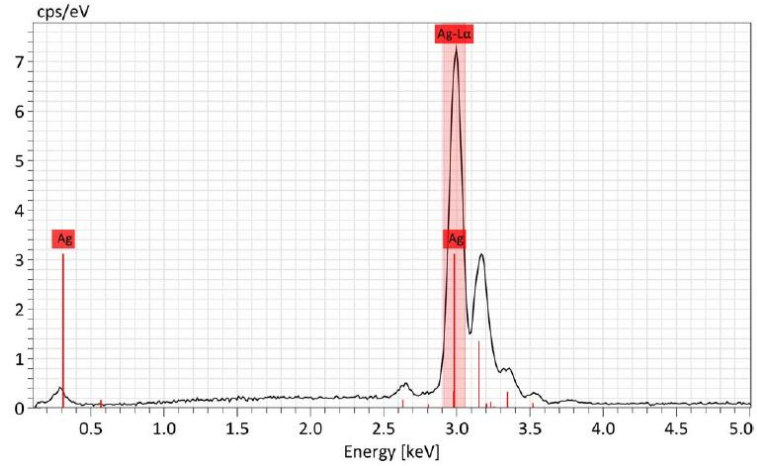

Figure 4.10. EDS analysis of AgNPs-based ink on photographic paper.

Table 4.2. Elemental quantification obtained from sample AgNPs-based ink spectra.

Element/spectral line	wt. %	at. %	Abs. error %
AgLα	97.66	100	3.12

4.5.3 Topography measurement by AFM

Surface topography mapping of sample AgNPs-based ink was conducted through AFM measurements, with an area analysis of 2.5 μm^2. Gwyddion 2.62 software was utilized for the image processing [229]. Both mapped films exhibit accumulated nanoparticles arranged irregular and compactly, demonstrating an agglomerated state consistent with previous reported works [229, 230].

For sample AgNPs-based ink, a horizontal and vertical scan along a marked line was performed. The marked line in figure 4.11(a) passes through a region displaying overlapping particles. In figure 4.11(b), it was determined that the maximum height profile for that region is 470 nm, with the minimum height measured around 200 nm. These particles are small and exhibit well-defined diameters less than 50 nm. The line marked in figure 4.11(c) depicts the arrangement of particles in a deeper region. The profile shown in figure 4.11(d) reveals that the particles have diameters ranging between 30 and 60 nm. Through this analysis, the relative uniformity of the spherical particles and their dimensions are confirmed, as observed in the SEM analysis.

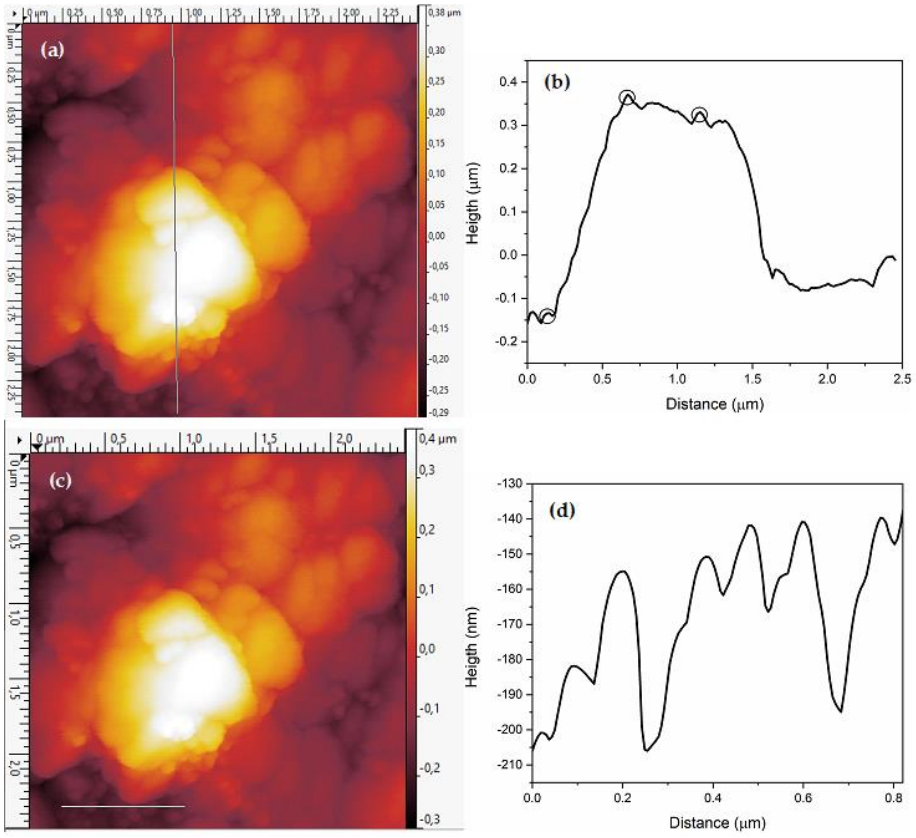

Figure 4.11. AFM topography measurements for AgNPs-based ink sample recorded the overlapping along (a) the mapped vertical gray line with (b) his corresponding profile height and (c) the mapped horizontal gray line with (d) his profile height reported on the figures.

4.5.4 Dynamic Light Scattering (DLS) and Zeta Potential Analysis

As shown in the Chapter 3, to determine the stability of the ink, particle size, size-distribution, and zeta potential is necessary to use the DLS technique. All parameters found are listed in Table 4.3.

Table 4.3. Particle size, polydispersity index and zeta potential values.

Sample	Particle size (nm)	Polydispersity index (PDI)	Polydispersity range	Zeta potential (mV)
AgNPs-SN3	64	0.57	Moderate	-32.2
AgNPs-based ink	50	0.59	Moderate	-30.5

The particle diameter size measured of sample AgNPs-SN3 was measured to be 64 nm, while that of AgNPs-based ink was found to be 50 nm. These values align closely with those obtained from both SEM and AFM investigations.

Both samples exhibited a moderate size distribution as indicated by the polydispersity index values: 0.571 to sample AgNPs-SN3 and 0.597 to sample AgNPs-based ink, which suggests moderate dispersion and potential instability. The standard error calculated from SEM analysis was used to verify the PDI, following the same methodology as the DLS technique [231]. The dispersion is moderate for both samples, 0.18 and 0.27 to sample AgNPs-SN3 and AgNPs-ink respectively.

Furthermore, the zeta potential measurements revealed values of -32.2 mV for SN3 sample and -30.5 mV for ink sample, which are consistent with the values associated with stable suspensions [155, 156]. The acquisition of ionic behavior (Ag^{+}) by the AgNPs due to the electron transfer from H_2O_2 to Ag^{0}, coupled with the negative zeta potential, confirms particle repulsion [232].

4.5.5 UV-Vis spectroscopy

Figure 4.12 shows the normalized absorbance curves for the sample AgNPs-SN3 and AgNPs ink. For sample, in SN3, the absorbance peak is observed at 389.93 nm, while for sample of AgNPs-based ink, the absorbance peak is shifted to a wavelength of 394.19 nm. If the maximum position change or not this will indicate the stability of AgNPs at a ratio or even to at a determined particle size [233]. However, the position of maximum absorption of a polydisperse sample does not provide accurate information about the size of nanoparticles, as conventionally used, because peaks separation cannot be observed from a specific nanoparticle population [176]. On another hand, agglomeration of nanoparticles leads to red-shifted peak toward longer wavelengths [174, 175].

In the case of AgNPs-based ink, a slight increase in the width of the absorption band is observed. However, as the red shift increases, it is observed that sample AgNPs-SN3 shows an increase absorption in the range of 600 to 800 nm [174]. This suggests that sample SN3 may have broader size distributions, as found in the sections 4.5.2 to 4.5.4.

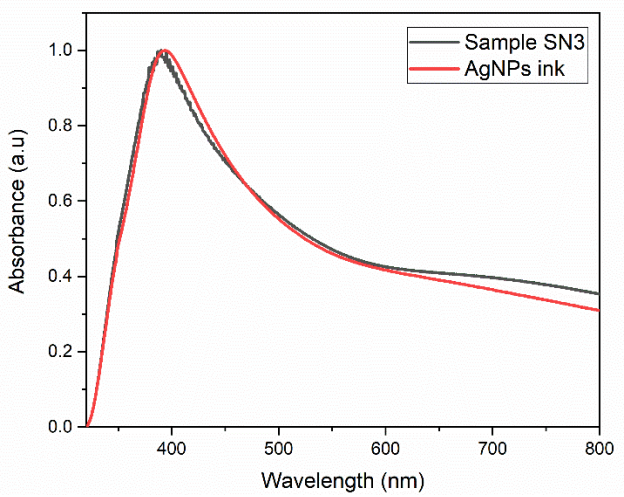

Figure 4.12. UV-Vis spectroscopy of conductive AgNPs (sample SN3) and AgNPs-based ink (after mixture in peroxide).

4.5.6 Electrical characterization

To realize the I-V measurements, the AgNPs-SN3 were deposited onto photographic paper and dried at room temperature. Current-voltage measurements were carried out with forward and reverse sweeps to detect possible hysteresis behaviors associated with material modifications and memory effects. The I-V curve in figure 4.13 exhibits linearity, indicating an ohmic behavior. Although a subtle hysteresis effect is observed but the material maintains its ohmic behavior. The calculated resistance was 4.35 Ω.

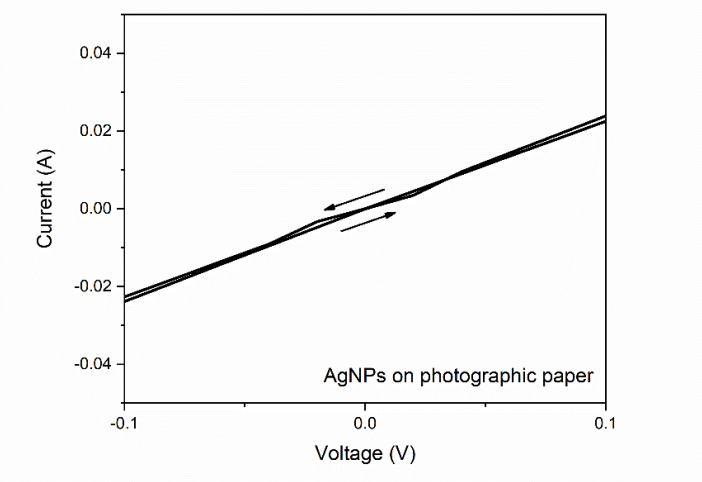

Figure 4.13. I-V curve of conductive AgNPs-SN3 on photographic paper.

To evaluate and compare the electrical behavior of the AgNPs-based ink deposited onto photographic paper, the I-V curve obtained shows a symmetric and reproducible graph compatible with ohmic contacts (figure 4.14). No hysteresis behaviors are observed, and the nominal resistance is measured to be 11.74 Ω when the substrate is flat.

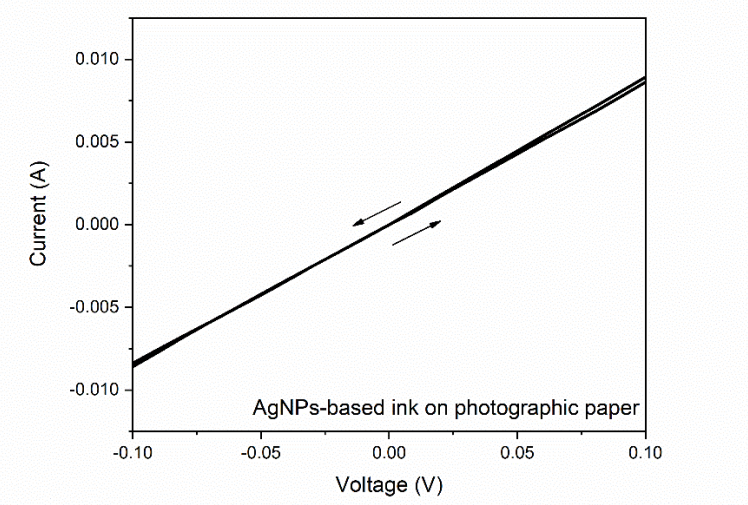

Figure 4.14. I-V curve of AgNPs-based ink on photographic paper.

Conventionally, to measure the mechanical stability, the substrate is initially measured in a flat position, and then the tension is increased at one or multiple radius and times, as shown in the figure 4.15.

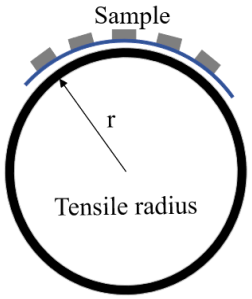

Figure 4.15. Tensile radius in a flexible substrate.

Using the following equation, mechanical stress can be calculated [234]:

$$Strain\ (\%) = \frac{St + Tt}{2r} x\ 100$$

Here, *St* is the substrate thickness of the substrate, *Tt* is the film thickness and *r* is the tensile radius of the substrate.

To observe memory effects of the AgNPs-based ink on photographic paper, flexions and bending cycles were applied to the substrate. Flexions were increase from 12.5 mm (when

the substrate was in a flat position) to 5 mm (when the substrate is at its maximum flexion) radius of curvature. When brought to a bending radius curvature of 12.5 mm, an increase in resistance to 17.99 Ω is observed [see figure 4.16(a)]. Subsequent bending cycles reveled minimal resistance increase that remained stable, when the radius of curvature decreased from 10 mm to 5 mm. The conductive wire is not significantly affected.

With a photographic paper thickness of 0.2032 mm and considering a film thickness of 200 nm (as determined from AFM images) bending at a curvature radius of 12.5 mm corresponds to a mechanical stress of ~0.8%, while at a curvature radius of 5 mm corresponds to a mechanical stress of 2%. All calculated parameters are summarized in Table 4.4, and an error rate of ±5% is considered for the bending curvature radius, indicating that the system remains operational under the applied mechanical constraints.

For bending cycles tests, an increasing cycle from 0 to 1000 is shown in figure 4.16(b). The measured current is close to 10^{-2} A and remains almost constant, showing a slight decrease in electrical resistance compared to the resistance values reported in the third column of Table 4.4. Similar to previous observations, no hysteresis effects are observed, indicating that the functionality of the ink is not altered with increasing bending cycles.

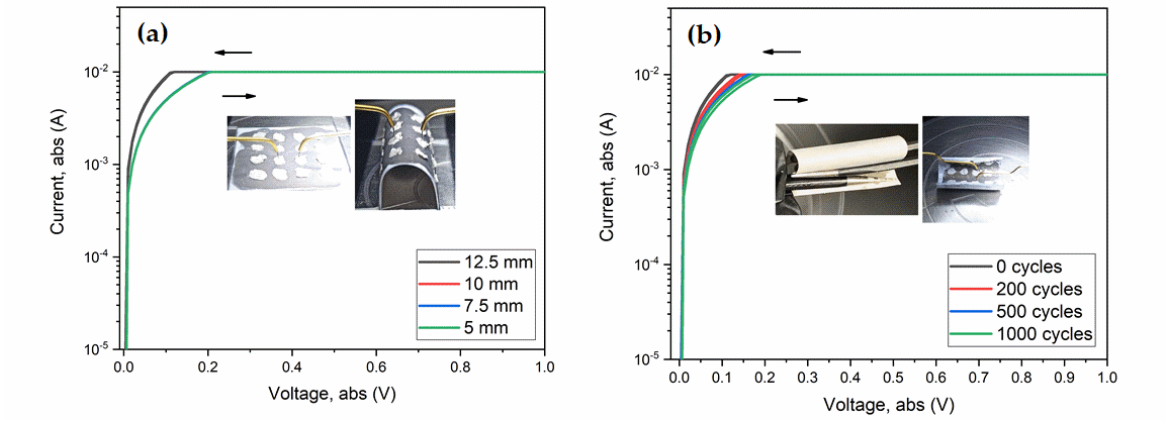

Figure 4.16. I-V measurement of the ink (a) with flexion and (b) bending cycles of photographic paper.

Table 4.4 Strain and resistance calculated for each radius of curvature of the substrate and resistance calculated by bending cycles increases.

Bending radius	Strain (%)	Resistance (Ω)	**Bending cycles**	Resistance (Ω)
12.5 mm	0.8	17.99	0	11.74
10 mm	1	20.11	200	14.00
7.5 mm	1.4	20.93	500	15.97
5 mm	2	20.96	1000	17.95

Finally, to illustrate one of the practical applications in which this ink could be implemented, the AgNPs ink was loaded inside a fountain pen with an extrafine point (0.6 mm) to trace a pattern by handwriting on the photographic paper, as illustrated in figure 4.17. The pattern consists of powering an LED by an external source connected through the printed conductive lines. This demonstration illustrates the potential of flexible and wearable electronics produced by the AgNPs ink reported in this work. The LED turns on and off when the voltage is applied or not. Despite being a basic demonstration of the ink´s functionality, this prototype showcases the capabilities of incorporating nanoparticles into inks to create electronic components that could facilitate the replacement of PCB boards in different operating systems, allowing the fabrication of flexible and more complex hybrid circuits.

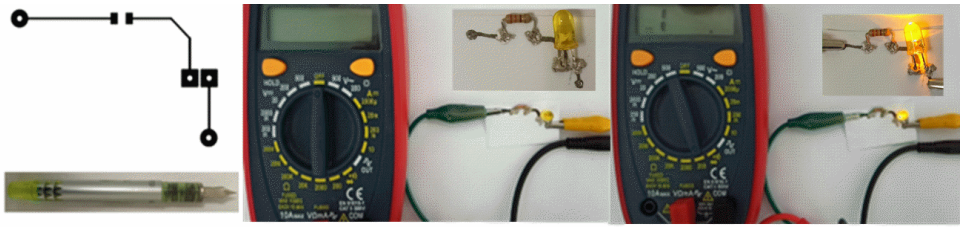

Figure 4.17. Design of drawing circuit with AgNPs ink with a fountain pen on photographic paper. Prototype to show a simple hybrid PCB.

Chapter 5
Conclusions and outlooks

During the synthesis of the silver nanoparticles, the control in the growth of the particles was observed through the addition of two reagents, sodium citrate at different concentrations (0.01 to 0.04 M) and sodium borohydride at 0.05 M, both reacting with silver nitrate 0.05 M, showing that with the concentration of 0.03 M of sodium citrate (sample named SC3), the reaction presented stoichiometric equilibrium, providing better properties for the nanoparticles obtained, such as the minimum particle size of ~52 nm, where a more uniform size distribution was observed and showing better stability. Despite this, sample SC3 showed poor conductive behavior calculating a resistance of $2.7X10^7$ Ω through I-V measurement of the sample on Corning glass. With the addition of silver nitrate at 0.15 M (sample named AgNPs-SN3) the conductive behavior improved significantly (5.78 Ω on Corning glass) without hysteresis effect and resistances between 2.86 to 4.35 Ω were observed using acetate, bond paper, opaline paper, photo paper and PET as flexible substrates. In all samples, the absence of hysteresis and an affinity of the particles with the surface of the substrates with different morphology were observed. Under these characteristics, the synthesis of the ink based on AgNPs was carried out.

Using conductive silver nanoparticles (AgNPs-SN3), the ink was prepared based on hydrogen peroxide diluted to 3% mixed with conductive AgNPs-SN3 at 20 wt.%. Although hydrogen peroxide has a high oxidative capacity, in this reaction it was confirmed that it did not affect the structural property of the Ag, nor the composition of the nanoparticles since no oxide phase or residues of it were found in the sample.

In order to demonstrate the electrical efficiency of the ink, an I-V characterization was performed, revealing a resistance of 11.74 Ω. It was observed that despite the dilution fraction, the particles exhibited optimal performance compared to the resistance value of the undiluted particles, and none of the samples exhibit hysteresis effects. With the addition of the AgNPs to hydrogen peroxide, the prepared mixture is electrically conductive due to the presence of free hydroxyl radicals and superoxide ions. The action of these ions was to promote successive redox reactions as well as the release of secondary chemicals. The concentration of silver added enhances the generation of free radicals without the addition of any acidic compound, which implies obtaining a sample with a low weight % ratio and high performance in the conductivity of the ink.

The performance of the ink was tested by flexing and bending tests of the flexible substrate, suggesting that the material remains functional under mechanical constraints. The maximum

stress found corresponds to 2%, being the fracture limit allowed for a metallic material. With respect to torsion, the increase in ink resistance was up to 17.95 Ω when 1000 cycles were exercised. No hysteresis effect was observed in any of the tests.

Finally, to test its application, a handwriting test was performed, in which a fountain pen loaded with the AgNPs ink was used to draw a basic PCB pattern on photographic paper. The efficiency of the ink adapted to this direct printing mechanism was demonstrated, and the efficiency of the device built by connecting an external voltage source was also observed.

We believe that this work contributes to the scientific community since the design of the synthesis of silver nanoparticle inks with controllable conditions, short time and without high energy cost has been demonstrated. Furthermore, the low concentrations of the reagents used, commercially available and inexpensive materials make the methodology established in this dissertation of interest for future large-scale applications, together with the compatibility of the ink on different substrates and its performance in the tests of bending and flexions provides relevant information for the fabrication of flexible hybrid devices.

Appendix A

Mask for depositing contacts.

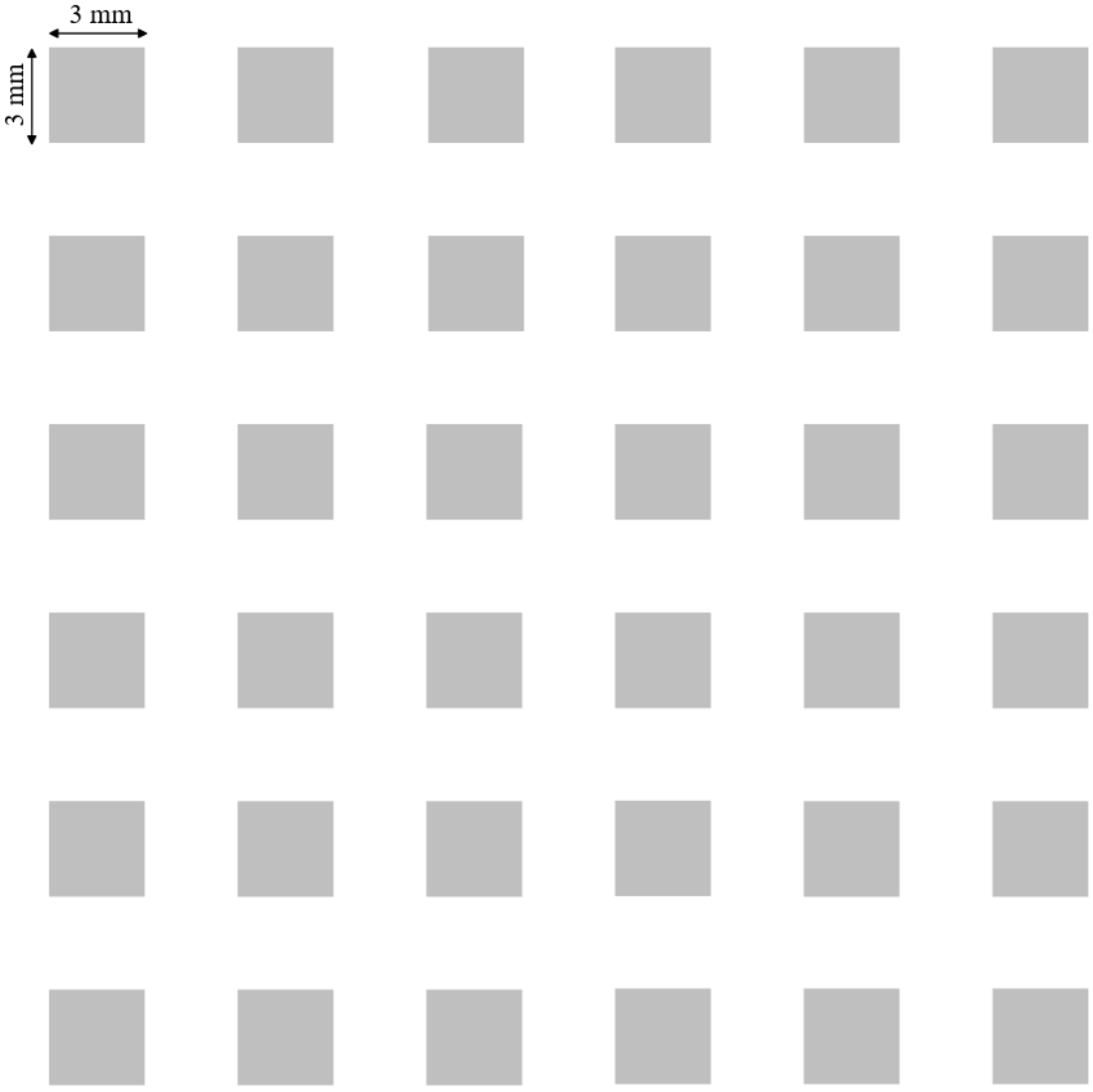

Appendix B

SEM images of AgNPs-based ink on different flexible substrates dry at room temperature.

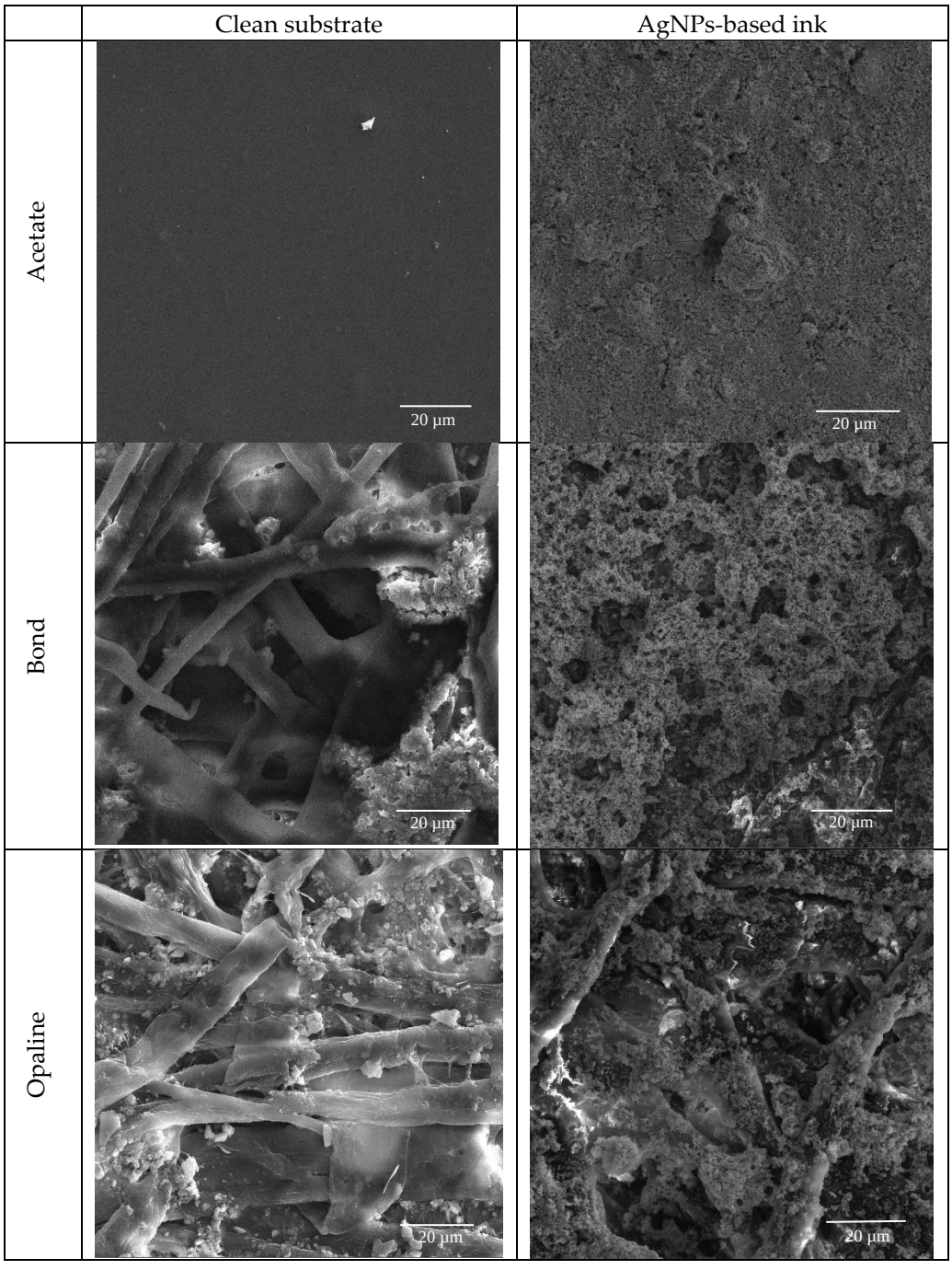

PET	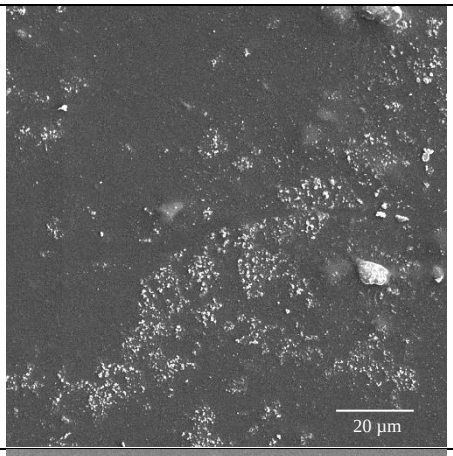	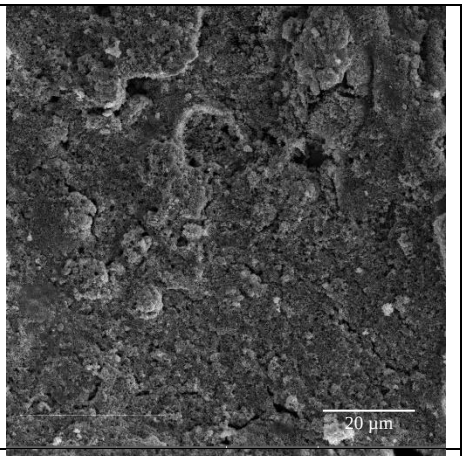
Photography	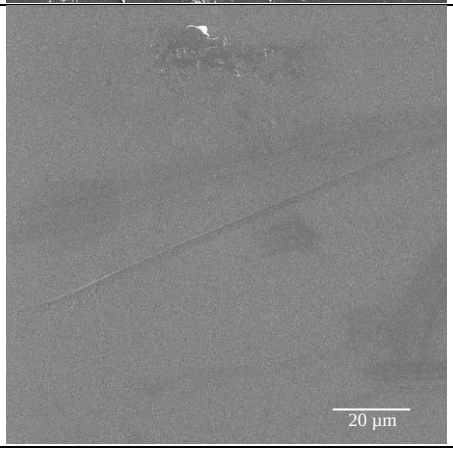	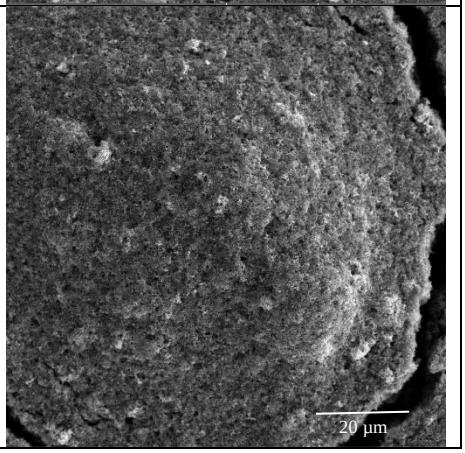

References

[1] Suja, F., Rahman, R. A., Yusof, A., & Masdar, M. S. (2014). e-Waste Management Scenarios in Malaysia. *J. Waste Manag.*, *2014*(609169), 1-7. https://doi.org/10.1155/2014/609169

[2] Awasthi, A.K., et al. (2019). Circular economy and electronic waste. *Nat. Electron.*, *2*, 86–89. https://doi.org/10.1038/s41928-019-0225-2

[3] Consumer Electronics—Worldwide. (2021). https://www.statista.com/outlook/dmo/ecommerce/electronics-media/consumer-electronics/worldwide

[4] Nikou, V. & Sardianou, E. (2023). Bridging the socioeconomic gap in E-waste: Evidence from aggregate data across 27 European Union countries. *Cleaner Production Letters*, 5, 100052. https://doi.org/10.1016/j.clpl.2023.100052

[5] Liu, K., Tan, Q., Yu, J., & Wang, M. (2023). A global perspective on e-waste recycling. *Circular Economy*, *2*(1), 100028. https://doi.org/10.1016/j.cec.2023.100028

[6] Forti, V., Balde, C. P. & Kuehr, R. (2018). *E*-waste statistics. *Guidelines on classification reporting and indicators.* 2nd ed. United Nations University, VIE-SCYCLE, Bonn, Germany.

[7] Chakraborty, M., Kettle, J., & Dahiya, R. (2022). Electronic Waste Reduction Through Devices and Printed Circuit Boards Designed for Circularity. *IEEE J-FLEX*, *1*(1), 4-23. https://doi.org/10.1109/JFLEX.2022.3159258.

[8] Grant, K., Zhang, S. & Kettle, J. (2023). Improving the sustainability of printed circuit boards through additive printing. *2023 IEEE Conference on Technologies for Sustainability (SusTech)*, Portland, OR, USA, 86-90, https://doi.org/10.1109/SusTech57309.2023.10129587.

[9] Li, W., et al. (2020). Biodegradable Materials and Green Processing for Green Electronics. *Adv. Mater.*, *32*, 2001591. https://doi.org/10.1002/adma.202001591

[10] Khan, Y., Thielens, A., Muin, S., Ting, J., Baumbauer, C., & Arias, A. C. (2019). A New Frontier of Printed Electronics: Flexible Hybrid Electronics. *Adv. Mater.*, *32*(15), 1905279. https://doi.org/10.1002/adma.201905279

[11] Tong, G., Jia, Z., & Chang, J. (2018). Flexible Hybrid Electronics: Review and Challenges, *2018 IEEE International Symposium on Circuits and Systems (ISCAS)*, Florence, Italy, 1-5, https://doi.org/10.1109/ISCAS.2018.8351806

[12] Tobjörk, D., & Österbacka, R. (2011). Paper Electronics. *Adv. Mater.*, *23*, 1935-1961. https://doi.org/10.1002/adma.201004692

[13] Brody, T.P. (1984). The thin film transistor—A late flowering bloom. *IEEE Trans. Electron Devices*, *31*(11), 1614-1628. https://doi.org/10.1109/T-ED.1984.21762.

[14] Wu, H., et al. (2014). Towards Practical Application of Paper based Printed Circuits: Capillarity Effectively Enhances Conductivity of the Thermoplastic Electrically Conductive Adhesives. *Sci. Rep. 4*, 6275. https://doi.org/10.1038/srep06275

[15] Martins, R.F.P., et al. (2013). Recyclable, Flexible, Low-Power Oxide Electronics. *Adv. Funct. Mater.*, *23*, 2153-2161. https://doi.org/10.1002/adfm.201202907

[16] Kamyshny, A., & Magdassi, S. (2014). Conductive Nanomaterials for Printed *Electronics. Small, 10,* 3515-3535. https://doi.org/10.1002/smll.201303000

[17] Xiang, D., et al. (2007). Printed circuit board recycling process and its environmental impact assessment. *Int. J. Adv. Manuf. Technol. 34*, 1030–1036. https://doi.org/10.1007/s00170-006-0656-6

[18] Bastola, A., et al. (2023). Formulation of functional materials for inkjet printing: A pathway towards fully 3D printed electronics. *Materials Today Electronics, 6,* 100058. https://doi.org/10.1016/j.mtelec.2023.100058

[19] Abdolmaleki, H., Hauge, A. B., Merhi, Y., Nygaard, J. V., & Agarwala, S. (2023). Inkjet-printed flexible piezoelectric sensor for self-powered biomedical monitoring. *Materials Today Electronics, 5,* 100056. https://doi.org/10.1016/j.mtelec.2023.100056

[20] Che, J., et al. (2023). Inkjet Printing of All Aqueous Inks to Flexible Microcapacitors for High-Energy Storage. *Adv. Funct. Mater., 33,* 2301544. https://doi.org/10.1002/adfm.202301544

[21] Sajedi-Moghaddam, A., Gholami, M., & Naseri, N. (2023). Inkjet Printing of MnO_2 Nanoflowers on Surface-Modified A4 Paper for Flexible All-Solid-State Microsupercapacitors. *ACS Appl. Mater. Interfaces, 15*(3), 3894-3903. https://doi.org/10.1021/acsami.2c08939

[22] Pendyala, N.K., Magdassi, S., & Etgar, L. (2023). Inkjet-Printed Flexible Semitransparent Solar Cells with Perovskite and Polymeric Pillars. *Sol. RRL, 7,* 2200988. https://doi.org/10.1002/solr.202200988

[23] Chennit, K., et al. (2023). Inkjet-Printed, Coplanar Electrolyte-Gated Organic Field-Effect Transistors on Flexible Substrates: Fabrication, Modeling, and Applications in Biodetection. *Adv. Mater. Technol., 8,* 2200300.https://doi.org/10.1002/admt.202200300

[24] Kant, C., Mahmood, S., & Katiyar, M. (2023). Large-Area Inkjet-Printed OLEDs Patterns and Tiles Using Small Molecule Phosphorescent Dopant. *Adv. Mater. Technol., 8,* 2201514. https://doi.org/10.1002/admt.202201514

[25] Dahiya, A.S., et al. (2020). High-performance printed electronics based on inorganic semiconducting nano to chip scale structures. *Nano Convergence, 7,* 33. https://doi.org/10.1186/s40580-020-00243-6

[26] Ferreira Cruz, S. M., A. Rocha, L. A., Viana, J. C., & Rackauskas, S. (2018). *Printing Technologies on Flexible Substrates for Printed Electronics*. IntechOpen, Chapter 3, 47-70. https://doi.org/10.5772/intechopen.76161

[27] Chang, J. S., Facchetti A. F., & Reuss, R. (2017). A Circuits and Systems Perspective of Organic/Printed Electronics: Review, Challenges, and Contemporary and Emerging Design Approaches. *IEEE J. Emerg. Sel. Top. Circuits Syst.*, *7*(1), 7-26. https://doi.org/10.1109/JETCAS.2017.2673863.

[28] Edgar, T. F. et al. (2000). Automatic control in microelectronics manufacturing: Practices, challenges, and possibilities. *Automatica*, *36*(11), 1567-1603. https://doi.org/10.1016/S0005-1098(00)00084-4

[29] Teng, K. & Vest, R. (1987). Liquid Ink Jet Printing with MOD Inks for Hybrid Microcircuits. *IEEE Transaction on Components, Hybrids, and Manufacturing Technology, 10*(4), 545-549. http://doi.org/10.1109/TCHMT.1987.1134794

[30] Ventaka, K. R. R., Ventaka, A. K., Karthik, P. S., & Surya, P. S. (2015). Conductive silver inks and their applications in printed and flexible electronics. *RSC Adv*., *5*, 77760-77790. https://doi.org/10.1039/C5RA12013F

[31] Scandurra, A., Francesco Indelli, G., Graziana Spartà, N., Galliano, F., Ravesi, S. & Pignataro, S. (2010), Low-temperature sintered conductive silver patterns obtained by inkjet printing for plastic electronics. *Surf. Interface Anal*., 42, 1163-1167. https://doi.org/10.1002/sia.3229

[32] Cai, Y., Yao, X., Piao, X., Zhang, Z., Nie, E., Sun, Z. (2019).Inkjet printing of particle-free silver conductive ink with low sintering temperature on flexible substrates. *Chem. Phys. Lett., 737*, 136857. https://doi.org/10.1016/j.cplett.2019.136857

[33] Lemarchand, J., Bridonneau, N., Battaglini, N., Carn, F., Mattana, G., Piro, B., Zrig, S., & Noël, V. (2012). Challenges, Prospects, and Emerging Applications of Inkjet-Printing Electronics: A Chemist's Point of View. *Angew. Chem. Int. Ed., 61*, e202200166.

[34] Yin, Z., Huang, Y., Bu, N. et al. (2010). Inkjet printing for flexible electronics: Materials, processes and equipments. *Chin. Sci. Bull. 55*, 3383–3407. https://doi.org/10.1007/s11434-010-3251-y

[35] Cano-Raya, C., Denchev, Z. Z., Cruz, S. F. & Viana, J. C. (2019). Chemistry of solid metal-based inks and pastes for printed electronics – A review. *Appl. Mater. Today*, *15*, 416–430. https://doi.org/10.1016/j.apmt.2019.02.012

[36] Orrill, M., Abele, D., Wagner, M.J., LeBlanc, S. (2021). Sterically Stabilized Multilayer Graphene Nanoshells for Inkjet Printed Resistors. *Electron. Mater.*, *2*, 394-412. https://doi.org/10.3390/electronicmat2030027

[37] Nallan, H. C., Sadie, J. A., Kitsomboonloha, R., Volkman, S. K., & Subramanian, V. (2014). Systematic Design of Jettable Nanoparticle-Based Inkjet Inks: Rheology, Acoustics, and Jettability. *Langmuir*, *30*(44), *13470–13477*. https://doi.org/10.1021/la502903y

[38] Sigma-Aldrich. Silver nanoparticles ink. (2024). https://www.sigmaaldrich.com/CA/en/product/aldrich/798738

[39] Henkel. Loctite. (2024). https://print-your-electronics-with-loctite.com

[40] Elephantech. List of Silver Nanoparticle Inks for Inkjet. (2021). https://info.elephantech.co.jp/ij-ink-catalog-en#Ag_ink_list

[41] Fernandes, I.J., Aroche, A.F., Schuck, A. et al. (2020). Silver nanoparticle conductive inks: synthesis, characterization, and fabrication of inkjet-printed flexible electrodes. *Sci. Rep. 10*, 8878. https://doi.org/10.1038/s41598-020-65698-3

[42] Mo, L., Guo, Z., Yang, L., Zhang, Q., Fang, Y., Xin, Z., Chen, Z., Hu, K., Han, L., & Li, L. (2019). Silver Nanoparticles Based Ink with Moderate Sintering in Flexible and Printed Electronics. *Int. J. Mol. Sci.*, *20*, 2124. https://doi.org/10.3390/ijms20092124

[43] Dang, M. C., Dang, T. M. D., & Fribourg-Blanc, E. (2014). Silver nanoparticles ink synthesis for conductive patterns fabrication using inkjet printing technology. (2015). *Adv. Nat. Sci: Nanosci. Nanotechnol. 6*, 015003. https://doi.org/10.1088/2043-6262/6/1/015003

[44] Shen, W., Zhang, X., Huang, Q., Xu, Q., & Song, W. (2014). Preparation of solid silver nanoparticles for inkjet printed flexible electronics with high conductivity. ***Nanoscale***, ***6***, 1622-1628. https://doi.org/10.1039/C3NR05479A

[45] Tam, S. K., Fung, K. Y., Poon, G. S. H., & Ng, K. M. (2016). *Product design: Metal nanoparticle-based conductive inkjet inks. AIChE Journal, 62*(8), *2740–2753.* https://doi.org/10.1002/aic.15271

[46] Sanchez-Duenas, L., Gomez, E., Larrañaga, M., Blanco, M., Goitandia, A.M., Aranzabe, E., & Vilas-Vilela, J.L. (2023). A Review on Sustainable Inks for Printed Electronics: Materials for Conductive, Dielectric and Piezoelectric Sustainable Inks. *Materials, 16,* 3940. https://doi.org/10.3390/ma16113940

[47] Dimitriou, E. & Michailidis, N. (2021). Printable conductive inks used for the fabrication of electronics: an overview. *Nanotechnology, 32,* 502009. https://doi.org/10.1088/1361-6528/abefff

[48] Jung, I., et al. (2012). A Simple Process for Synthesis of Ag Nanoparticles and Sintering of Conductive Ink for Use in Printed Electronics. *J. Electron. Mater. 41,* 115–121. https://doi.org/10.1007/s11664-011-1761-3

[49] Keskinen, M. (2012). End-of-life options for printed electronics. *Waste Electrical and Electronic Equipment (WEEE) Handbook,* 352–364. https://doi.org/10.1533/9780857096333.3.352

[50] Aleeva, Y., & Pignataro, B. (2014). Recent advances in unscalable wet methods and ink formulation for printed electronics. *J. Mater. Chem. C, 2,* 6436-6453. https://doi.org/10.1039/C4TC00618F

[51] Ferreira de Oliveira, A. E., Pereira, A. C., & Ferreira, L. F. (2022). Fully handwritten electrodes on paper substrate using rollerball pen with silver nanosilver nanoparticle ink, marker pen with carbon nanotube ink and graphite pencil. *Anal. Methods, 14,* 1880-1888 https://doi.org/10.1039/D2AY00373B

[52] Zhao, C.-F., Wang, J., Zhang, Z.-Q., & Sun, Z., & Maimaitimin, Z. (2022). Silver-Based Conductive Ink on Paper Electrodes Based on Micro-Pen Writing for Electroanalytical Applications. *Chem. Electro. Chem., 9*, e202200948. https://doi.org/10.1002/celc.202200948

[53] Cui, Z. (2016). *Printed Electronics: Materials, Technology and Applications.* Singapore: John Wiley & Sons.

[54] Sudheshwar, A., Malinverno, N., Hischier, R., Nowack, B., & Som, C. (2023). The need for design-for-recycling of paper based printed electronics-a prospective comparison with printed circuit boards. *Resources, Conservation and Recycling, 189,* 106757. https://doi.org/10.1016/j.resconrec.2022.106757

[55] Nayak, L., Mohanty, S., Nayak, S. K., & Ramadoss, A. (2019). A review on inkjet printing of nanoparticle inks for flexible electronics. *J. Mater. Chem. C, 7*(29), 8771–8795. https://doi.org/10.1039/C9TC01630A.

[56] Wack, S., Popa, P. L., Adjeroud, N., Vergne, C., & Leturcq. (2020). Two-Step Approach for Conformal Chemical Vapor-Phase Deposition of Ultra-Thin Conductive Silver Films. *ACS Appl. Mater. Interfaces, 12*(32), 36329-36338. https://doi.org/10.1021/acsami.0c08606

[57] Jara N., Milán N.S., Rahman A., Mouheb L., Boffito D.C., Jeffryes C., & Dahoumane S.A. (2021). Photochemical Synthesis of Gold and Silver Nanoparticles—A Review. *Molecules*, 26(15), 4585. https://doi.org/10.3390/molecules26154585

[58] Liang, J., Liu, Q., Li, T., Luo, Y., Lu, S., Shi, X., Zhang, F., Asiri, A. M., & Sun, X. (2021). Magnetron sputtering enabled sustainable synthesis of nanomaterials for energy electrocatalysis. *Green Chem., 23,* 2834-286. https://doi.org/10.1039/D0GC03994B

[59] Zhang, D., Li, Z. & Sugioka, K. (2021). Laser ablation in liquids for nanomaterial synthesis diversities of targets and liquids. *J. Phys. Photonics, 3*, 042002. https://doi.org/10.1088/2515-7647/ac0bfd

[60] Garcia, P. R. A. F., Prymak, O., Grasmik, V., Pappert, K., Wlysses, W., Otubo, L., Epple, M., & Oliveira, C. L. P. (2020). An in situ SAXS investigation of the formation of silver nanoparticles and bimetallic silver-gold nanoparticles in controlled wet-chemical reduction synthesis. *Nanoscale Adv., 2*, 225-238. https://doi.org/10.1039/C9NA00569B

[61] Yaqoob, A. A., Umar, K., & Ibrahim, M. N. M. (2020). Silver nanoparticles: various methods of synthesis, size affecting factors and their potential applications-a review. *Appl. Nanosci., 10*, 1369-1378. https://doi.org/10.1007/s13204-020-01318-w

[62] Zeng, X., He, P., Hu, M., Zhao, W., Chen, H., Liu, L., Sun, J., & Yang, J. (2022). Copper ink for printed electronics: a review. *Nanoscale, 14*, 16003-16032. https://doi.org/10.1039/D2NR03990G

[63] Rajan, K., Roppolo, I., Chiappone, A., Bocchini, S., Perrone, D., & Chiolerio, A. (2016). Silver nanoparticle ink technology: state of the art. *Nanotechnol. Sci. Appl., 11*(9), 1-13, https://doi.org/10.2147/NSA.S68080

[64] Gangwar, C., Yaseen, B., Kumar, I., Singh, N. K., & Naik, R. M. (2021). Growth Kinetic Study of Tannic Acid Mediated Monodispersed Silver Nanoparticles Synthesized by Chemical Reduction Methods and Its Characterization. *ACS Omega, 6*(34), 22344-22356. https://doi.org/10.1021/acsomega.1c03100

[65] Ma, Z., et al. (2022). Preparation of nano-silver nanoparticles for conductive ink and the correlations with its conductivity. *Appl. Nanosci., 12*, 1657–1665. https://doi.org/10.1007/s13204-022-02340-w

[66] Zhuo, L., et al. (2020). Cost-effective silver nano-ink for inkjet printing in application of flexible printing in application of flexible electronic devices. *Chem. Phys. Lett., 757*, 137904. https://doi.org/10.1016/j.cplett.2020.137904

[67] Kant, T., et al. (2020). Flexible printed paper electrode with silver nano-ink for electrochemical applications. *Microchemical Journal, 155*, 104687. https://doi.org/10.1016/j.microc.2020.104687

[68] Kumar, A., & Goia, D. V. (2022). Preparation of concentrated stabilizer-free dispersion of uniform silver nanoparticles. *Polyhedron, 219*, 115804. https://doi.org/10.1016/j.poly.2022.115804

[69] Lee, Y.-C., Ahn, J.-H., & Lee, C.-Y. (2021). Grid-type sensors using resistance change ratio for micro-crack detection. *Eng. Fail. Anal., 119*, 104973. https://doi.org/10.1016/j.engfailanal.2020.104973

[70] Fujifilm-Dimatix. Dimatix Materials Printer Jettable Fluid Formulation Guidelines. Support and Contact Center. (2013). https://asset.fujifilm.com/www/us/files/202104/c80cdd17080a06095c34a26d6221c81a/PDS00085.pdf

[71] Lee, A., Sudau, K., Ahn, K. H., Lee, S. J., & Willenbacher, N. (2012). Optimization of Experimental Parameters to Suppress Nozzle Clogging in Inkjet Printing. *Industrial & Engineering Chemistry Research, 51*(40), *13195–13204.* https://doi.org/10.1021/ie301403g

[72] Li, M., Zhang, L., Wang, D., Agbo, C., & Fu, S. (2017). Influence of nano-coated pigment ink formulation on ink-jet printability and printing accuracy. *Color. Techno, 133*(6), *476–484.* https://doi.org/10.1111/cote.12299

[73] Yang, W., Mathies, F., Unger, E. L. Hermerschmidt, F., List-Kratochvil, E. J. W. (2020). One-pot synthesis of stable and cost-effective silver particles-free ink for inkjet-printed flexible electronics. *J. Mater. Chem. C., 8*, 16443-16451. https://doi.org/10.1039/D0TC03864D

[74] Towne, S., Viswanathan, V., Holbery, J. & Rieke, P. (2007). Fabrication of polymer electrolyte membrane fuel cell MEAs utilizing inkjet print technology. *J. Power Sources*, *171*, 575–584

[75] Magdassi, S., Bassa, A., Vinetsky, Y., & Kamyshny, A. (2003). Silver Nanoparticles as Pigments for Water-Based Ink-Jet Inks. *Chem. Mater*., *15*, 2208-2217. https://doi.org/10.1021/cm021804b

[76] Winter, C., et al. (2023). Development of a Workflow to Engineer Tailored Microparticles Via Inkjet Printing. *Pharm. Res.*, *40*, 281–294. https://doi.org/10.1007/s11095-022-03426-4

[77] Li, N., Li, J., Wan, X., Niu, Y., Gu, Y., Chen, G., & Ju, S. (2023). Preparation of Micro-Size Spherical Silver Particles and Their Application in Conductive Silver Paste. *Materials*, *16*, 1733. https://doi.org/10.3390/ma16041733

[78] Wang, Z., et al. (2017). Facile synthesis of monodisperse silver nanoparticles for screen printing conductive inks. *J. Mater. Sci.: Mater. Electron, 28*, 16939–16947. https://doi.org/10.1007/s10854-017-7614-y

[79] Hussain, M. H., Bakar, N. F. A., Mustapa, A. N., Low, K.-F., Othman, N. H., Adam, F. (2020). Synthesis of Various Size Gold Nanoparticles by Chemical Reduction Method with Different Solvent Polarity. *Nanoscale, Res. Lett., 15*, 140. https://doi.org/10.1186/s11671-020-03370-5

[80] Seitkalieva, M. M., Samoylenko, D. E., Lostman, K. A., Rodygin, K. S., & Ananikov, V. (2021). Metal nanoparticles in ionic liquids: Synthesis and catalytic applications. *Coord. Chem. Rev., 445*, 213982. https://doi.org/10.1016/j.ccr.2021.213982

[81] Wang, X., Zhang, M., Zhang, L., Xu, J., Xiao, X., & Zhang, X. (2022). Inkjet-printed flexible sensors: From function materials, manufacture process, and applications perspective. *Mater. Today Commun., 31*, 103263. https://doi.org/10.1016/j.mtcomm.2022.103263

[82] Ragonese, E., Fattori, M., & Cantatore, E. (2021). Printed Organic Electronics on Flexible Foil: Circuit Design and Emerging Applications. *IEEE Trans. Circuits Syst. II Express Briefs*, *68*(1), 42-48. https://doi.org/10.1109/TCSII.2020.3040707

[83] Eshkeiti, A., et al. (2015). Screen Printing of Multilayered Hybrid Printed Circuit Boards on Different Substrates. *IEEE Trans. Compon. Packag. Manuf. Technol*., *5*(3), 415-421. https://doi.org/10.1109/TCPMT.2015.2391012

[84] Rocha, H., Semprimoschning, C., & Nunes, J. P. (2021). Sensors for process and structural health monitoring of aerospace composites A review. *Eng. Struct., 237*, 112231. https://doi.org/10.1016/j.engstruct.2021.112231

[85] Li, W., Zhang, C., Lan, D., Ji, W., & Wang, Y. (2022). Solution Printing of Electronics and Sensors: Applicability and Application in Space. *Adv. Eng. Mat., 24*, 2200173. https://doi.org/10.1002/adem.202200173

[86] Karakurt, I., & Lin, L. (2020). 3D printing technologies: techniques, materials, and post-processing. *Curr. Opin. Chem. Eng*., *28*, 134-143. https://doi.org/10.1016/j.coche.2020.04.001

[87] Fapanni, T., Sardini, E., Borghetti, M., Serpelloni, M., & Bellotti. S. (2023). Preliminary Results on Fully-Printed and Silver-Based Temperature Sensors for Aerospace Industry. *2023 IEEE International Workshop on Metrology for Industry 4.0 & IoT (MetroInd4.0&IoT)*, Brescia, Italy, 200-204. https://doi.org/10.1109/MetroInd4.0IoT57462.2023.10180153

[88] Charles, A., Hofer, A., Elkaseer, A., & Scholz, S.G. (2021). *Additive Manufacturing in the Automotive Industry and the Potential for Driving the Green and Electric Transition*. In: Scholz, S.G., Howlett, R.J., Setchi, R. (eds) Sustainable Design and Manufacturing. KES-SDM 2021. Smart Innovation, Systems and Technologies, vol. 262. Springer, Singapore. https://doi.org/10.1007/978-981-16-6128-0_32

[89] Hariri, H., Kim, J., Kim, W. S., Frechette, L. G., & Masson, P. (2017). Performance validation of printed strain sensors for active control of intelligent tires. *Appl. Acoust.*, *123*, 73-84. https://doi.org/10.1016/j.apacoust.2017.03.011

[90] Andrews, J. B., et al. (2018). Fully Printed and Flexible Carbon Nanotube Transistors for Pressure Sensing in Automobile Tires. *IEEE Sens. J.*, *18*(19), 7875-7880. https://doi.org/10.1109/JSEN.2018.2842139

[91] Escobedo, P., Bhattacharjee, M., Nikbakhtnasrabadi, F., & Dahiya, R. (2021). Flexible Strain and Temperature Sensing NFC Tag for Smart Food Packaging Applications. *IEEE Sens. J.*, *21*(23), 26406-26414. https://doi.org/10.1109/JSEN.2021.3100876

[92] Liao, Y., Zhang, R., & Qian, J. (2019). Printed electronics based on inorganic conductive nanomaterials and their applications in intelligent food packaging. *RSC. Adv.*, *9*, 29154-29172. https://doi.org/10.1039/C9RA05954G

[93] Zhang, Y., Anderson, N., Bland, S., Nutt, S., Jursich, G., & Joshi, S. (2017). All-printed strain sensors: Building blocks of the aircraft structural health monitoring system. *Sens. Actuator A Phys*., *253*, 165-172. https://doi.org/10.1016/j.sna.2016.10.007

[94] Herbert, R., Lim, H.-R., & Yeo, W.-H. (2020). Printed, Soft, Nanostructured Strain Sensors for Monitoring of Structural Health and Human Physiology. *ACS Appl. Mater. Interfaces*, *12*(22), 25020-25030. https://doi.org/10.1021/acsami.0c04857

[95] Gao, Y., Yu, L., Yeo, J. C., & Lim, C. T. (2019). Flexible Hybrid Sensors for Health Monitoring: Materials and Mechanisms to Render Wearability. *Adv. Mater., 1902133*, 1-31. https://doi.org/10.1002/adma.201902133

[96] Boutry, C.M., et al. (2019). Biodegradable and flexible arterial-pulse sensor for the wireless monitoring of blood flow. *Nat. Biomed. Eng.*, *3*, 47–57. https://doi.org/10.1038/s41551-018-0336-5

[97] Zheng, Y., et al. (2014). Personal electronics printing via tapping mode composite liquid metal ink delivery and adhesion mechanism. *Sci. Rep. 4*, 4588. https://doi.org/10.1038/srep04588

[98] Zheng, Y., et al. (2013). Direct Desktop Printed-Circuits-on-Paper Flexible Electronics. *Sci. Rep., 3*, 1786. https://doi.org/10.1038/srep01786

[99] Htwe, Y. Z. N., & Mariatti, M. (2022). Printed graphene and hybrid conductive inks for flexible, stretchable, and wearable electronics: Progress, opportunities, and challenges. *J. Sci.: Adv. Mater. Devices*, *7*(2), 100435. https://doi.org/10.1016/j.jsamd.2022.100435

[100] Buga, C. S., & Viana, J. C. (2022). The role of printed electronics and related technologies in the development of smart connected products. *Flex. Print. Electron., 7*, 043001. https://doi.org/10.1088/2058-8585/ac91de

[101] Kim, K.-T. & Park, Y.-W. (2008). Feasibility of low-cost microarray printing with inkjet printer. *2008 International Conference on Control, Automation and Systems*, 1932-1935. https://doi.org/10.1109/ICCAS.2008.4694413.

[102] Beedasy, V., & Smith, P.J. (2020). Printed Electronics as Prepared by Inkjet Printing. *Materials*. *13*(3), 704. https://doi.org/10.3390/ma13030704

[103] Oliveira, J., Correia, V., Castro, H., Martins, P., & Lanceros-Mendez, S. (2018). Polymer-based smart materials by printing technologies: Improving application and integration. Additive Manufacturing, *21*, 269-283. https://doi.org/10.1016/j.addma.2018.03.012

[104] Tan, H. W., An, J., Chua, C. K., & Tran, T. (2019). Metallic Nanoparticle Inks for 3D Printing of Electronics. *Adv. Electron. Mater.*, *5*, 1800831. https://doi.org/10.1002/aelm.201800831

[105] Berdozzi, N. et al. (2020). Rapid Fabrication of Electro-Adhesive Devices With Inkjet Printed Electrodes. *IEEE Robotics and Automation Letters*, *5*(2), 2770-2776. https://doi.org/10.1109/LRA.2020.2972838.

[106] Yoon, K. J., et al. (2019). Electrically-generated memristor based on inkjet printed silver nanoparticles. *Nanoscale Adv.*, *1*(8), 2990–2998. https://doi.org/10.1039/C9NA00329K.

[107] Abu-Khalaf, J. M., Al-Ghussain, L., & Al-Halhouli, A. (2018). Fabrication of Stretchable Circuits on Polydimethylsiloxane (PDMS) Pre-Stretched Substrates by Inkjet Printing Silver Nanoparticles. *Materials*, *11*(12), 2377. https://doi.org/10.3390/ma11122377.

[108] Tao, R. et al. (2018). Inkjet Printed Electrodes in Thin Film Transistors. *IEEE J. Electron Devices Soc.*, *6*, 774–790. https://doi.org/10.1109/JEDS.2018.2852288.

[109] Sundriyal, P., & Bhattacharya, S. (2018). *Inkjet-Printed Sensors on Flexible Substrates*. In: Bhattacharya, S., Agarwal, A., Chanda, N., Pandey, A., Sen, A. (eds) Environmental, Chemical and Medical Sensors. Energy, Environment, and Sustainability. Springer, Singapore. https://doi.org/10.1007/978-981-10-7751-7_5

[110] Ealias, A. M., & Saravanakumar, M. P. (2017). A review on the classification, characterisation, synthesis of nanoparticles and their application. *OP Conf. Ser.: Mater. Sci. Eng*., *263*, 032019. http://doi.org/10.1088/1757-899X/263/3/032019

[111] Ijaz, I., Gilani, E., Nazir, A., & Bukhari, A. (2020). Detail review on chemical, physical and green synthesis, classification, characterizations and applications of nanoparticles, *Green Chem. Lett. Rev*., *13*(3), 223-245. http://doi.org/10.1080/17518253.2020.1802517

[112] Jamkhande, P. D., Ghule, N. W., Bamer, A. H., & Kalaskar, M. G. (2019). Metal nanoparticles synthesis: An overview on methods of preparation advantages and disadvantages, and applications. *J. Drug Deliv. SCI TEC.*, *53*, 101174. https://doi.org/10.1016/j.jddst.2019.101174

[113] Loza, K., Heggen, M., & Epple, M. (2020). Synthesis, Structure, Properties, and Applications of Bimetallic Nanoparticles of Noble Metals. *Adv. Funct. Mater.*, *30*, 1909260. https://doi.org/10.1002/adfm.201909260

[114] Beyene, H. D., Werkneh, A. A., Bezabh, H. K., & Ambaye, T. G. (2017). Synthesis paradigm and applications of silver nanoparticles (AgNPs), a review. *Sustainable Materials and Technologies*, *13*, 18-23. https://doi.org/10.1016/j.susmat.2017.08.001

[115] Dauthal, P., & Mukhopadhyay, M. (2016). Nobel Metal Nanoparticles: Plant-Mediated Synthesis, Mechanistic Aspects of Synthesis, and Applications. *Ind. Eng. Chem. Res*., *55*, 9557−9577. https://doi.org/10.1021/acs.iecr.6b00861

[116] Dhand, C., et al. (2015). Methods and strategies for the synthesis of diverse nanoparticles and their applications: a comprehensive overview. *RSC Adv*., *5*, 105003. https://doi.org/10.1039/c5ra19388e

[117] Gawande, M. B., et al. (2015). Core-shell nanoparticles: synthesis and applications in catalysis and electrocatalysis. *Chem. Soc. Rev*., *44*, 7540. https://doi.org/10.1039/c5cs00343a

[118] Pryschchepa, O., Pomastowski, P., & Buszewski, B. (2020). Silver nanoparticles: Synthesis, investigation technique, and properties. *Adv. Colloid Interface Sci*., *284*, 102246. https://doi.org/10.1016/j.cis.2020.102246

[119] Rane, A. V., Kanny, K., Abitha, V. K., & Thomas, S. (2018). Chapter 5-Methods for Synthesis of Nanoparticles and Fabrication of Nanocomposites. In *Synthesis of Inorganic Nanomaterials*, 121-139. https://doi.org/10.1016/B978-0-08-101975-7.00005-1

[120] Rao, C. N. R., Ramakrishna Matte, H. S. S., Voggu, R., & Govindaraj, A. (2012). Recent progress in the synthesis of inorganic nanoparticles. *Dalton Trans*., *41*, 5089. https://doi.org/10.1039/c2dt12266a

[121] Harish, K. K., Nagasamy, V., Himangshu, B., & Anuttam, K. (2018). Metallic Nanoparticle: A Review. *Biomed. J. Sci. &Tech. Res*., *4*(2), 3765-3775. https://doi.org/10.26717/ BJSTR.2018.04.001011.

[122] Wei, L., Lu, J., Xu, H., Patel, A., Chen, Z.-S., & Chen, G. (2015). Silver nanoparticles: synthesis, properties, and therapeutic applications. *Drug Discov. Today*, *20*(5), 596-601. https://doi.org/10.1016/j.drudis.2014.11.014

[123] Xu, L. Wang, Y.-Y., Huang, J., Chen, C.-Y., Wang, Z.-X., & Xie, H. (2020). Silver nanoparticles: Synthesis, medical applications and biosafety. *Theranostics*, *10*(20), 8996-9031. https://doi.org/10.7150/thno.45413

[124] Tran, Q. H., Nguyen, V. Q., & Le, A.-T. (2018). Corrigendum: Silver nanoparticles: synthesis, properties, toxicology, applications and perspectives. *Adv. Nat. Sci.: Nanosci. Nanotechnol*., *9***,** 049501. https://doi.org/10.1088/2043-6254/aad12b

[125] Whitehead, C. B., Özkar, S., & Finke, R. G. (2019). LaMer´s 1950 Model for Particle Formation of Instantaneous Nucleation and Diffusion-Controlled Growth: A Historical Look at the Model´s Origins, Assumptions, Equations, and Underlying Sulfur Sol Formation Kinetics Data. *Chem. Mater*., *31*, 7116−7132. https://doi.org/10.1021/acs.chemmater.9b01273

[126] McCoy, B. J. (2001). Distribution Kinetics Modeling of Nucleation, Growth, and Aggregation Processes. *Ind. Eng. Chem. Res***.,** *40*, 5147-5154. https://doi.org/10.1021/ie001034i

[127] Vreeland, E. C., et al. (2015). Enhanced Nanoparticle Size Controñ by Extending LaMer's Mechanics. *Chem. Mater*., *27*, 6059−6066. https://doi.org/10.1021/acs.chemmater.5b02510

[128] Chen, D., Qiao, X., Qiu, X., & Chen, J. (2009). Synthesis and electrical properties of uniform silver nanoparticles for electronic applications. *J. Mater. Sci*., *44*, 1076-1081. https://doi.org/10.1007/s10853-008-3204-y

[129] Khodashenas, B., & Ghorbani, H. R. (2019). Synthesis of silver nanoparticles with different shapes. *Arab. J. Chem*., *12*, 1823-1838. https://doi.org/10.1016/j.arabjc.2014.12.014

[130] Reverberi, A. P.; Kuznetsov, N. T., Meshalkin, V. P., Salerno, M., & Fabiano, B. (2016). Systematical Analysis of Chemical Methods in Metal Nanoparticles Synthesis. *Theor. Found. Chem. Eng*., *50*(1), 59-66. *ISSN 0040_5795*,

[131] Gudikandula, K., & Maringanti, S. C. (2016). Synthesis of silver nanoparticles by chemical and biological methods and their antimicrobial properties. *J. Exp. Nanosci*., *11*(9), 714-721. https://doi.org/10.1080/17458080.2016.1139196

[132] Dragieva, I., Stoynov, Z. B., & Klabunde, K. J. (2001). Synthesis of nanoparticles by borohydride reduction and their applications. *Scripta mater*., *44*, 2187-2191. https://doi.org/10.1016/S1359-6462(01)00901-0

[133] Wuithschick, M. et al. (2015). Turkevich in New Robes: Key Questions Answered for the Most Common Gold Nanoparticle Synthesis. *ACS Nano*, *9*(7), 7052-7071. https://doi.org/10.1021/acsnano.5b01579

[134] Pillai, Z. S., & Kamat, P. V. (2004). What Factors Control the Size and Shape of Nanoparticles in the Citrate Ion Reduction Method? *J. Phys. Chem. B*., *108*, 945-951. https://doi.org/10.1021/jp037018r

[135] Wan, Y., Guo, Z., Jiang, X., Fang, K., Lu, X., Zhang, Y., & Gu, N. (2013). Quasi-spherical silver nanoparticles: Aqueous synthesis and size control by the seed-mediated Lee-Meisel method. *J. Colloid. Interface Sci*., *394*, 263-268. https://doi.org/10.1016/j.jcis.2012.12.037

[136] Evanoff, D. D., & Chumanov, G. (2005). Synthesis and Optical Properties of Silver Nanoparticles and Arrays. *Chem. Phys. Chem*., *6*, 1221-1231. https://doi.org/10.1002/cphc.200500113

[137] Krutyakov, Y. A., Kudrinskiy, A. A., Olenin, A. Y., & Lisichkin, G. V. (2008). Synthesis and properties of silver nanoparticles: advances and prospects. *Russ. Chem. Rev*., *77*, 233. https://doi.org/10.1070/RC2008v077n03ABEH003751

[138] Creighton, J. A., Blatchford, C. G., & Albrecht, M. G. (1976). Plasma Resonance Enhancement of Raman Scaterring by Pyridine Adsorbed on Silver or Gold Sol Particles of Size Comparable to the Excitation Wavelength. ***J. Chem. Soc., Faraday Trans. 2*****(75)**, 790-798. https://doi.org/10.1039/F29797500790

[139] Mulfinger, L., Solomon, S. D., Bahadory, M., Jeyarajasingam, A. V., Rutkowsky, S. A., & Boritz, C. (2007). Synthesis and Study of Silver Nanoparticles. *J. Chem. Educ. 84*(2), 322. https://doi.org/10.1021/ed084p322

[140] Van Dong, P., et al. (2012). Chemical synthesis and antibacterial activity of novel-shaped silver nanoparticles. *Int. Nano. Lett. 2*, 9. https://doi.org/10.1186/2228-5326-2-9

[141] Dong, X., Ji, X., Jing, J., Li, M., Li, J., & Yang, W. (2010). Synthesis of Triangular Silver Nanoprisms by Stepwise Reduction of Sodium Borohydride and Triangular Citrate. *J. Phys. Chem. C. 115*(5), 2070-2074. https://doi.org/10.1021/jp909964k

[142] García-Barrasa, J., López-de-Luzuriaga, J. M., & Monge, M. (2011). Silver nanoparticles: synthesis through chemical methods in solution and biological applications. *Cent. Eur. J. Chem*., *9*(1), 7-19. https://doi.org/10.2478/s11532-010-0124-x

[143] Pyatenko, A., Pomastowski, P., & Buszewski, B. (2020). Silver nanoparticles: Synthesis, investigation technique, and properties. *Adv. Colloid Interface Sci*., *284*, 102246. https://doi.org/10.1016/j.cis.2020.102246

[144] Eckelman, M. J., & Graedel, T. E. (2007). Silver Emissions and their Environmental Impacts: A Multilevel Assessment. *Environ. Sci. Technol*., *41*(17), 6283-6289. https://doi.org/10.1021/es062970d

[145] Desmukh, S. P., Patil, S. M., Mullani, S. B., & Delekar, S. D. (2019). Silver nanoparticles as an effective disinfectant: A review. *Mater. Sci. Eng. C, 97*, 954-965. https://doi.org/10.1016/j.msec.2018.12.102

[146] National Center for Biotechnology Information (2024). PubChem Compound Summary for CID 24470, Silver Nitrate. Retrieved March 12, 2024 from https://pubchem.ncbi.nlm.nih.gov/compound/Silver-Nitrate.

[147] Santos, D. M. F., & Sequeira, C. A. C. (2011). Sodium borohydride as a fuel for the future. *Renewable Sustainable Energy Rev., 15*, 3980-4001. https://doi.org/10.1016/j.rser.2011.07.018

[148] Retnamma, R., Novais, A. Q., & Rangel, C. M. (2011). Kinetics of hydrolysis of sodium borohydride for hydrogen production in fuel cell applications: A review. *Int. J. Hydrogen Energy*, *36*, 9772-9790. https://doi.org/10.1016/j.ijhydene.2011.04.223

[149] Rivarolo, M., Improta, O., Magistri, L., Panizza, M., & Babucci, A. (2018). Termo-economic análisis of a hydrogen production system by sodium borohydride ($NaBH_4$). *Int. J. Hydrogen Energy*, *43*, 1606-1614. https://doi.org/10.1016/j.ijhydene.2017.11.079

[150] Ouya, ng, L. Z., Zhong, H., Li, Z. M., Cao, Z. J., Wang, H., Liu, J. W., Zhu, X. K., & Zhu, M. (2014). Low-cost method for sodium borohydride regeneration and the energy efficiency of its hydrolysis and regeneration process. *J. Power Sources*, *269*, 768-772. https://doi.org/10.1016/j.jpowsour.2014.07.074

[151] National Center for Biotechnology Information (2024). PubChem Compound Summary for CID 6224, Sodium Citrate. Retrieved March 12, 2024 from https://pubchem.ncbi.nlm.nih.gov/compound/Sodium-Citrate.

[152] Hoyt, H.L., & Gewanter, H.L. (1992). Citrate. In: *de Oude*, N.T. (eds) Detergents. Anthropogenic Compounds, vol. 3/3F. Springer, Berlin, Heidelberg. https://doi.org/10.1007/978-3-540-47108-0_6

[153] PDI from an individual peak in DLS. (2015). https://www.malvernpanalytical.com/en/learn/knowledge-center/insights/pdi-from-an-individual-peak-in-dls

[154] Worldwide, M. I. (2011). Dynamic Light Scattering, Common Terms Defined, Inform White Paper. Malvern Instruments Limited: Malvern, UK.

[155] Gupta, V.; Trivedi, P. (2018). Chapter 15-In vitro and in vivo characterization of pharmaceutical topical nanocarriers containing anticancer drugs for skin cancer treatment. In Lipid Nanocarriers for Drug Targeting; Grumezescu, A.M., Ed.;William Andrew Publishing: Norwich, NY, USA. pp. 563–627. http://doi.org/10.1016/B978-0-12-813687-4.00015-3.

[156] Raval, N.; Maheshwari, R.; Kalyane, D.; Youngren-Ortiz, S.R.; Chougule, M.B.; Tekade, R.K. (2019). Importance of Physicochemical Characterization of Nanoparticles in Pharmaceutical Product Development. In Basic Fundamentals of Drug Delivery; Academic Press: Cambridge, MA, USA, pp. 369–400. http://doi.org/10.1016/B978-0-12-817909-3.00010-8.

[157] Vokhidova, N. R., & Rashidova, S. Sh. (2022). The influence of synthesis conditions on the film morphology of chitosan-stabilized silver nanoparticles. *Polym. Bull.*, *79*, 3419-3436. https://doi.org/10.1007/s00289-021-03669-y

[158] Shikha, S., Dureja, S., Sapra, R., Babu, J., Haridas, V., & Pattanayek, S. K. (2021). Interaction of borohydride stabilized silver nanoparticles with sulfer-containing organophosphates. *RCS Adv.*, *11*, 32286. https://doi.org/10.1039/d1ra06911j

[159] Gakiya-Teruya, M., Palomino-Marcelo, L., & Rodriguez-Reyes, J.C.F. (2019). Synthesis of Highly Concentrated Suspensions of Silver Nanoparticles by Two Versions of the Chemical Reduction Method. *Methods Protoc.*, *2*, 3. https://doi.org/10.3390/mps2010003

[160] Stewart, A., Murray, S., & Bell, S. E. J. (2015). Simple preparation of positively charged silver nanoparticles for detection of anions by surface-enhanced Raman spectroscopy. Analyst, 140, 2988-2994. https://doi.org/10.1039/C4AN02305F

[161] Dehsari, H.S.; Ribeiro, A. H., Ersöz, B., Tremel, W., Jakob, G., & Asadi, K. (2017). Effect of precursor concentration on size evolution of iron oxide nanoparticles. Cryst. Eng. Comm., 19, 6694-6702. https://doi.org/10.1039/C7CE01406F

[162] Vaseen, M., et al. (2022). High-conductivity screen-printable silver nanowire Ink for optically transparent flexible radio frequency electronics. *Flex. Print. Electron*., *7(4),* 044001. https://doi.org/10.1088/2058-8585/ac97a4

[163] McClary, F.A., et al. (2013). Enhanced localized surface plasmon resonance dependence of silver nanoparticles on the stoichiometric ratio of citrate stabilizers. *J. Nanopart. Res.* 15, 1442. https://doi.org/10.1007/s11051-013-1442-7

[164] Paswan, S. K., et. al. (2021). Optimization of structure-property relationships in nickel ferrite nanoparticles annealed at different temperature. *J. Phys. Chem. Solids*, *151*, 109928. http://doi.org/10.1016/j.jpcs.2020.109928.

[165] Arguelles, A. P., & Turner, J. A. (2017). Ultrasonic attenuation of polycrystalline materials with a distribution of grain sizes. *J. Acoust. Soc. Am.*, *141*, 4347–4353. http://doi.org/10.1121/1.4984290.

[166] Gao, P., Zhang, T. S., Wei, J. X., & Yu, Q. J. (2018). Evaluation of RRSB distribution and lognormal distribution for describing the particle size distribution of graded cementitious materials. *Powder Technol*., *331*, 137–145. http://doi.org/10.1016/j.powtec.2018.01.079.

[167] Jana, N. R., Gearheart, L., & Murphy, C. J. (2001). Evidence for Seed-Mediated Nucleation in the Chemical Reduction of Gold Salts to Gold Nanoparticles. *Chem. Mater*., *13*(7), 2313-2322. https://doi.org/10.1021/cm000662n

[168] Stöber, W., Fink, A., & Bohn, E. (1996). Controlled growth of monodisperse silica spheres in the micron size range. *J. Colloid Interface Sci*., *26*(1), 62-69. http://doi.org/10.1016/0021-9797(68)90272-5

[169] Matyi, R. J., Schwartz, L. H., & Butt, J. B. (1987). Particle Size, Particle Size Distribution, and Related Measurements of Supported Metal Catalysts, *Catalysis Reviews*, *29*(1), 41-99, http://doi.org/10.1080/01614948708067547

[170] Austin, J., et al. (2020). Nanoparticle number concentration measurements by multi-angle dynamic light scattering. *J. Nanopart. Res.*, *22*, 108. https://doi.org/10.1007/s11051-020-04840-8

[171] Raza, M. A., Kanwal, Z., Rauf, Anum., Sabri, A. N., Riaz, S., & Naseem, S. (2016). Size-and Shape-Dependent Antibacterial Studies of Silver Nanoparticles Synthesized by Wet Chemical Routes. *Nanomaterials*, *6*, 74. https://doi.org/10.3390/nano6040074

[172] Monowar, T., Sayedur Rahman, Md., Bhore, S. J., Raju, G., & Sathasivam, K. V. (2018). Silver Nanoparticles Synthesized by Using the Endophytic Bacterium Pantoea ananatis are Promising Antimicrobial Agents agains Multidrug Resistant Bacteria. *Molecules*, *23*(12), 322. https://doi.org/10.3390/molecules23123220

[173] Zhang, W., Yao, Y., Sullivan, N., & Chen, Y. (2011). Modeling the primary Size Effects of Citrate-Coated Silver Nanoparticles on Their Ion Release Kinetics. *Environ. Sci. Technol., 45*(10), 4422-4428. https://doi.org/10.1021/es104205a

[174] Zook, M., Rastogi, V., MacCuspe, R. I., Keene, A. M., & Fagan, J. (2011). Measuring Agglomerate Sie Distribution and Dependence Localized Surface Plasmon Resonance Absorbance on Gold Nanoparticle Agglomerate Size Using Analytical Ultracentrifugation. *ACS Nano, 5*(10), 8070-8079. https://doi.org/10.1021/nn202645b

[175] Rocha, F.S., Gomes, A.J., Lunardi, C.N., Kaliaguine, S. & Patience, G.S. (2018), Experimental methods in chemical engineering: Ultraviolet visible spectroscopy—UV-Vis. *Can. J. Chem. Eng.*, *96*, 2512-2517. https://doi.org/10.1002/cjce.23344

[176] Tomaszewska, E., Soliwoda, K., Kadziola, K., Tkacz-Szczesna, B., Celichowski, G., Cichomski, M., Szmaja, W., & Grobelny, J. (2013). Detection Limits of DLS and UV-Vis Spectroscopy in Characterization of Polydisperse Nanoparticles Colloids, *J. Nanomater., 2013*, 313081. https://doi.org/10.1155/2013/313081

[177] Mariam, R., Rodrigues, M., Loidl, M., Pierre, S., & Lourenço, V. (2022). Determination of L-X ray absolute emision intensities of 238Pu, 244Cm, 237Np and 233Pa radionuclides using a metallic magnetic calorimeter. *Spectrochim. Acta B: At.*, *187*, 106331. https://doi.org/10.1016/j.sab.2021.106331

[178] Armstrong, J. T. (1999). Determination of Chemical Valence State by X-ray Emission Analysis Using Electron Beam Instruments: Pitfalls and Promises. *Anal. Chem, 71*, 2714-2724. https://doi.org/10.1021/ac981214q

[179] Krukowski, S., Karasiewicz, M., & Kolodziejski, W. (2017). Convenient UV-spectrophotometric determination of citrates in aqueous solutions with applications in the pharmaceutical analysis of oral electrolyte formulations. *JDFA, 25*(3), 717-722. https://doi.org/10.1016/j.jfda.2017.01.009

[180] Velgosova, O., Mačák, L., Lisnichuk, M., & Vojtko, M. (2022). Synthesis and Analysis of Polymorphic Silver Nanoparticles and Their Incorporation into the Polymer Matrix. *Polymers, 14*, 2666. https://doi.org/10.3390/polym14132666

[181] La Spina, R., Mehn, D., Fumagalli, F., Holland, M., Reniero, F., Rossi, F., & Gilliland, D. (2020). Synthesis of Citrate-Stabilized Silver Nanoparticles Modified by Thermal and pH Preconditioned Tannic Acid. *Nanomaterials, 10*, 2031. https://doi.org/10.3390/nano10102031

[182] Ali, Md. H., Kalam Azad, Md. A., Khan, K. A., Obaidur Rahman, Md, Chakma, U., & Kumer, A. (2023). Analysis of Crystallographic Structures and Properties of Silver Nanoparticles Synthesized Using PKL Extract and Nanoscale Characterization Techniques. *ACS Omega, 8*(31), 28133-28142. https://doi.org/10.1021/acsomega.3c01261

[183] Bhagat, M., et al. (2015). Biological and electrical properties of biosynthesized silver nanoparticles. *Bull. Mater. Sci., 38*, 1253–1258 (2015). https://doi.org/10.1007/s12034-015-1007-8

[184] Wu, W., Wang, Z., Jiang P., & Tang, Z. (2017). Effect of Electroplating Variables on Electrodeposition of Ni Rich Ni-Ir Allys from Citrate Aqueous Solutions. *J. Electrochem. Soc., 164* (14), D985. https://doi.org/10.1149/2.0771714jes

[185] Chadha, R., Maiti, N., & Kapoor, S. (2014). Reduction and aggregation of silver ions in aqueous citrate solutions. *Mater Sci. Eng. C, 38*, 192-196. https://doi.org/10.1016/j.msec.2014.01.041

[186] Bhadra, J., Al-Thani, N. J., Karmakar, S., & Madi, N. K. (2019). Photo-reduced route of polyaniline nanofiber synthesis with embedded silver nanoparticles. *Arab. J. Chem*., *12*(8), 4848-4860. https://doi.org/10.1016/j.arabjc.2016.10.001

[187] Zhao, Y.-Y., Ren, X.-L., Zheng, M.-L., Jin, F., Liu, J., Dong, X.-Z., Zhao, Z.-S., & Duan, X.-M. (2021). Plasmon-enhanced nanosoldering of silver nanoparticles for high-conductive nanowires electrodes. *Opto-Electron. Adv.*, ***4***, 200101. 10.29026/oea.2021.200101

[188] Chettri, P., Tripathi, A., & Tiwari, A. (2022). Effect of silver nanoparticles on electrical and magnetic properties of reduced graphene oxide. *Mater. Res. Bull.*, *150*, 111752. https://doi.org/10.1016/j.materresbull.2022.111752

[189] Männl, U., van den Berg, C., Magunje, B., Härting, M., Britton, D. T., Jones, S., van Staden M. J., & Scriba, M. R. (2014). Nanoparticle composites for printed electronics. *Nanotechnology*, *25*(9), 094004. https://doi.org/10.1088/0957-4484/25/9/094004

[190] Abry, P., et al. (2015). Multiscale Anisotropic Texture Analysis and Classification of Photographic Prints: Art scholarship meets image processing algorithms. *IEEE Signal Process. Mag.*, *32*(4), 18-27. https://doi.org/10.1109/MSP.2015.2402056

[191] Pedrosa, J.F.S., Alves, L., Neto, C.P., Rasteiro, M.G., & Ferreira, P.J.T. (2022). Assessment of the Performance of Cationic Cellulose Derivatives as Calcium Carbonate Flocculant for Papermaking. *Polymers*, *14*, 3309. https://doi.org/10.3390/polym14163309

[192] Jasmee, S., Omar, G., Masripan, N. A. B., Kamarolzaman, A. A., Ashikin, A. S., & Che Ani, F. (2018). Hydrophobicity performance of polyethylene terephthalate (PET) and thermoplastic polyurethane (TPU) with thermal effect. *Mater. Res. Express*, *5*, 096304. https://doi.org /10.1088/2053-1591/aad81e

[193] Ihalainen, P., Määttänen, A., Järnström, J., Tobjörk, D., Österbacka, R., & Peltonen, J. (2012). Influence of Surface Properties of Coated Papers on Printed Electronics. *Ind. Eng. Chem. Res*., *51*(17), 6025-6036. https://doi.org/10.1021/ie202807v

[194] Potts, S.-J., Phillips, C., Claypole, T., & Jewell. E. (2020). The Effect of Carbon Ink Separation Mechanisms in Screen-Printing. *Coatings*, *10*(10), 1008. https://doi.org/10.3390/coatings10101008

[195] Gustafsson, O., Gustafsson, S., Manukyan, L., & Mihranyan, A. (2018). Significance of Brownian Motion for Nanoparticle and Virus Capture in Nanocellulose-Based Filter Paper. *Membranes*, *8*, 90. https://doi.org/10.3390/membranes8040090

[196] Asper, M., Hanrieder, T., Quellmalz, A., & Mihranyan, A. (2015). Removal of xenotropic murine leukemia virus by nanocellulose based filter paper. *Biologicals*, *43*(6), 452–456. https://doi.org/10.1016/j.biologicals.2015.

[197] Praveena, S. M., Han, L. S., Than, L. T. L., & Aris, A. Z. (2016). Preparation and characterization of silver nanoparticle coated on cellulose paper: evaluation of their potential as antibacterial water filter. *J. Exp. Nanosci.*, *11*(17), 1307-1319. https://doi.org/10.1080/17458080.2016.1209790

[198] Andò, B., et. al. (2019). Low Cost Inkjet Printed Sensors: From Physical to Chemical Sensors. *Lect. Notes Electr. Eng.*, *539*, 297– 308, https://doi.org/10.1007/978-3-030-04324-7_38

[199] Cheng, T., Narumi, K., Do, Y., Zhang, Y., Ta, T. D., Sasatani, T., Markvicka, E., Kawahara, Y., Yao, L., Abowd, G. D., & Oh, H. (2020). Silver Tape: Inkjet-Printed Circuits Peeled-and-Tranferred on Versatile Substrates. *Proceedings of the ACM on Interactive, Mobile, Wearable and Ubiquitous Technologies, 4*(1), 1–17. https://doi.org/10.1145/3381013

[200] Zhao, P., Huang, J., Nan, J., Liu, D., & Meng, F. (2020). Laser sintering process optimization of microstrip antenna fabricated by inkjet printing with silver-based MOD ink, *J. Mater. Process. Technol.*, *275*, 116347. https://doi.org/10.1016/j.jmatprotec.2019.116347

[201] Komuro, N., et al. (2013). Inkjet printed (bio)chemical sensing devices. *Anal. Bioanal. Chem.*, *405*, 5785–5805. https://doi.org/10.1007/s00216-013-7013-z

[202] Dimatrix Materials Printer DMP-2850. (2024). https://www.fujifilm.com/us/en/business/inkjet-solutions/inkjet-technology-integration/dmp-2850

[203] Fujifilm Dimatix DMP-2831 inkjet printer. (2024). https://www.labx.com/item/fujifilm-dimatix-dmp-2831-ink-jet-printer-with-fiducial/DIS-86979-4026

[204] Cho, H., Parameswaran, M. (Ash), & Yu, H.-Z. (2007). Fabrication of microsensors using unmodified office inkjet printers. *Sensors and Actuators B: Chemical*, *123*(2), 749–756. https://doi.org/10.1016/j.snb.2006.10.022

[205] Kumar, S., Bhat, V., Vinoy K. J. & Santhanam, V. (2014). Using an Office Inkjet Printer to Define the Formation of Copper Films on Paper. *IEEE Trans. Nanotechnol.*, *13*(1), 160-164. https://doi.org/10.1109/TNANO.2013.2295765.

[206] Chae, H., et al. (2016). Thermoelectric temperature sensors by printing with a simple office inkjet printer. *TechConnect Briefs*, *4*, 151-155.

[207] Zhuo, L., et al. (2023). Direct pen writing and atomic-scale molecular dynamics simulation study of a novel silver nano-ink. *J Mater Sci: Mater Electron.*, *34*, 2182. https://doi.org/10.1007/s10854-023-11628-8

[208] Quain, E., Mathis, T. S., Kurra, N., Maleski, K., Van Aken, K. L., Alhabeb, M., Alshareef, H. N., & Gogotsi, Y. (2019). Direct Writing of Additive-Free MXene-in-Water Ink for Electronics and Energy Storage. *Adv. Mater. Technol.*, *4*, 1800256. https://doi.org/10.1002/admt.201800256

[209] Loghin, F. C., Falco, A., Albrecht, A., Salmeron, J. F., Becherer, M., Lugli, P., & Rivadeneyra, A. (2018). A handwriting method for low-cost gas sensors. *ACS Appl. Mater. Interfaces*, *10*(40), 34683–34689. https://doi.org/10.1021/acsami.8b08050

[210] Bower, I. A., Taylor, C., & Sitaraman, S. K. (2020). Study of inkjet-printed serpentine structure on flexible substrates deformed over sculptured surfaces. *Flex. Print. Electron.*, *5*(1), 15010. https://doi.org/10.1088/2058-8585/ab670b

[211] Calvert, P. (2017). *Reactive Inkjet Printing: A Chemical Synthesis Tool*. ed. P. J. Smith and A. Morrin, The Royal Society of Chemistry. 222-239. https://doi.org/10.1039/9781788010511-00222

[212] Kamyshny, A., Ben-Moshe, M., Aviezer, S., & Magdassi, S. (2005). Ink-Jet Printing of Metallic Nanoparticles and Microemulsions. *Macromol. Rapid Commun.*, *26*(4), 281–288, 2005. https://doi.org/10.1002/marc.200400522

[213] Huang, Q., & Zhu, Y. (2019). Printed Conductive Nanomaterials for flexible and Stretchable Electronics: A Review of Materials, Processes, and Applications *Adv. Mater. Technol.*, *4*, 1800546. https://doi.org/10.1002/admt.201800546

[214] Soum, V., Lehmann, V., Lee, H., Khan, S., Kwon, O.-S., & Shin, K. (2023). A Novel Polymeric Substrate with Dual-Porous Structures for High-Performance Inkjet-Printed Flexible Electronic Devices. *Macromol. Mater. Eng.*, *308*, 2300107. https://doi.org/10.1002/mame.202300107

[215] Fardim, P., & Holmbom, B. (2005). ToF-SIMS imaging: a valuable chemical microscopy technique for paper and paper coatings. *Appl. Surf. Sci*., *249*(1-4), 393-407. https://doi.org/10.1016/j.apsusc.2004.12.041

[216] Saha, T. K., Knaus, T. N., Khosla, A., & Sekhar, P. K. (2018). Investigation of Printing Properties on Paper Substrate. *J. Electrochem. Soc.*, *165*(8), B3163--B3167. https://doi.org/10.1149/2.0211808jes

[217] Kabekkodu, S. N., Faber, J., & Fawcett, T. (2002). New Powder Diffraction File (PDF-4) in relational database format: advantages and data-mining capabilities. *Acta Crystallogr. Sect. B Struct. Sci., 58*, 333–337. http://doi.org/10.1107/s0108768102002458.

[218] Alim-Al-Razy, M., Asik Bayazid, G. M., Ur Rahman, R., Bosu, R., & Samim Shamma, S. (2020). Silver nanoparticle synthesis, UV-Vis spectroscopy to particle size and measure resistance of colloidal solution. *J. Phys.: Conf. Ser., 1706*, 012020. http://doi.org/10.1088/1742-6596/1706/1/012020

[219] Zhang, X., Zhao, X., Zhu, P., Alder, Z., Wu, Z.-Y., Liu, Y. & Wang, H. (2022). Electrochemical oxygen reduction to hydrogen peroxide at practical rates in strong acidic media. *Nat. Commun., 13*, 2880. https://doi.org/10.1038/s41467-022-30337-0

[220] Gatemala, H., Ekgasit, S., & Wongravee, K. (2017). High purity silver microcrystals recovered from silver wastes by eco-friendly process using hydrogen peroxide. *Chemosphere*, *178*, 249-258. https://doi.org/10.1016/j.chemosphere.2017.03.051

[221] Parnklang, T., Lamlua, B., Gatemala, H., Thammacharoen, C., Kuimalee, S., & Lohwongwatana, B. (2015). Shape transformation of silver nanospheres to silver nanoplates induced by redox reaction of hydrogen peroxide. *Mater. Chem. Phys.*, *153*, 127-134. https://doi.org/10.1016/j.matchemphys.2014.12.044

[222] Meng, F., Zhu, X., & Miao, P. (2015). Study of autocatalytic oxidation reaction of silver nanoparticles and the application for nonenzymatic H_2O_2 assay. *Chem. Phys. Lett. 635*, 213-216. http://doi.org/10.1016/j.cplett.2015.06.068.

[223] Wang, G.-L., Zhu, X.-Y., Dong, Y.-M., Jiao, H.-J., Wu, X.-M., & Li, Z.-J. (2013). The pH-dependent interaction of silver nanoparticles and hydrogen peroxide: A new platform for visual detection of iodide with ultra-sensitivity. Talanta, 107, 146-153. http://doi.org/10.1016/j.talanta.2012.12.029.

[224] He, D., Garg, S., & Waite, D. (2012). H_2O_2-Mediated Oxidation of Zero-Valent Silver and Resultant Interactions among Silver Nanoparticles, Silver Ions, and Reactive Oxygen Species. *Langmiur, 28*, 10266-10275. http://doi.org/10.1021/la300929g.

[225] Riera-Franco de Sarabia, E., Gallego-Juárez, J. A., Rodríguez-Corral, G., Elvira-Segura, L., & González-Gómez, I. (2000). Application of high-power ultrasound to enhance fluid/solid particle separation processes. *Ultrasonics*, *38*, 642–646. http://doi.org/10.1016/s0041-624x(99)00129-8.

[226] Krause, B., Mende, M., Pötschke, P., & Petzold, G. (2010). Dispersability and particle size distribution of CNTs in an aqueous surfactant dispersion as a function of ultrasonic treatment time. *Carbon*, *48*, 2746–2754. http://doi.org/10.1016/j.carbon.2010.04.002.

[227] Shigemune, H., et al. (2017). Printed Paper Robot Driven by Electrostatic Actuator. *IEEE Robot. Autom. Lett.*, *2*(2), 1001-1007. https://doi.org/10.1109/LRA.2017.2658942

[228] Jiang, H. et al. (2021). Low content and low-temperature cured silver nanoparticles/silver ion composite ink for flexible electronic applications with robust mechanical performance. *Appl. Surf. Sci.*, *564*, 150447. https://doi.org/10.1016/j.apsusc.2021.150447

[229] Chicea, D., Nicolae-Maranciuc, A., Doroshkevich, A. S., Chicea, L. M., & Ozkendir, O. M. (2023). Comparative Synthesis of Silver Nanoparticles: Evaluation of Chemical Reduction Procedures, AFM and DLS Size Analysis. *Materials*, *16*, 5244. http://doi.org/10.3390/ma16155244.

[230] Viguié, J.-R., Sukmanowski, J., Nölting, B., & Royer, F.-X. (2007). Study of agglomeration of alumina nanoparticles by atomic force microscopy (AFM) and photon correlation spectroscopy (PCS). *Colloids Surf. A: Physicochem. Eng.*, *302*(1-3), 269–275. https://doi.org/10.1016/j.colsurfa.2007.02.03

[231] Baalousha, M., & Lead, J. R. (2013). Nanoparticles dispersity in toxicology. *Nature Nanotech.*, *8*, 308-309. http://doi.org/10.1038/nnano.2013.78.

[232] Aadil, K. R., Barapatre, A., Meena, A, S., & Jha, H. (2016). Hydrogen peroxide sensing and cytotocity activity of Acacia lignin stabilized silver nanoparticles. *Int. J. Biol. Macromol.*, *82*, 39-47. https://doi.org/10.1016/j.ijbiomac.2015.09.072

[233] Perevezentseva, D., Gorchakov, E., Petrushin, M., Hismutdinov, I., & Bimatov, V. (2016). Influence of silver nanoparticles conditions synthesis on their electrochemical properties. *AIP Conf. Proc.*, *1772*, 020005. https://doi.org/10.1063/1.4964527

[234] Jang, J., Cho, K., Lee, S., & Kim, S. (2008). Transparent and flexible thin-film transistors with channel layers composed of sintered HgTe nanocrystals. *Nanotechnology*, *9*, 015204. https://doi.org/10.1088/0957-4484/19/01/015204